2017

Cell-bioactive glass scaffold interactions: Biological response to chemistry and topology

Tia Kowal
Lehigh University

Cell-bioactive glass scaffold interactions: Biological response to chemistry and topology

by

Tia Kowal

A Dissertation

Presented to the Graduate and Research Committee

of Lehigh University

in Candidacy for the Degree of

Doctor of Philosophy

in

Cell & Molecular Biology

Lehigh University

May 22, 2017

Approved and recommended for acceptance as a dissertation in partial fulfillment of the requirements for the degree of Doctor of Philosophy

Tia Kowal
Cell-bioactive glass scaffold interactions: Biological response to chemistry and topology

_____
Defense Date

_____
Matthias M. Falk, Ph.D.
Dissertation Director

_____
Approved Date

Committee Members:

_____
Himanshu Jain, Ph.D.

_____
Lynne Cassimeris, Ph.D.

_____
M. Kathryn Iovine, Ph.D.

_____
Paul Janmey, Ph.D.

ACKNOWLEDGMENTS

This dissertation is devoted to my Grandmother. She was the most wonderful and caring woman. She was always supportive and pushed me to be just a little bit better than I thought I was. Grandmother was a confident and progressive woman that I am proud to have known and loved. Pep, Vim, and Vitality.

I would like to thank my advisor, Matthias Falk, for his support. I am incredibly thankful to him for giving me the opportunity to be in his lab and to work on such a unique project. I am also thankful that he allowed me to participate in gap junction discussions and publications, although I was not a part of that project, it made me a well-rounded scientist. Most importantly, I am thankful to him for exposing me to different imaging techniques. My passion for microscopy has really been fostered by the experiences I had in his lab. I would also like to thank my co-advisor, Himanshu Jain, for opening his lab to me and pioneering the project initially. Thanks to him, I was easily able to be trained on instruments that are not readily accessible to the biology department and in-turn, he has also played a pivotal role in my love for microscopy.

The support of my wonderful committee members was crucial to my maturation into a scientist. Thank you to Kathy Iovine, who is always available for moral and scientific support. Thank you to Lynne Cassimeris for being so passionate about science and having an invested interest in those you mentor. I appreciate our discussions including lunch room banter. Thank you to Paul Janmey for taking an interest in this project and for always making the long haul to Lehigh for some always insightful discussions. I must also mention Jutta Marzillier for initial training on the project.

I of course must thank my Falk lab compadres. Rachael's ability to listen to science or non-science related matters is unmatched, and I am blessed to find such an amazing friend disguised as a co-worker. I could always count on Chuck for a smile and more hugs than one would ever need. John was the big brother in the lab, and always set a good example for grad student etiquette. Thank you to Ana for being a strong, motivated, and determined woman (and role model), and of course a great friend. Natalie

was the best undergrad a grad student could ask for, offered a fresh perspective on the project and a lasting friendship. Last but not least, the honorary Falk lab member Tee. This project could never have succeeded without his sincere interest in the venture. He will probably never understand how much I appreciate all of his help and discussions. I am so lucky to have developed all of these friendships with the Falk lab members, and I hope we can all continue to support each other.

The staff members in the biology department are unparalleled superheroes. Thank you to Lee Graham, Maria Brace, Vicki Ruggiero, Heather Sohora, and Delia Chetlani for all of the support and patience you give to graduate students in the Biology department. The department would not be successful without the effort of these individuals.

Although I truly think my family would support me in any endeavor, even one as crazy as pursuing a PhD, I have to say that their patience with me throughout this process has been remarkable. I appreciate my parents for giving me all the opportunities I have had, for taking an interest in the things that are important to me, and expanding my mind by sharing with me the things that are important to them. I have been incredibly lucky to be able to share this journey with my youngest and shortest sister Mikala, who also pursued a degree in biology at Lehigh. It has been so enjoyable to have noodles with her on Wednesdays, talk about what classes she should take next semester, and go rock climbing with her at the gym. Although our other sister Sasha didn't join us in our studies at Lehigh, I frequently confided in her and often lived vicariously through stories of her travels with Disney on Ice. We may have bickered as youngsters but I couldn't imagine anyone I'd rather share a whole jar of pickles with than her. Aunt Mary has been there always, no matter what, with a fresh smile and open mind. A special thank you to my extended "family" Lou, Bec, Erin, and Nancy, to my crazy wonderful neighbors Jay and Feldie, and to my family-to-be, the Fiorinis. Finally, Johnny Fiorini is the love of my life, my rock, my forever and for always. He has been nothing less than amazing, and I cannot wait to take on our next adventure together.

TABLE OF CONTENTS

LIST OF FIGURES

ABSTRACT

The medical community is transitioning from replacement to regeneration with the advent of tissue engineering; yet, it is not well understood how cells of the body can interact with the biologically active scaffolds used to guide tissue regeneration. In order to design the ideal material for the regeneration of different tissues, we must first have a comprehensive understanding of the fundamental mechanisms that allow cells to not only attach to these bioscaffold materials, but to also take cues from them as to what tissue should be regenerated. The Jain lab in Lehigh University's Material Science and Engineering department developed a bioactive glass scaffold with a 70 mol% SiO_2 -30 mol% CaO composition, termed TAMP (Tailored Amorphous Multi Porous), for which many parameters of the material may be controlled independently including chemical composition, surface roughness, porosity and pore distribution, and surface area. The worked described here aimed to determine how characteristics of bioactive TAMP scaffolds influence cellular behavior (e.g. attachment, morphology, function, proliferation) and how proteins that absorb to the scaffold surface modify cellular response. Not only did we find that cells attached to the surface and proliferated on and inside the TAMP scaffolds, but we also demonstrate that cells are able to sense and respond to topographical features of their substrate that are 1000 times smaller than the cells themselves. This sensitivity is likely influenced by nano-structure imposed by either the natural glass surface or hydroxyapatite, which forms when glass is exposed to physiological solutions and in-turn influences the conformation of adsorbed proteins on the surface. Using immunofluorescence, qRT-PCR, immunological and enzymatic assays, potential applications for TAMP scaffolds were explored including for hard (bone) tissue, for which we determined that MC3T3-E1 pre-osteoblast cells differentiated and BMD pre-cursor cells matured into active osteoclasts. Furthermore, soft tissue applications were explored including analyses of skin regeneration and polarization of uterine epithelium in culture. The data described here support the potential utility of this novel scaffold material for tissue engineering applications.

Chapter 1: Introduction

1.1 - The Problem

Tissue engineering has become a major new frontier in medicine with the potential for regenerating tissue with the patient's own cells, rather than replacing it from a donor, other part of the body, or foreign material [1] Medicine has seen over the past few decades that replacing tissue can work, but not in all instances, and often not efficiently or permanently. For example, bone tissue is often replaced with metals, like titanium or stainless steel, which are not bioactive meaning that cells of the body cannot interact with them. Therefore, instead of incorporating the metal implant into the existing tissue structure, scar tissue forms around the foreign material. This scar tissue may cause discomfort and over time can break free from the material, necessitating the removal and replacement of the original implant [2]. To circumvent this issue, metals are often textured or coated to allow cells to attach [3-5], but still the metals are not of the same mechanical properties as the tissue. In addition to metallic implants, the medical community also replaces tissue with other tissue, which is called grafting. Grafting has its drawbacks too with issues of donor compatibility and immunological rejection in the case of allografting (transplant from one person to another), along with extended surgery times and creation of a new defect with autografting (transplant from one location to another on the same person) [6, 7]. Tissue regeneration using a bioactive material offers an alternative to both of these techniques, while addressing each of their drawbacks directly.

1.2 - A solution

In the 1960's, Larry Hench developed a novel material for tissue regeneration, which he called Bioglass®. He began this pursuit after being intrigued by a Vietnam war veteran's account of amputations that were necessary because of surgeons' lack of

appropriate material in the field. His innovative material was composed of 45%SiO_2-24.5%Na_2O-24.5%CaO-6%P_2O_5 (mol%) [8]. When the 45S5 Bioglass® was placed into solution it quickly formed a layer of hydroxyapatite ($Ca_5(PO_4)_3OH$), which is the main inorganic component of bone. Additionally, analysis of 45S5 Bioglass® implanted into the femur and tibias of rat, canine and monkeys showed that cells of the bone bonded to the glass, which suggested it was a bioactive material.

Since the advent of 45S5, there have been several versions of bioactive glasses developed. Hench's 45S5 Bioglass® was produced using the melt-quench method which results in a dense bulk material that lacks pores. Researchers have moved to using alternative strategies (reviewed in Jones et. al. 2015), including the sol-gel method (described below), for manufacturing bioactive glasses, which allow for greater flexibility in the structure and improved functionality of the glass.

1.3 - Our solution

A scaffold material should provide the body's native cells with cues to prompt regeneration of damaged tissue. Therefore, the ideal material to do this would be bioactive, contain pores to allow for nutrient exchange, mimic the structure/morphology of the tissue to be regenerated, and be a temporary scaffold that resorbs into the body after the regeneration process. We have previously reported in Marquez et. al. 2009 about TAMP (Tailored Amorphous Multi-Porous) scaffolds, a material that could fulfill these requirements. They are named as such because these scaffolds can be "Tailored," meaning many of the parameters of the material may be controlled independently. These include chemical composition, surface roughness, porosity and pore distribution, and surface area [9-11]. Through this "Tailored" fabrication, scaffolds can be customized to the specific needs of a patient or tissue. TAMP scaffolds are prepared through a novel sol-gel process (Figure 1) [10, 11] resulting in a glass and therefore "Amorphous" material. Finally, the scaffolds are "Multi-Porous" in the sense that they have two or more types of pores, macropores which are important for allowing cells to enter into and colonize the scaffold, and nanopores which are critical for fluid exchange and large

surface area. The chemical composition that we have chosen to work with is 70 mol% SiO2 -30 mol% CaO because of its simplicity, bioactivity, and potential osteoinductive properties [12, 10, 11, 8].

1.4 - Results

The material resulting from the sol-gel process is a dual-porous disc shaped TAMP scaffold with a diameter of app. 1.3 cm and a composition of 70 mol% SiO_2 and 30 mol% CaO [10, 11] (Figure 2A). TAMP scaffolds featured interconnected macro-pores ranging from app. 20-200μm measured by mercury porosimetry and imaged by SEM (Figure 2B), and interconnected nano-pores ranging from app. 2.5-20nm measured by BET nitrogen adsorption and imaged by SEM (Figure 2C). From the BET analysis, we also learned that these scaffolds have a surface area of on average 90.2 ± 5.5m^2 per gram (Figure 2D). Additionally, when incubated in simulated body fluid (SBF) or cell culture medium, TAMP scaffolds become coated with a crystalline layer of hydroxyapatite which further contributes to the glass' biocompatibility (Figure 2E) [10]. Further, the glass slowly dissolved with a half-life dissolution rate of 15.4 days under quasi-dynamic conditions [13]. Taken together TAMP material fulfills all principle parameters desirable of an advanced bioactive tissue regeneration scaffold.

1.5 – Materials and Methods

1.5.1 – TAMP scaffold preparation

70 mol% SiO_2-30 mol% CaO TAMP scaffolds were produced using a modified sol-gel method previously described by Wang et al 2011 [12]. In brief, 1.4g polyethylene oxide (PEO) was dissolved in 20ml 0.05N acetic acid followed by addition of 9ml tetramethyl orthosilicate (TMOS) and 6.18g $Ca(NO_3)_2$-$4H_2O$. 2.5% Hydrofluoric acid (HF) was added to catalyze the gelation process and the sol was pipetted into 24-well plates to gel. The gel was allowed to mature at 40°C for 24 hrs before 1N NH_4OH was added for

solvent exchange (also at 40°C) over the next 3 days. The samples were dried slowly over 3 days by increasing temperature from 24°C to 180°C in a controlled humidity environment, followed by sintering at 700°C. Nanoporosity and surface area were confirmed using BJH (Barrett-Joyner-Halenda) and BET (Brunauer-Emmett-Teller) nitrogen adsorption (ASAP 2020; Micromimetics) by loading 0.6g of TAMP into the chamber of the BET which was evacuated and heated to 150°C to remove moisture before analysis [14]. Additionally, mercury porosimetry was performed by Micromerictics' AutoPore IV 9500 to confirm the macropore size. After sintering, the samples were sanded to produce a smooth surface and then autoclaved to ensure sterility for cell culture testing. Before cells were seeded onto the TAMPs, the scaffolds were pre-incubated in phosphate buffered saline (PBS) for 3 days to allow for complete hydration and formation of hydroxyapatite.

1.6 - Conclusion

While the logic behind the design and preparation of the TAMP scaffolds has been explained above, the goals of my dissertation are to characterize cell-substrate interactions on a fundamental level by exploring how surface topology affects protein adsorption and cellular response. This knowledge may then be utilized to design materials for regeneration of different tissues. To achieve these goals, I characterized the scaffolds on a biological level, including: an in-depth characterization of cellular response on the mRNA and protein level (Chapter 2), I investigated how cells are able to sense and respond to the topology of the scaffold (Chapter 3), and I explored the utility of scaffolds for tissue regeneration and other tissue engineering purposes (Chapters 2 and 4).

1.7 - Figures

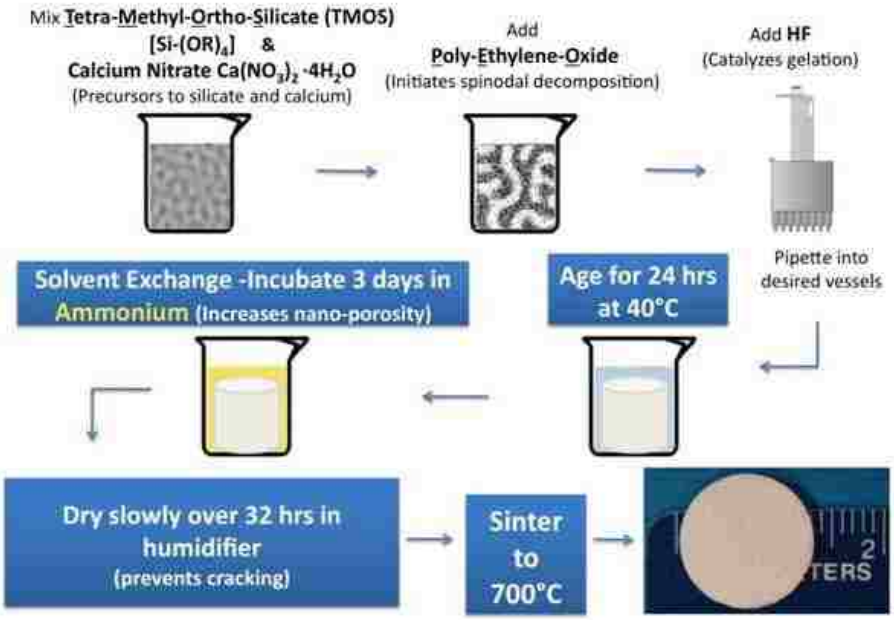

Figure 1: TAMP scaffolds produced using a novel sol-gel method

This scheme outlines how the sol-gel process is used for fabrication of TAMP scaffolds. Precursors, TMOS and $Ca(NO_3)^2$, are mixed together with PEO, the polymer that forms macropores. HF is added to this sol to start the gelification process before pipetting the sol into a vessel that defines the glass shape. The glass ages at 40°C before ammonium is added for the solvent exchange process. Finally the glass is dried in a controlled humidity environment to prevent cracking and sintered to strengthen the structure.

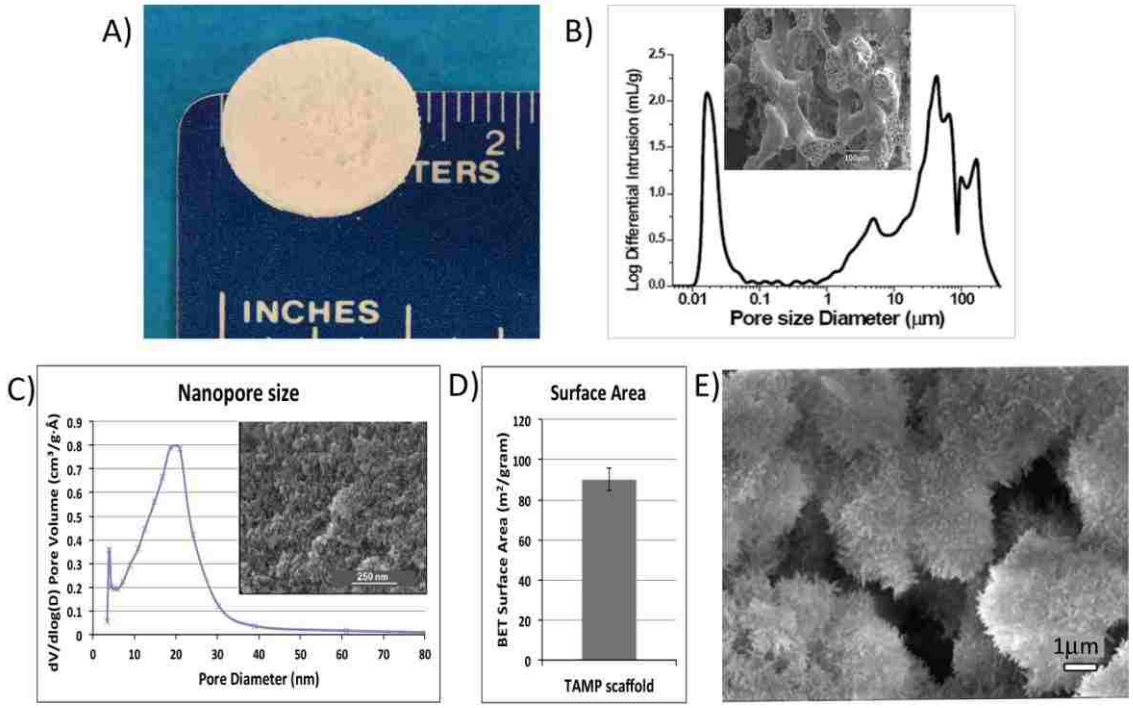

Figure 2: TAMP scaffolds contain the necessary features for a tissue regenerative scaffold

As the product of a novel sol-gel process, highly porous TAMP scaffolds are 1.3cm diameter opaque discs (A). By SEM analysis, the highly porous structure of the TAMP scaffolds can be observed including macropores (B) and nanopores (C). The macropores range in size from 20-200mm as measured by mercury porosimetry [10, 11] (B) while nanopores range from 2.5-20nm as measured by BET nitrogen adsorption (C). Also measured by BET is surface area which is approximately 90.2 ±5.5m^2/gram (E), and a layer of hydroxyapatite (HA) forms on the surface after incubation in physiological fluids such as simulated body fluid as observed by SEM [10]

Chapter 2- Characterization of osteoblast and osteoclast response to TAMP bioactive glass scaffolds

(Kowal et. al. 2017 – in preparation)

2.1 - Abstract

Tissue regeneration is a significantly improved alternative to tissue replacement and requires porous bioscaffolds for the restoration of natural tissue rather than relying on bio-inactive, often metallic implants. Recently, we have developed technology for fabricating novel, nano-macroporous bioactive 'Tailored Amorphous Multi-Porous scaffolds' (TAMPs) using a 70 mol% SiO_2-30 mol% CaO model composition. The TAMPs are fabricated by a modified sol-gel process, and have shown excellent biocompatibility via the rapid formation of hydroxyapatite in simulated body fluid as well as in early tests with bone forming cells. Our results from imaging, gene expression, protein expression, and enzyme activity analyses demonstrate that MC3T3-E1 pre-osteoblast cells adhere, proliferate, colonize, and differentiate on and inside the bioactive TAMP scaffolds. Additionally, BMD precursor cells matured into active osteoclasts highlighting the exceptional qualities of this novel scaffold material for bone tissue regeneration.

2.2 - Introduction

The word “scaffold” implies that the framework in future no longer will be needed to support the newly generated structure; however, most if not all traditional implant materials violate this definition as they remain in the body over time. In contrast, bioactive glass ceramics have been shown to dissolve over time in biological fluids and when implanted, especially (1) when the material is highly porous allowing cells to colonize the scaffolds, and (2) when reactive surface area is increased and fluid exchange is enhanced by superimposed interconnected nanoporosity as is the case in our TAMP scaffolds [9-11]. Moreover, ions leaching from the dissolving bioactive glass have been reported to behave osteogenically, by stimulating the differentiation of osteoblast precursors into mature calcified matrix producing osteoblasts [15-17]. We have previously reported on the enhanced bioactivity of porous, sol-gel derived TAMP scaffolds [9-11], however a careful analysis of the biological performance of this material using advanced in vitro proliferation and differentiation assays has not been performed.

In contrast to studies performed by others in which bioactive glass performance was judged by adding conditioned medium (medium exposed to glass) to cells [15-17], we seeded cells directly onto TAMP scaffolds. Enzymatic, RNA, and protein analyses demonstrate that cells quickly and robustly attach to TAMP through the formation of focal adhesions and that MC3T3-E1 cells differentiate into mature bone producing osteoblasts. Additionally, bone marrow derived (BMD) precursor cells were found to differentiate into active osteoclasts (bone degrading cells) supporting the extraordinary qualities of this novel bioactive material for bone tissue regeneration.

2.3 - Results

2.3.1 - Pre-osteoblast cells adhere to the surface of TAMP scaffolds

TAMP scaffolds opaqueness due to porosity (Figure 2A) interferes with simple detection of cells growing on the scaffold surface by standard transmission light

microscopy. Instead, scanning electron microscopic (SEM) analyses were preformed (Figure 3A). In addition, to determine whether cells were forming stable cell adhesions when growing on the scaffolds, cells were fluorescently stained for actin (Alexa488-labeled phalloidin, green), chromatin (cell nuclei, DAPI, blue), and vinculin (using anti-vinculin specific and Alexa568-labeled secondary antibodies, red), a protein component of focal adhesion complexes responsible for forming cellular attachments to substrates (Figure 3B). One hour post seeding MC3T3-E1 pre-osteoblasts onto the scaffolds, cells remained largely rounded, however had attached to the scaffold surface as indicated by the formation of numerous filopodial anchoring extensions (Figure 3A, 1 hour, depicted with white arrows). Additionally, actin remained diffuse and located cortically as indicated by the brighter staining at the cell periphery as is typical for not yet well-attached cells stained shortly after cell seeding (Figure 3B, top panel). Vinculin was visible after 1 hour mainly as a soluble cytoplasmic pool as is typical for vinculin that is not bound to focal adhesions [18]. After 2 (Figure 3A, B, second row) and especially after 8 hours post seeding (Figure 3A, B, third row), cells were spreading acquiring their typical flat morphology including numerous lamellipodial extensions. Actin began to form distinct stress fibers as indicated by the filamentous staining pattern (Figure 3B, third row, yellow arrows). After 3 days, a dense layer of cells, partially growing on top of each other featuring numerous filopodial and lamellipodial extensions were observed by SEM analyses (Figure 3A, bottom row), and pronounced focal adhesion complexes formed at the tip of robust actin stress fibers as is typical of cells growing on stiff substrates [19-21] (Figure 3B, bottom row, orange arrows) indicating that cells had established healthy attachments to the surface of the TAMP scaffold material. Consistent with these data, cells could not easily be removed even after extended exposure to trypsin, a protease commonly used to release MC3T3-E1 and other cell types from tissue culture plates, suggesting that the cells attach robustly to TAMP scaffolds or that trypsin activity may in some way be blocked. Average surface area per cell was quantitated for 30-40 cells/time point using the outline function of Image J software package (Figure 3C) and showed that cells were indeed spreading over time. Note the relatively large standard

deviations that are due to the 3D nature of the TAMP scaffolds that allows cells to grow in many different angles in relation to the image plane.

2.3.2 - MC3T3-E1 cells colonize the inside of TAMP scaffolds.

As analyses by SEM showed that: (1) cells covered the majority of the scaffold surface after 8 hours (Figure 4A, top panel) and 3 days post seeding (Figure 4A, bottom panel), (2) cells continued to proliferate to form a dense monolayer on the TAMP scaffold surface (Figure 5, days 10 and 21), and (3) cells were growing at the entrance of macro-pores (Figure 4A), we investigated whether MC3T3-E1 cells would also colonize the TAMP scaffold interior. Cells were seeded onto the TAMP scaffolds and fixed 10 days post seeding, then a center section was cut out, turned on its side and mounted (Figure 6). SEM analyses of these cross-sections showed cells growing inside the TAMP scaffolds indicating that cells had migrated into the macro-pores and were also colonizing the inside (Figure 4B).

Next we wanted to determine the rate of cell proliferation on TAMP scaffolds. To do this, we needed to find a technique that allowed us to accurately determine the number of cells on and inside the scaffolds at progressive time points. Imaging would not capture cells inside the scaffolds, and proteins from cell culture medium, e.g. bovine serum albumin (BSA, MW: 66kDa), an abundant serum component of fetal bovine serum, robustly absorbed to TAMP scaffolds (Figure 7, marked with arrow) and interfered with standard quantitative colorimetric protein assays such as Bradford and MTS. We instead detected and quantified the levels of a constitutively expressed housekeeping protein, α-adaptin (a component of the endocytic adaptor protein 2 (AP-2) [22] complex) by Western blot using α-adaptin specific antibodies (Figure 4C). The large molecular weight of α-adaptin (MW: 112kDa) allowed for its accurate detection and quantification, as the detection and resolution of smaller, standardly used house-keeping proteins such as actin, tubulin, and GAPDH, which migrate faster on SDS-PAGE gels than BSA was impeded (Figure 7). Based on these analyses, we found that MC3T3-E1 cells proliferating on TAMP scaffolds entered the logarithmic growth phase of

proliferation by approximately day 2 and growth slowed to reach a plateau at approximately day 10 (Figure 4D). Logarithmic growth resulted in a duplication time of app. 3 days under standard cell culture conditions, slower than proliferation on tissue culture plastic (app. 38 hours (ATCC)), with one possible explanation for this being that cells are differentiating (see below).

2.3.3 - MC3T3-E1 cells differentiate into mature osteoblasts when grown on TAMP scaffolds : quantitative transcription analyses

To assess whether MC3T3-E1 pre-osteoblasts differentiate into mature osteoblasts we quantitatively analyzed transcription of osteoblast differentiation-related genes (including genes related to (1) cell adhesion [orange], (2) extracellular matrix and remodeling [light blue], (3) proliferation [olive], (4) differentiation [grey], (5) collagen expression [off red], (6) bone specific transcription regulation [yellow], and (7) expression of osteoblast calcified matrix-specific proteins [purple]) by quantitative PCR analyses (qRT-PCR) using a commercially available 84-gene bone differentiation array (SA-Biosciences, Qiagen) supplemented by a few additional well-known bone cell marker proteins (osteocalcin, osteopontin, Figure 8A). Genes that were not evaluated because they showed unrealistically high up-regulation profiles, did not obviously fall into one of the above described categories, their relation to bone-cell differentiation remains unclear, or their expression pattern remained unchanged are shown in white.

RNA was isolated, quantified, and normalized on days 1, 7, 14, and 26 post seeding cells onto the scaffolds. We found that representative genes were either up (Figure 8A, labeled red) or down regulated (Figure 8A, labeled green), or that their expression remained unchanged (Figure 8A, grey). The gene expression profiles of differentiating MC3T3-E1 cells has been well characterized [23-25] and the overall trends in gene expression observed here are consistent with MC3T3-E1 pre-osteoblast cells attaching to their substrate, proliferating, and differentiating into mature, calcified matrix secreting osteoblasts. For example, the overall trend in gene expression for cell adhesion proteins (Figure 8B-1, black polynomial average line indicates functional group

trend) such as those encoding integrins (Itgam, Itga3, Itgb1, and Itga2b) was initially high post seeding and down regulated over time indicating that cells were expressing genes necessary to make initial attachments to the TAMP surface. Additionally, secreted extracellular matrix and matrix remodeling proteins such as fibronectin (Fn1), biglycan (bgn), Serpin h1 peptidase inhibitor (Serpinh1), and matrix metalloproteases (Mmp9 & Mmp2) (Figure 8B-2) were up regulated at day 1. In addition, several growth factors related to proliferation are more highly expressed on day 1 with down regulation overtime (Figure 8B-3) such as Tgfb1, Vegfa, Fgf2, Pdgfa, egf, vegfb; whereas other growth factors related to differentiation of MC3T3-E1 cells (Figure 8B-4) are expressed consistently, for example, Nfkb1, Fgf2, Tgfb3, Tgfbr2, Tgfbr3, Tfgb2, BMP1, BMP4 suggesting that cells may stop proliferating to differentiate. The two main transcription factors for bone cell differentiation are both up regulated early, with Sox9 elevated at day 1 and RunX2 elevated at day 7 (Figure 8B-5). Collagens were upregulated both early and late (Figure 8B-6). Finally, alkaline phosphatase (ALP), an enzyme that is up regulated during differentiation into mature osteoblasts was up regulated early on the mRNA level (Figure 8A). Osteocalcin (OCN) and osteopontin (OPN), both late indicators of bone cell differentiation, were up regulated as expected at later time points (Figure 8B-7). Taken together, these quantitative RNA expression analyses indicate that MC3T3-E1 cells express genes necessary for cellular adhesion, proliferation, and differentiation into mature osteoblasts when grown for 4 weeks on TAMP scaffolds.

2.3.4 - MC3T3-E1 cells differentiate into mature osteoblasts when grown on TAMP scaffolds – protein level

Alkaline phosphatase (ALP) expression and activity is a canonical indicator of osteoblast differentiation and is known to be up regulated during osteoblast differentiation [26, 27]. Increased expression of the ALP gene in MC3T3-E1 cells growing on TAMP scaffolds was observed and described above (Figure 9A, B). Consistent with these data, colorimetrically assessed enzymatic ALP activity increased almost three-fold from day 3 to day 21 (Figure 9A). These data are also in agreement with the decreased proliferation rate of MC3T3-E1 cells grown for 3-4 weeks on TAMP

scaffolds (Figure 7C) as cell proliferation and differentiation are known to be cross-correlated [28].

Mature osteoblasts are also known to express and secrete proteins such as osteocalcin (OCN) and osteopontin [OPN] that aid in the formation of secreted calcified bone-specific extracellular matrix. To verify that the observed up regulation of mRNA expression for OCN and OPN was also detectable as an up regulation in protein expression, we used specific antibodies and immunofluorescence microscopic analyses to examine OCN and OPN protein expression of MC3T3-E1 cells growing on TAMP scaffolds over time (Figure 9B, C). OCN staining on day 3 presented as a diffuse perinuclear staining, whereas staining on day 10 resulted in both, diffuse perinuclear staining and some defined puncta localized in the cytoplasm and/or extracellular matrix that increased in number and size by days 16 and 32, while diffuse cellular staining diminished (Figure 9B, labeled with arrows). Since OCN is a late differentiation marker, its expression/staining pattern is consistent with the expected and previously observed late mRNA up regulation of this secreted protein. OPN is another late up regulated, bone-specific matrix protein. Consistently, only diffuse OPN staining was observed on days 3, 10, and 16 (Figure 9C), that either indicates early cytoplasmic expression similar to the expression profile observed for OPN, or unspecific background staining (Figure 10). In contrast, a prominent punctate OPN stain comparable to the late OCN stain was detected on day 32 (Figure 9C, labeled with arrows), suggesting a robust OPN expression of MC3T3-E1 cells growing on TAMP scaffolds at later time points. Taken together, these quantitative and qualitative marker protein expression analyses reiterate that MC3T3-E1 cells appear to differentiate into mature osteoblasts when growing on TAMP scaffolds.

2.3.5 - TAMP scaffolds support growth of a co-culture of osteoblasts and osteoclasts

Since bone is a highly dynamic organ that is constantly remodeled by synthesis and degradation (via osteoblasts and osteoclasts, respectively) [29], we wanted to test whether TAMP scaffolds also support the growth of osteoclasts and whether co-culture of osteoblasts and osteoclasts would remodel TAMP scaffolds similarly to natural bone.

Osteoclasts feature a number of morphological characteristics including a very large cell size, multiple cell nuclei, relatively large vesicular inclusions, and a sealing zone composed of actin and vinculin. Because osteoclasts mature via the fusion of several precursor cells and thus contain multiple cell nuclei, they no longer proliferate making it necessary to differentiate these cells from their precursors located in bone marrow. Bone marrow was extracted from rat long bones and bone marrow derived (BMD) cells corresponding to ½ bone were mixed and grown together with 200,000 MC3T3-E1 cells. Co-cultures were maintained in complete α-MEM culture medium supplemented with macrophage colony stimulating factor (MCSF) to promote the survival and differentiation of the osteoclast precursor cells (reviewed in:[30-32]). MC3T3-E1 cells are known to enhance osteoclastogenesis [33, 34] through secretion of receptor activator of nuclear factor kappa-B ligand (RANKL), the main cytokine that regulates osteoclast differentiation and activation [30-32]. After 10 days of co-culture on microscopic cover slips, mature osteoclasts were clearly recognizable based on the above described morphological features by both Differential Interference Contrast (DIC) as well as fluorescent images (after staining nuclear chromatin and actin) (Figure 11A). Remarkably, co-culturing these cells for 10 days on TAMP scaffolds resulted in the formation of a complex bone-like tissue structure that consisted of a dense network of MC3T3-E1 osteoblasts recognizable by their small size, and interspersed osteoclasts recognizable by their large size, multiple cell nuclei, and their typical actin-based sealing zones (Figure 11B, labeled with OC and outlined with dashed lines). Single channel black and white images of actin (Figure 11B, top) and DAPI (cell nuclei, Figure 11B, bottom) further supported these distinctive osteoclast features (depicted with arrows). Quantitative analyses revealed a ratio of 179+/-53 osteoblasts per osteoclast, a ratio similar to the ratio of these two cell types in human iliac crest bone [35] (Figure 11C).

To further support our conclusion that the large multi-nucleated cells indeed represented osteoclasts, we treated co-cultured TAMP scaffolds with Cellstripper (Corning), a proprietary mixture of chelators that gradually removes cells according to their size/adhesion strength, followed by staining remaining cells for actin, vinculin and chromatin (Figure 11C). Osteoblasts/osteoclasts co-cultured in control on cover glasses

were analyzed in parallel. As expected, treating TAMP scaffolds with Cellstripper removed the small-sized/less adherent osteoblasts, while large-sized/strongly adherent osteoclasts remained on the scaffolds. Vinculin (red) and actin (green) robustly colocalized in the sealing zones resulting in yellow, the overlay color of red and green as typical for osteoclasts (Figure 11C, depicted with arrows).

Finally, to test whether osteoclasts are active when grown on TAMP scaffolds, we stained osteoclasts with antibodies specific for tartrate resistant acid phosphatase (TRAP). TRAP is an enzyme found in active osteoclasts that aids in the degradation of of the bone matrix by dephosphorylating bone matrix phosphoproteins such as osteopontin [36-38]. In immunofluorescence images, TRAP (green) was detected as a diffuse as well as punctate, perinuclear stain (Figure 11D). A similar staining pattern was observed on coverslips with TRAP being present in addition at the sealing zone of cells (Figure 11D, panel i). The positive TRAP staining of osteoclasts co-cultured on TAMP scaffolds correlated with the enzymatic detection of TRAP activity that was demonstrated using a colorimetric acid phosphatase kit (Sigma). The assay utilizes the TRAP substrate Naphthol AS-BI, which on hydrolysis couples with fast garnet GBC to form an insoluble pink product. The presence of tartrate in the staining solution renders all other acid phosphatases inactive making the stain specific to only TRAP positive cells [39-41]. A strong pink staining of the co-cultured TAMP scaffold was detected, clearly indicating robust TRAP enzyme activity (Figure 12A, panel 1 and quantified in B). No pink product was detected on control scaffolds seeded with MC3T3-E1 cells only, or scaffolds not seeded with cells (Figure 12A, panels 2 and 3, B). Samples were counter-stained with DAPI to verify the presence of cells on scaffolds i and ii. No cells were detected on scaffold iii (Figure 12A, inserts, top left). Pink scaffold color intensity in 3 independent experiments was measured quantitatively comparing pixel intensities using ImageJ image analyses software. Taken together these analyses convincingly demonstrated that TAMP scaffolds support the growth of robustly TRAP-producing osteoclasts suggesting the active remodeling of TAMP scaffolds under osteoblast/osteoclast co-culture conditions, similarly to the dynamic remodeling of normal bone occurring in situ.

2.4 - Discussion

Tissue regeneration using bioactive materials has many advantages over replacing tissue with inert, non-biological materials. 45S5 Bioglass® has been found to provide such bioactivity [8]. and its application in e.g. bone regeneration is well established [42]. However, Bioglass® is a solid material and allows cells to bond to its surface only. Here, we demonstrate by performing a comprehensive biological characterization utilizing bone cells growing directly on the scaffolds, that next-generation TAMP ceramics due to their high rate of interconnected macro and nanoporosity overcome these limitations. TAMP bioscaffolds exhibit superior qualities for e.g. bone regeneration that include cell bonding and penetration, cell differentiation, and scaffold remodeling by co-cultured osteoblasts and osteoclasts. Osteoblasts are the main, calcified matrix-secreting cell type in bone. Comprehensive SEM and immunofluorescence analyses show that MC3T3-E1 pre-osteoblast cells rapidly attach to TAMP scaffolds (within 1 hour) and quickly spread out on the surface and inside the TAMP scaffolds. The formation of distinct actin stress fibers and robust focal adhesions are indicative of cells forming stable attachments to this stiff substrate [21, 19]. Cell proliferation analyses based on a quantitative Western blot-based assay revealed a cell-duplication time of approximately 3 days, somewhat slower than the 38 hours reported by ATCC for these cells. As cell proliferation is known to be inversely coupled to cell differentiation [43, 25] a slower proliferation rate observed for MC3T3-E1 cells growing on/in TAMP scaffolds thus may support cell differentiation (as detailed below). Additionally, ions known to leach from TAMP and other sol-gel derived bioactive glass materials have been found to be osteoinductive and to induce osteoblast precursor cells to differentiate [44, 16, 15], potentially further contributing to the differentiation of pre-osteoblasts growing on TAMP scaffolds.

As cell differentiation involves the specific up- and down-regulation of many different proteins, we performed quantitative mRNA-based RT-PCR analyses of MC3T3-E1 cells growing for 1, 7, 14, and 26 days on TAMP scaffolds using an oligonucleotide array probing 84 different bone cell-specific proteins (SABioscience). For example, we found that integrins and growth factors were up-regulated early supporting our previous findings that MC3T3-E1 cells attached to, and proliferated on the TAMP scaffolds. These

findings are consistent with an earlier study performed by Xynos et al., who reported that human osteoblasts treated with conditioned cell culture medium (medium exposed to bioactive glass for some time, consequently containing the ionic dissolution products of the glass material) exhibited up-regulation of proliferative factors and of other genes responsible for cell attachment [15]. Furthermore, we observed the up-regulation of distinct collagens, such as Collagen 1a1, indicating bone cell differentiation. MC3T3-E1 cell differentiation is further supported by the regulated expression of bone cell differentiation specific transcription factors. We found that Sox9 expression is high early, then drops as RunX2 expression increases. This is expected, since it is known that Sox9 expression must decrease to allow for RunX2 expression to increase and differentiation to occur [45]. Expression of bone-specific secreted extracellular matrix proteins indicative of osteoblast differentiation (OPN and OCN) was up-regulated as well. These data are corroborated by studies done by others [17, 16, 15, 46], although several experimental differences including the use of cell types, time points of analyses, glass compositions, and most importantly, the use of conditioned medium in all other studies compared to growing and analyzing cells directly on TAMP scaffolds.

Differentiation of MC3T3-E1 pre-osteoblasts when growing on TAMP scaffolds was further supported when analyzing differentiation markers on protein level. ALP enzyme activity was observed to continuously increase over time with a steeper increase towards longer time points (days 17, 21), correlating with observed reduced proliferation rates at these later times. Upregulation of ALP activity correlates with data reported by Christodoulou et. al., who observed from day 7 to 14 a 4- to 8-fold increase in ALP activity of fetal osteoblasts exposed to low or high concentrations of bioactive glass conditioned medium respectively [17]. OCN and OPN, proteins known to be secreted by mature osteoblasts into the extracellular calcified matrix [47-49], were detected by immunofluorescence staining as well. OCN was first detected as diffuse and perinuclear punctate labeling that later matured into larger, more distantly located puncta. These results are consistent with Filova et al. who observed a punctate perinuclear stain of OCN in differentiating MG63 cells grown on hydroxyapatite [50]. Interestingly, punctate OPN was detected only at later time points (day 32) consistent with reports by Przybylowki et

al., Ruckh et al., and Tsutsumi et al. [51-53], who also detected osteopontin at late time points as a punctate golgi-like stain. Taken together, our analyses strongly suggest MC3T3-E1 pre-osteoblastic cells differentiate into mature bone-producing osteoblasts when cultivated on TAMP scaffolds.

Bone, however not only consists of osteoblasts but also of several distinct other cell types that interact to maintain strong and healthy bone, as well as a sufficient amount of calcium in the blood [54]. Indeed, bone is remodeled continually, it is built by osteoblasts and degraded by osteoclasts (reviewed in [55, 56, 30, 57]. Osteoclasts generally have 3-20 cell nuclei [58], indicating that e,g, 12 precursor cells may fuse to form a single osteoclast [59]. Typically these cells are very large, ranging from 100 – 200 µm in diameter (but may be much larger in vitro) and characteristically form a sealing zone of actin and vinculin around the periphery of the cell [55, 56, 30, 32, 60]. This sealing zone provides a contained, low pH environment necessary for the activity of secreted enzymes that degrade the bone matrix. Osteoclasts are clearly distinguishable from other cells based on these unique morphological features.

To mimic the natural in situ environment, we co-cultured MC3T3-E1 pre-osteoblasts together with bone marrow derived (BMD) hematopoietic stem cells that we isolated and differentiated in vitro resulting in a ratio of 179+/-53, similar to ratios reported in humans [35]. Osteoclast identity was confirmed via their typical morphological features that were apparent in white-light microscopic images as well as by immunofluorescent labeling (actin, vinculin, and cell nuclei). Remarkably, the co-cultured osteoblastic and osteoclastic cells formed a complex tissue-like structure when cultured on TAMP scaffolds. . In order to degrade calcified bone structure, osteoclasts produce specific enzymes, e.g. tartrate resistant acid phosphatase (TRAP), that are secreted into the resorption lacunae, a compartment formed basally between the bone surface, sealing zone, and ruffled boarder (a specialized invaginated membrane that resembles late endosomal membrane that serves to secrete substances required for degradation and resorption of the bone matrix) [55, 61]. Once proteins have been degraded, they are resorbed into the osteoclasts and follow a transcytotic pathway until they are secreted into the extracellular space at the apical side of the cell. TRAP has been

described to be secreted, but to also localize to these transcytotic vesicles to further degrade collagen before secretion to the extracellular space [62, 32]. Using immunofluorescence detection of TRAP, these vesicles were observed in osteoclasts co-cultured on TAMP scaffolds. TRAP biosynthesis and secretion indicates that the osteoclasts actively degraded TAMP scaffold matrix, while osteoblasts secreted bone matrix, suggesting active remodeling of the scaffold material. Our findings are consistent with results by Yamada et al., Detsch et al., and Monchau et al. [63-65], who showed that osteoclasts degraded hydroxyapatite in vitro. TRAP biosynthesis and secretion indicates that the osteoclasts actively degraded TAMP scaffold matrix, while osteoblasts secreted bone matrix, suggesting active remodeling of the scaffold material.

2.5 - Conclusion

Here we show for the first time that MC3T3-E1 pre-osteoblasts attach, proliferate and differentiate into mature, calcified matrix secreting osteoblasts, and BMD cells differentiate into active, TRAP secreting osteoclasts when cultured on TAMP scaffolds, indicating that this bioactive glass material can mimic the dynamic remodeling activities that are required for successful bone growth and repair. Our in vitro results are supported by results obtained in situ using subcutaneous rabbit skin and human mandible implant studies [66, 9]. As TAMP scaffold chemistry and porosity are easily "tailored", modifications in the chemical composition promise that TAMP scaffolds will meet the many challenging specifics of various bone regeneration applications.

2.6 – Materials and Methods

2.6.1 – Osteoblasts culture on TAMP scaffolds

MC3T3-E1 subclone 4 mouse pre-osteoblast cells (CRL-2593) were purchased from American Type Culture Collection (ATCC, Manassas,VA). Cells were maintained using standard culture conditions at 37°C in a 5% CO2 atmosphere and 100% humidity in alpha-Modified Eagles Medium without ascorbic acid (α-MEM, Gibco/Invitrogen, Grand Island, NY, Cat. No. A10490-01) supplemented with 10% fetal bovine serum

(Atlanta Biologicals, Flowery Branch, GA Cat. No. S11150), 1% L-glutamine (HyClone, Logan, UT Cat. No. 25-005-C1) and 1% penicillin/streptomycin (Corning, Corning, NY Cat. No.30-001-Cl). MC3T3-E1 cells were counted using a hemocytometer and seeded onto the TAMP glass disks placed into either 3.5cm diameter or 24-well polystyrene tissue culture plates (Genesee, San Diego, CA Cat. #25-107) at a density of 30,000 cells/cm2.

2.6.2 - Osteoclasts / osteoblasts co-culture on TAMP scaffolds

Osteoclasts were derived from bone marrow collected from the long bones of SAS Sprague Dawley wild type rats. Rats were anesthetized with isoflurane and euthanized in accordance with federal animal welfare guidelines and protocols reviewed and approved by the Lehigh Institutional Animal Care and use Committee (IACUC). Long bones were isolated and both ends of the bones were cut off. After transferring the bones to 1.5ml eppendorff tubes, they were centrifuged at 2000 rpm for 15 seconds to extract the marrow (modified from [67]). Bone marrow derived (BMD) cells were seeded onto either glass coverslips or TAMP scaffolds with the addition of MC3T3-E1 cells. Approximately 400,000 MC3T3-E1 cells were seeded for every bones worth of BMD cells seeded. The co-cultures were maintained in complete α-MEM as described above for osteoblasts with the addition of 50ng/ml Macrophage Colony Stimulating Factor (MCSF) (Prospec, Israel, Cat. # cyt-046) to promote survival of the osteoclast precursor cells. In order to allow for better imaging of osteoclasts, most other cells from the co-culture were removed by incubation with Cellstripper® (Corning, Inc, Corning, NY, Cat. # 25-056-CI) using the following procedure. Medium was removed and each sample was washed with PBS. Cell stripper was added to the dish and incubated for 10 min. at 37°C. The Cellstripper® solution was pipetted aggressively over the sample to ensure the removal of unwanted cells was complete. The samples now containing only osteoclasts were fixed for visualization by immunofluorescence detection as described below. The ratio of osteoblasts to osteoclasts was estimated by counting the number of nuclei not found in an osteoclast as determined by DAPI and Alexa488-phallodin staining.

2.6.3 - Scanning Electron Microscopy (SEM) detection

Cells were fixed in 4% gluteraldehye at 4°C overnight followed by incubation in a series of ethanol dilutions (35%, 35%, 60% - 10 min each, 80%, 90%, 100% ethanol – 15 min each). Finally samples were incubated for 10 min in hexamethyldisilazane (HMDS; Sigma, St. Louis, MI, cat. # 52619) to ensure the removal of moisture was complete [3]. Samples were stored in a desiccator until analysis. Just before examination by SEM, the samples were sputter coated with iridium using a turbo pumped sputter coater (Electron Microscopy Sciences – EMS575X) for 1min to prevent charging. A Hitachi 4300 FEGSEM was used to image samples using secondary electron collection mode and 5.0kV accelerating voltage.

2.6.4 - Determining cell proliferation on TAMP scaffolds

MC3T3-E1 cells were seeded onto TAMP scaffolds as described above. To quantitatively obtain accurate cell numbers, a constitutively expressed protein, α-adaptin (MW, 112kDa, mouse monoclonal, BD. Biosciences, San Jose, CA, Cat. # 610501) was analyzed by Western blot. To collect the samples to be analyzed, the TAMP scaffolds were crushed in 4x sample buffer, boiled for 5 min, centrifuged to pellet the scaffold debris, and the supernatants were loaded onto a 10% SDS-PAGE gel. Gels were electrophoresed at 120V for 90 min followed by transfer to nitrocellulose membranes for 90 min at 120V on ice. After transfer, the membranes were blocked in 5% fat free dry milk solution prepared in TBST (TBS with 1% Tween) for 1 hr at room temperature, rinsed briefly with TBS to remove excess blocking solution, and probed with primary antibody (1:2,000 dilution in 5% BSA solution) overnight at 4°C. The membranes were incubated with HRP conjugated goat-anti-mouse secondary antibody (1:5,000 – Life Technologies, Eugene, OR. Cat. # G21040) at room temperature for 1 hr, and protein was detected using X-ray film and Enhanced Chemiluminescent (ECL) reagent. Densitometry was performed using ImageJ. The number of cells per TAMP scaffold

(n=4) was calculated by generating a standard curve of α-adaptin using a Western blot sample with a known number of cells (1 million MC3T3-E1 cells).

2.6.5 - Immunofluorescent staining of cells on TAMP scaffolds

Cells were processed for analysis by fluorescence detection of nuclei by incubating in DAPI (Molecular Probes, Eugen, OR, Cat. # D1306), actin using Alexa488 (or Alexa568)-phalloidin (Molecular Probes, Grand Island, Ny, Cat. # A-12379), and specific proteins by immuno-staining for vinculin (mouse monoclonal-Sigma, St. Louis, MO, Cat. # V9131), osteopontin (rabbit polyclonal – AnaSpec, Fremont, CA, Cat. # 55455), osteocalcin (rabbit polyclonal – Abbiotec, San Diego, CA Cat. # 250483), and TRAP (goat polyclonal -Santa Cruz, Dallas, TX Cat. # sc-30833). In brief, cells were fixed using 3.7% formaldehyde followed by permeabilization with 0.2% Triton X-100 for staining with the vinculin, osteocalcin, and TRAP antibodies. Alternatively cells were fixed and permeabilized using ice cold ethanol for osteopontin staining. Cells were then blocked in 5% BSA/PBS at room temperature overnight. The primary antibodies were diluted in blocking solution to 1:200 and incubated with cells at room temperature for 1 hr. Blocking solution containing DAPI (1µg/ml), Alexa488-phalloidin (1:100) and secondary antibody (1:200) Alexa568-conjugated goat-anti-mouse (Molecular Probes/Invitrogen, Grand Island, NY, Cat. # A11031) for vinculin, Alexa568-phalloidin (1:100) and secondary antibody (1:200) Alexa488-conjugated donkey-anti-goat (Molecular Probes/Invitrogen, Grand Island, NY, Cat. # A11055) for TRAP, and Alexa488-conjugated goat-anti-rabbit (Molecular Probes/Invitrogen, Grand Island, NY, Cat. # A11008) for osteopontin and osteocalcin was incubated with the cells at room temperature for 1 hr. Samples were imaged by submersing the scaffolds in PBS on a glass bottom 3.5cm tissue culture plate with the side on which cells were seeded facing the glass bottom. Imaging was performed using a Nikon Eclipse TE2000-E inverted fluorescence microscope equipped with 10x air, 20x air, 40x oil and a forced-air cooled Photometrics CoolSnap HQ CCD camera (Roper Scientific, Martinsried, Germany).

Images were captured using MetaVue (Molecular Devices, Sunnyvale, CA) software version 6.1r5.

2.6.6 - qRT-PCR analysis of cells grown on TAMP scaffolds

MC3T3-E1 cells were seeded onto TAMP scaffolds and grown for 1, 7, 16, and 32 days before collection of RNA using either Arcturus® Picopure RNA isolation kit (Applied Biosystems, Carlsbad, CA Cat # Kit0204) or Qiagen RNeasy mini kit (Qiagen, Valencia, CA, Cat. # 74104). cDNA was synthesized from these samples using SuperScript III First-strand synthesis (ThermoFisher, Carlsbad, CA, Cat # 18080-051). Analysis of these samples was performed using either Osteogeneisis PCR array (SABiosciences, Frederick, MD, Cat # PAMM-026Z) and RT^2 Real-time SYBR green PCR master mix (SABiosciences, Frederick, MD, PA-012-12) on a model 7300 Thermocycler (Applied Biosystems), or SYBRgreen-Rotorgene PCR kit (Qiagen, Valencia, CA, Cat. # 204074) and sets of custom-designed oligonucleotides (Integrated DNA Technologies, Coralville, IA) that corresponded to the mRNAs encoding the relevant proteins on a Rotor-gene real-time PCR cycler. GAPDH was analyzed in parallel and used as expression reference. Fluorescence signal detection within 35 PCR cycles was considered significant. mRNA level fold-change was normalized against GAPDH expression and compared to day 0.

2.6.7 - Alkaline phosphatase (ALP) activity assay

MC3T3-E1 cells were grown on TAMP scaffolds and samples were collected for ALP activity analysis on days 3, 7, 11, 14, and 21. Samples were prepared by washing in TBS followed by incubation in 500µl lysis buffer (TBS, 0.5% SDS, and protease inhibitor cocktail (1:100), Sigma, Cat. # P8340) with agitation for 15 minutes on ice. 20µl of cell lysate was mixed with 20µl of 2x sample buffer and boiled for determination of cell number as described above. ALP activity was quantitatively detected using a

colorimetric Quantichrom ALP detection kit (BioAssay Systems, Hayward, CA, Cat. # DALP-250). Briefly, 50µl of cell lysate was incubated with 150 µl of ALP buffer (containing 10 mM p-nitrophenol phosphate (pNPP) and 5 mM MgAcetate) per reaction at room temperature for 1 hr. The activity of ALP was determined by measuring the absorbance at 405nm using a Tecan Infinite M200 PRO plate reader spectrophotometer. ALP activity was normalized to cell number as determined by Western blot detection of α-adaptin (n=4).

2.6.8 - TRAP staining of osteoclasts grown on TAMP scaffolds

A co-culture of MC3T3-E1 and BMD cells were grown on TAMP scaffolds in parallel to TAMP scaffolds containing only MC3T3-E1 cells for 10 days as described above. Next, the samples were fixed in 3.7% formaldehyde, stained with DAPI and imaged. The same samples were then stained for TRAP activity using an Acid Phosphatase, Leukocyte (TRAP) Kit (Sigma, St. Loius, MO, Cat. # 387A-1KT). In brief, scaffolds were incubated for 1 hr in staining solution, which contained tartrate to render all other phosphatases inactive and the substrate Naphthol AS-BI, which couples with fast garnet GBC on enzymatic hydrolysis to form a pink insoluble product. The samples were washed 3 times in dH_2O following staining and imaged at 4x using a Nikon SMZ1500 dissection scope equipped with an HR plan Apo 1x WD 54 Nikon objective, a Nikon Digital DS-Fi2 camera using NIS Elements F4 32bit build 764. The stain was quantified in ImageJ by analyzing the amount of red in each image of 5 images per condition (n=3) and normalized by subtracting background obtained on TAMP scaffolds stained without cells.

2.6.9 - Statistical analyses

Unpaired student t-tests were used to analyze statistical significance. Data are presented as mean +/- SEM with a p-value < 0.05 to be considered significant.

2.7 – Figures

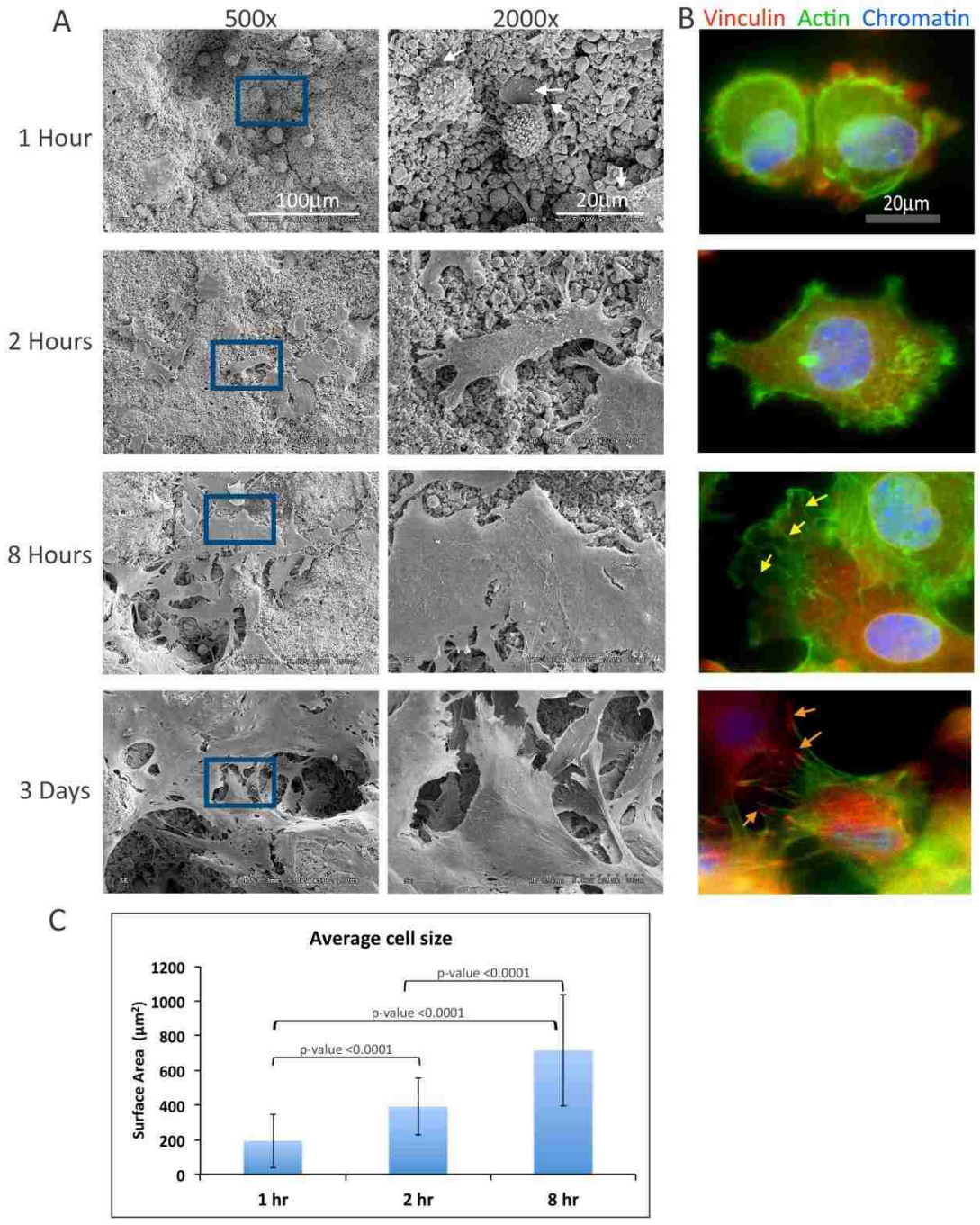

Figure 3: MC3T3-E1 pre-osteoblasts adhere and colonize TAMP scaffold surface

MC3T3-E1 pre-osteoblast cells were observed attaching to TAMP scaffolds after 1 hour by SEM analysis (A, 500x and 2000x, blue box defines the region imaged at 2000x). Thin extensions that are likely probing the environment can be seen as early as 1 hour after seeding (A, 2000x, white arrows). These cells can be seen progressively spreading out over the period of 2 and 8 hours (A, middle 2 sets of panels). After 3 days on the scaffold, the cells appear fully spread and begin to form lamellipodial- and filopodial-like structures (A, bottom panels). Immunofluorescence was performed for the corresponding time points (B) to visualize vinculin (red), actin (green), and chromatin (cell nuclei, blue). These images show that cells spread over time (1 hour to 2 hours) and begin to form definitive actin structures like stress fibers (8 hours, yellow arrows) and stable attachments like focal adhesions (3 days, orange arrows). (C) Cell size increased over time as measured through ImageJ analyses of SEM images. Large standard deviations here result from the 3-dimensionality of the TAMP scaffold surface captured by SEM. Cells deep in pores appear smaller as a result of depth perception (compare 1hour SEM and fluorescent images).

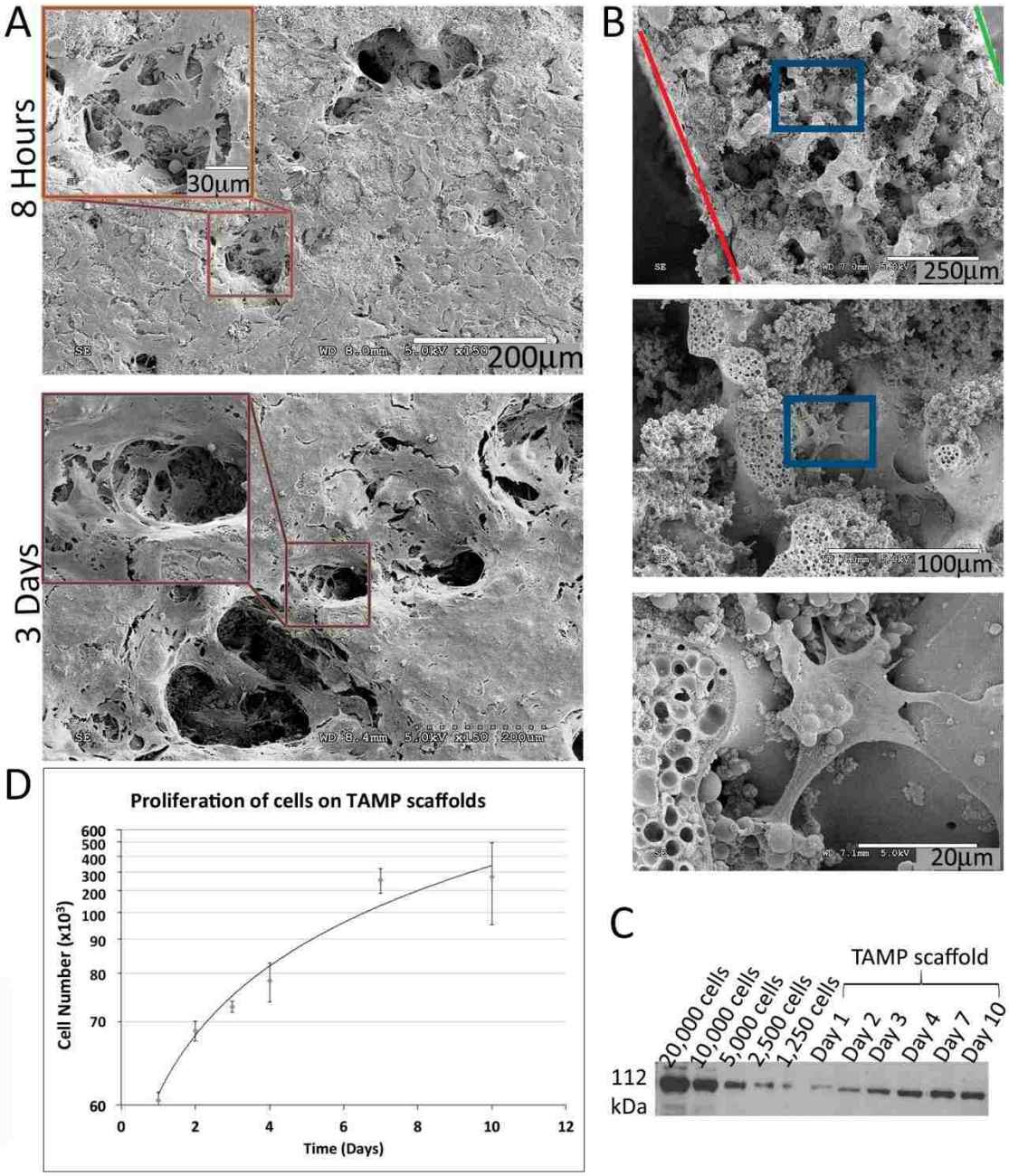

Figure 4: MC3T3-E1 cells colonize the interior of TAMP scaffolds
SEM analysis reveals that cells spread over the surface of the TAMP scaffolds by 8 hours (A, top panel) and form a monolayer of cells after 3 days (A, bottom panel) indicating that the cells are proliferating on the surface of the TAMP. Additionally, cells can be observed in macropores suggesting that they are crawling into the scaffold (A, purple

insets highlight macropores). Further analysis of the interior of a TAMP shows that cells are utilizing the macropores to enter into the scaffolds (B, red line indicates top of scaffold where cells were seeded, while green line indicates side that was on bottom of cell culture dish, orange boxes indicate magnified region in the image below). Analyses of cellular proliferation on/in TAMP scaffolds were performed using an AP-2 Western blotting protocol (C, example blot) and revealed that cells initially proliferate slowly, reach a logarithmic phase, and eventually plateau in growth (D).

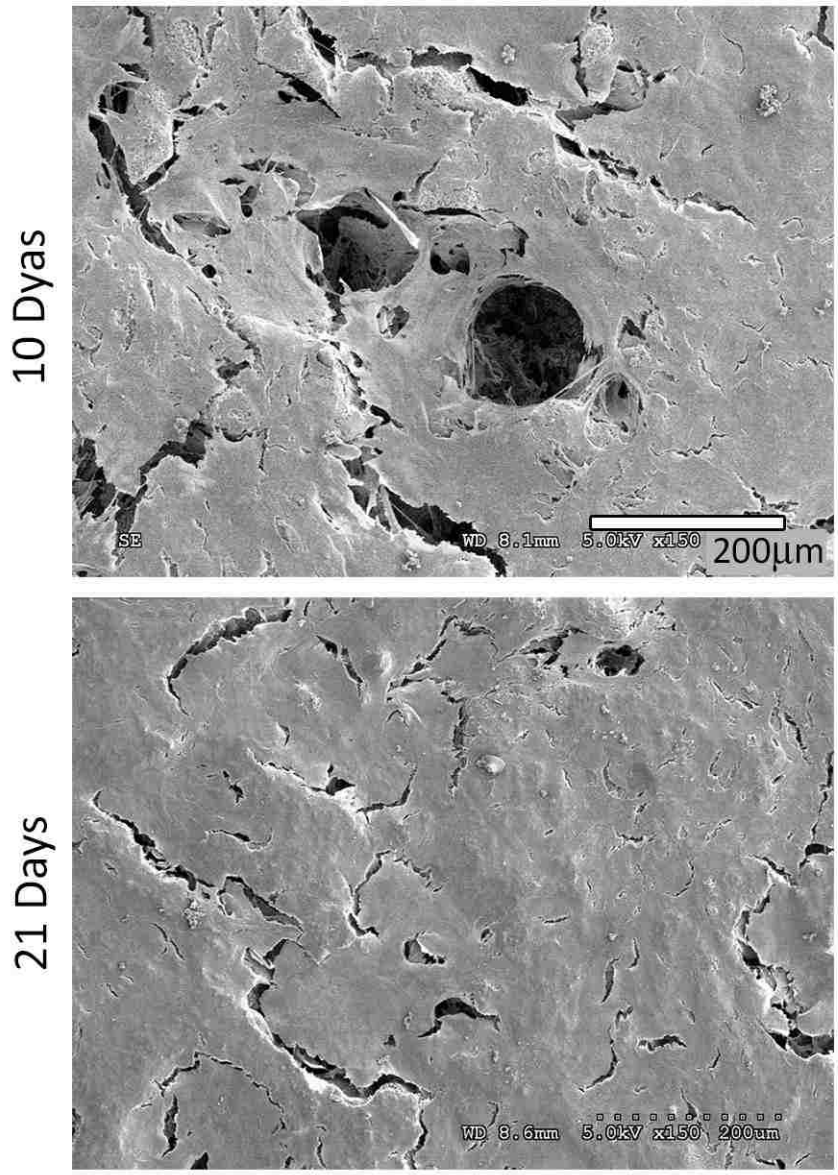

Figure 5: Cells continue to grow over extended periods of time on TAMP scaffolds
MC3T3-E1 continue to form a monolayer on the surface of the TAMP scaffold over 10 and 21 days

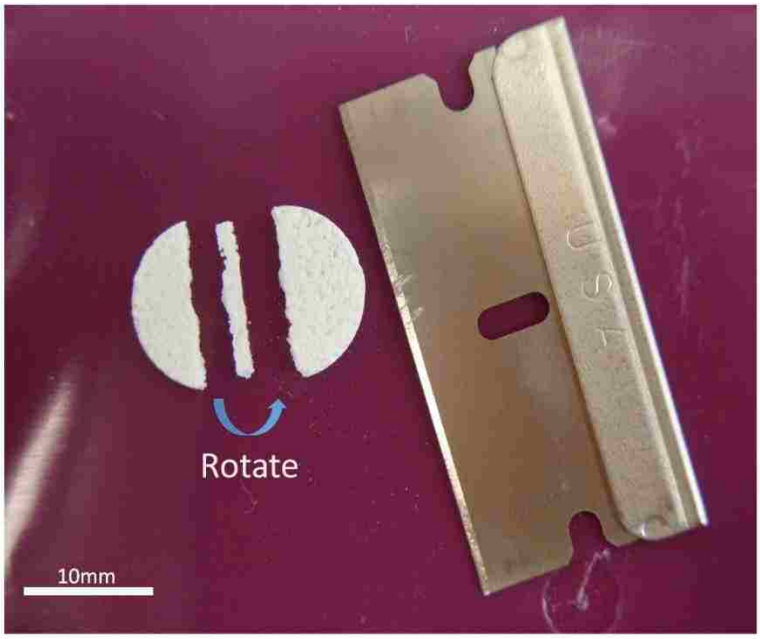

Figure 6: Section from TAMP scaffold for SEM analyses
Cells were seeded on the top of the scaffold then fixed before a slice was cut from the center and mounted on its side for SEM analysis of the TAMP scaffold interior.

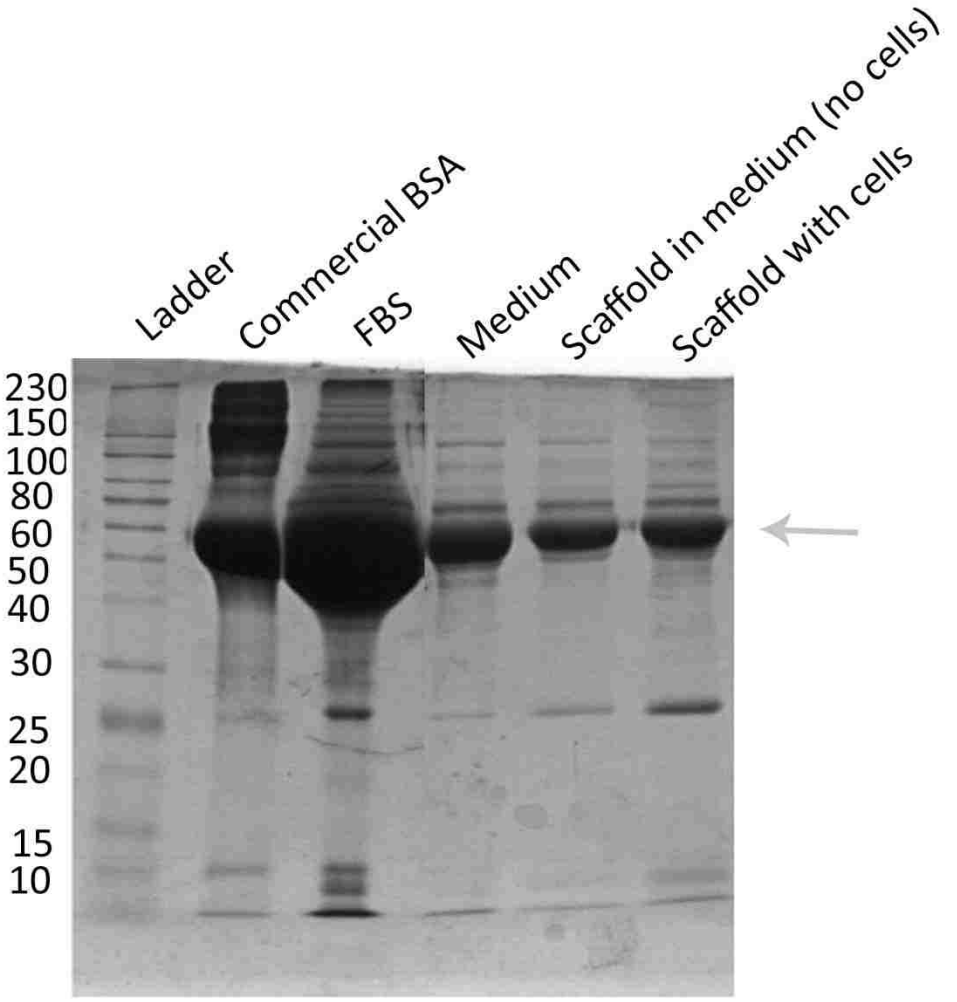

Figure 7: BSA adsorbs abundantly to TAMP scaffolds
Coomasie stained gel demonstrating the amount of protein adsorbed to a TAMP scaffold from the cell culture medium. A large band near 60kDa in all lanes corresponds to the band for BSA indicating that the scaffold adsorbs large amounts of BSA from the medium.

A)

Symbol	Gene Name	Array Loc.	Day 1	Day 7	Day 14	Day 26
Dmp1	dentin matrix acidic phosphoprotein 1	C10	67.1	24.4	21.9	10.8
Itgam	integrin, alpha M	E3	350.4	20.7	20.5	8.8
Ahsg	alpha-2-HS-glycoprotein	A1	66.8	24.4	3.0	3.0
OCN	osteocalcin	N/A	-	5.3	18.7	45.3
Col4a2	collagen, type IV, alpha 2	C1	24.9	3.0	4.2	4.6
Itga3	integrin, alpha 3	E2	7.7	3.3	2.8	1.3
Nfkb1	nuclear fact. of κ light polypep. gene enhanc. in B-cells 1	E11	7.2	4.3	3.4	1.5
Tgfb1	transforming growth factor, beta 1	F12	6.5	2.7	5.2	5.5
Vegfa	vascular endothelial growth factor a	G11	16.5	4.3	3.6	1.9
Col4a1	collagen, type IV, alpha 1	B12	3.2	4.3	4.1	6.6
Phex	phosphate regulating endopeptidase homolog, X-linked	F1	4.4	-1.1	7.3	2.0
BSP	Bone Sialo Protein	N/A	-	3.5	1.8	6.6
Mmp9	matrix metallopeptidase 9	E9	6.4	1.3	1.5	2.0
Col1a1	collagen, type I, alpha 1	B8	3.1	3.9	3.2	5.4
Fgf2	fibroblast growth factor 2	D2	2.5	4.8	3.8	1.7
Col5a1	collagen, type V, alpha 1	C2	3.1	2.7	2.1	3.1
Fn1	fibronectin 1	D7	4.0	2.6	2.4	3.5
Ctsk	cathespsin K	C9	3.1	1.6	2.8	2.9
Scarb1	scavenger receptor class B, member 1	F3	1.9	2.1	1.5	1.5
Tgfb3	transforming growth factor, beta 3	G2	2.4	1.3	4.2	2.9
Anxa5	annexin A5	A4	1.8	2.2	1.4	1.6
Col6a2	collagen, type VII, alpha 2	C4	2.4	1.8	-1.1	1.7
Bmp4	bone morphogenetic protein 4	A9	2.6	1.5	-1.2	1.6
Bgn	biglycan	A5	1.2	2.6	2.2	2.8
Pdgfa	platelet-derived growth factor alpha polypeptide	E12	-1.0	2.7	2.3	2.4
Itgb1	integrin, beta 1	E5	2.1	2.2	1.4	1.4
Itgav	integrin, alpha V, vitronectin receptor	E4	1.7	1.5	1.1	1.4
Cd36	CD36 molecule, thrombospondin receptor	B2	1.4	2.3	1.3	1.8
Serpinh1	serpin peptidase inhibitor, clade H, member 1	F4	1.1	1.7	1.2	1.8
Cdh11	cadherin 11, type 2, OB-cadherin	B3	1.2	1.6	-1.2	1.2
Bmpr1b	bone morphogenetic protein receptor, type IB	B1	192.2	188.0	-	-
Itga2	integrin, alpha 2	D12	-	35.5	20.0	-
Col7a1	collagen, type VII, alpha 1	C5	-	49.5	-	5.2
Icam1	intercellular adhesion molecule 1	D9	-	62.8	-	6.3
Fgf1	fibroblast growth factor 1	D1	-	-	12.4	-
Ambn	ameloblastin, enamel matrix protein	A3	-	-	-	3.5
Bmp3	bone morphogenetic protein 3	A8	-	-	-	1.5
Tuft1	tuftelin 1	G7	-	-	-	4.5
Bmp6	bone morphogenetic protein 6	A11	12.0	2.4	4.0	-4.4
Tgfbr2	transforming growth factor, beta receptor 2	G4	-1.6	3.9	2.5	2.0
Flt1	fms-related tyrosinase kinase 1	D6	2.1	3.1	-1.0	-1.5
Sox9	SRY box 9	F10	4.4	1.9	-1.3	-1.8
Itga2b	integrin, alpha 2b	E1	6.5	2.1	1.2	-2.0
Alpl	alkaline phosphatase, liver/bone/kidney	A2	5.2	1.0	-4.3	2.8
Tfip11	tuftelin interacting protein 11	F11	-2.2	2.5	1.5	-1.3
Col12a1	collagen, type XII, alpha 1	B6	-1.3	3.2	1.1	1.6
Bmp 1	bone morphogenetic protein 1	A6	2.8	1.2	1.3	-1.6
Comp	cartilate oligomeric matrix protein	C6	3.5	-1.4	-6.4	-1.3
Smad3	SMAD family member 3	F7	1.3	1.8	1.3	-1.6
Vegfb	vascular endothelial growth factor b	G12	-1.5	1.4	1.7	1.3
Runx2	runt-related transcription factor 2	F2	-2.0	2.4	1.0	-1.1
Fgfr1	fibroblast growth factor receptor 1	D4	1.7	1.3	-4.2	-2.3
Col2a1	collagen, type II, alpha 1	B10	5.8	-2.4	1.6	-2.4
Smad2	SMAD family member 2	F6	3.0	-2.0	-1.1	-1.8
Col11a1	collagen, type XI, alpha 1	B5	-1.8	-1.7	-1.3	2.3
Egf	epidermal growth factor	C11	3.2	-1.6	-7.0	-2.2
Col10a1	collagen, type X, alpha 1	B4	-2.6	-2.2	-3.5	2.9
Msx1	msh homeobox 1	E10	1.2	1.3	-2.0	-1.5
Igf1r	insulin-like growth factor 1 receptor	D11	-1.4	1.4	-1.6	-1.1
Twist1	twist homolog 1	G8	-1.4	1.3	-2.0	-1.4
Tgfbr3	transforming growth factor, beta receptor 3	G5	-1.3	-3.7	1.1	1.3
Smad4	SMAD family member 4	F8	-1.0	1.2	-1.4	-1.1
Col6a1	collagen, type VI, alpha 1	C3	1.0	1.1	-1.7	-1.1
Bmpr1a	bone morphogenetic protein receptor, type IA	A12	-2.8	-1.4	-2.1	-1.5
Igf1	insulin-like growth factor 1	D10	-8.1	-1.0	-3.9	-1.3
Tgfb2	transforming growth factor, beta 2	G1	-2.1	-3.1	-1.1	-1.4
Smad1	SMAD family member 1	F5	-1.3	-3.1	-1.5	-2.1
Vdr	vitamin D receptor	G10	-1.3	-2.4	-4.1	-4.6
Vcam1	vascular cell adhesion molecule 1	G9	-1.5	1.3	-1.9	-1.8
Col3a1	collagen, type III, alpha 1	B11	-1.9	-1.6	-2.4	-1.3
Col1a2	collagen, type I, alpha 2	B9	-2.1	-1.5	-2.3	1.1
Mmp2	matrix metallopeptidase 2	E7	-1.5	-2.4	-2.1	-1.4
Fgfr2	fibroblast growth factor receptor 2	D5	-9.8	-3.3	-3.3	-4.5
Csf2	colony simulating factor 2	C7	-	-	-	-
Enam	enamelin	C12	-	-	-	-
Fgf3	fibroblast growth factor 3	D3	-	-	-	-
Gdf10	growth differentiation factor 10	D8	-	-	-	-
Mmp10	matrix metallopeptidase 10	E6	-	-	-	-
MmpB	matrix metallopeptidase 8	E8	-	-	-	-
Sost	sclerostin	F9	-	-	-	-
Tgfbr1	transforming growth factor, beta receptor 1	G3	-	-	-	-
Tnf	tumor necrosis factor	G6	-	-	-	-

>-6	-4.6 to-6.0	-3.1 to -4.5	-1.5 to -3.0	-1.4 - 1.4	1.5-3.0	3.1-4.5	4.6-6.0	>6
Fold down-regulation								Fold up-regulation

(1) Cell Adhesion
(2) Extracellular matrix & remodeling proteins
(3) Proliferative growth factors
(4) Differentiation growth factors
(5) Bone Specific transcription factors
(6) Collagens
(7) Osteoblast specific proteins

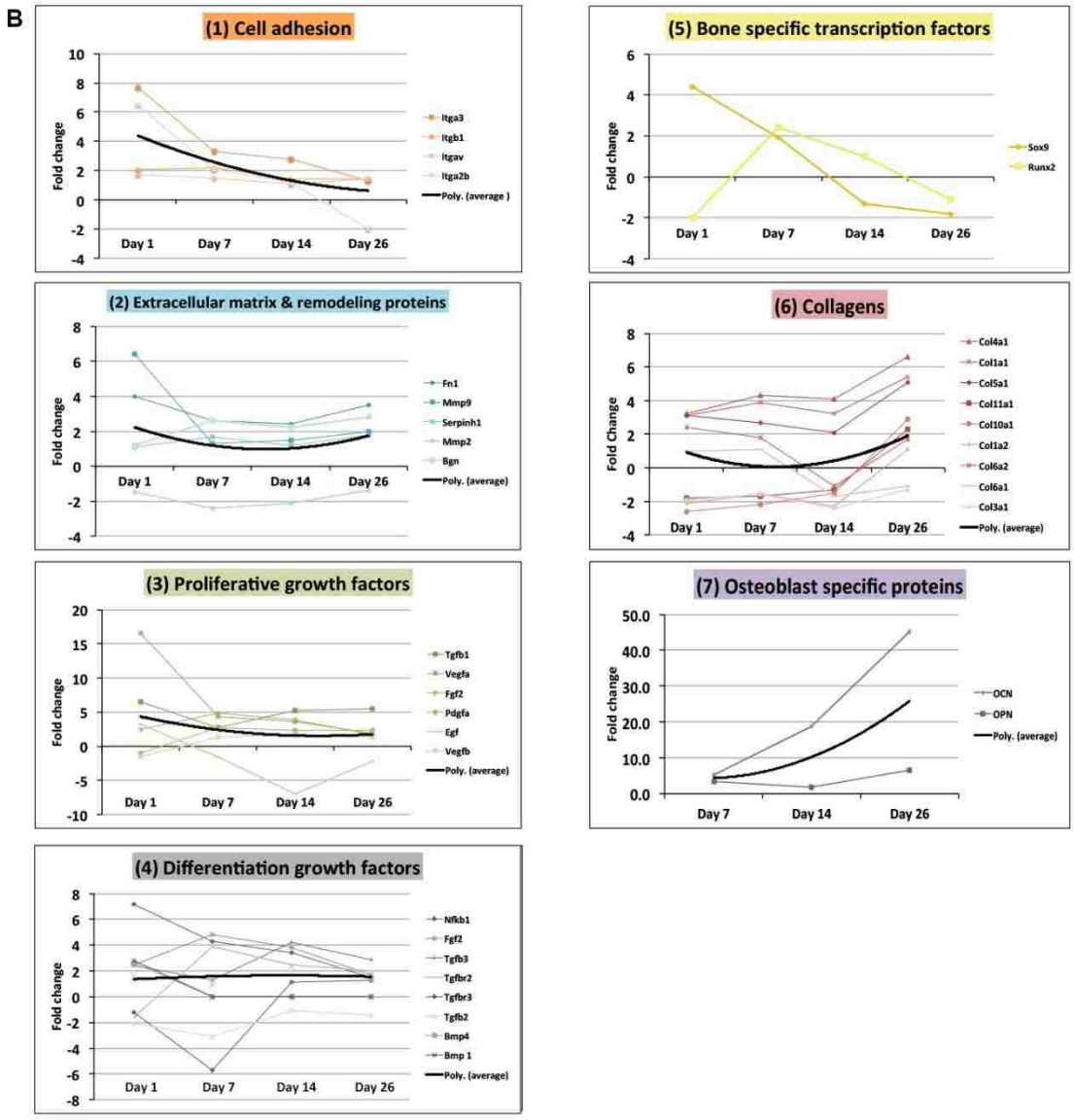

Figure 8 : MC3T3-E1 cells differentiate into mature bone producing osteoblasts on the mRNA level

A microarray from SA biosciences / Qiagen was used to analyze expression of bone cell differentiation related genes (A). Highlighted genes were grouped into categories based on their function and summarized by trendlines in the graphs of (B). Early up-regulation occurs for genes related to cell attachment (1), extracellular matrix and remodeling proteins (2), and proliferative growth factors (3), followed by expression of differentiation growth factors (4). Importantly, expression of known bone cell differentiation transcription factor, Sox9, is high early and is down-regulated as RunX2 is

up-regulated (5). Additionally, extracellular matrix components of bone, primarily collagens (6) and osteoblast specific extracellular matrix protein genes (7) were found to be expressed at late time points as anticipated.

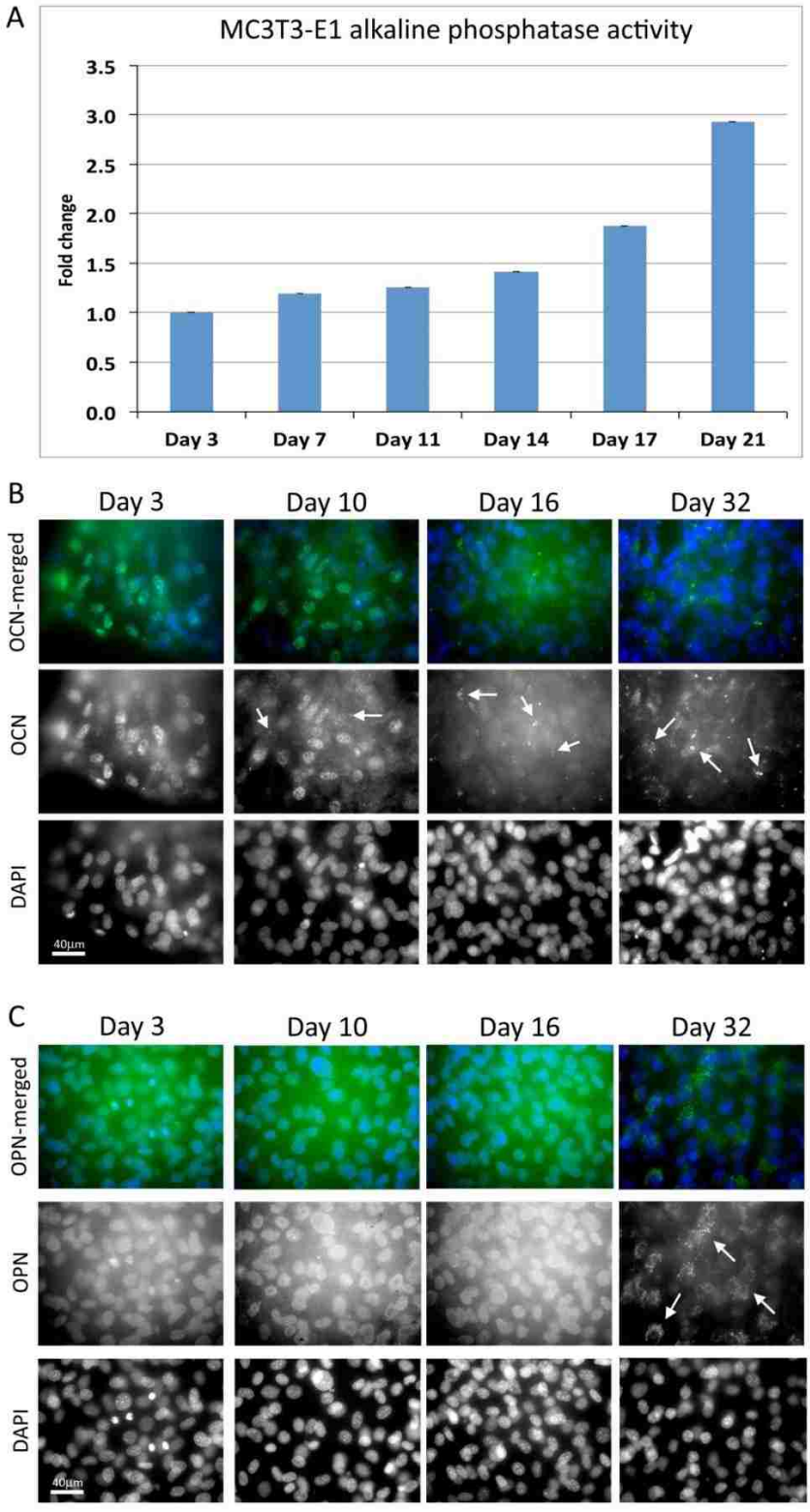
A
MC3T3-E1 alkaline phosphatase activity
Fold change
3.5
3.0
2.5
2.0
1.5
1.0
0.5
0.0
Day 3
Day 7
Day 11
Day 14
Day 17
Day 21
B
Day 3
Day 10
Day 16
Day 32
OCN-merged
OCN
DAPI
40μm
C
Day 3
Day 10
Day 16
Day 32
OPN-merged
OPN
DAPI
40μm

Figure 9: MC3T3-E1 cells produce osteoblast specific proteins
Alkaline phosphatase enzyme activity was analyzed colorimetrically and indicated that MC3T3-E1 cells were differentiating on the TAMP scaffolds (A). Immunofluorescence analyses for osteocalcin (B) and osteopontin (C) indicate that MC3T3-E1 cells grown on pelleted TAMP scaffolds differentiate into mature bone secreting osteoblasts. Osteocalcin appears as a punctate nuclear stain during early time points (B, OCN in green and nuclei in blue, days 3 and 10) and becomes a punctate cytoplasmic / extracellular matrix protein stain by days 10, 16, and 32 (arrows). Additionally, osteopontin staining is not evident until day 32 (C, OPN in green and nuclei in blue). Positive staining for these late stage protein markers at day 32 suggests that the cells are differentiating into mature osteoblasts.

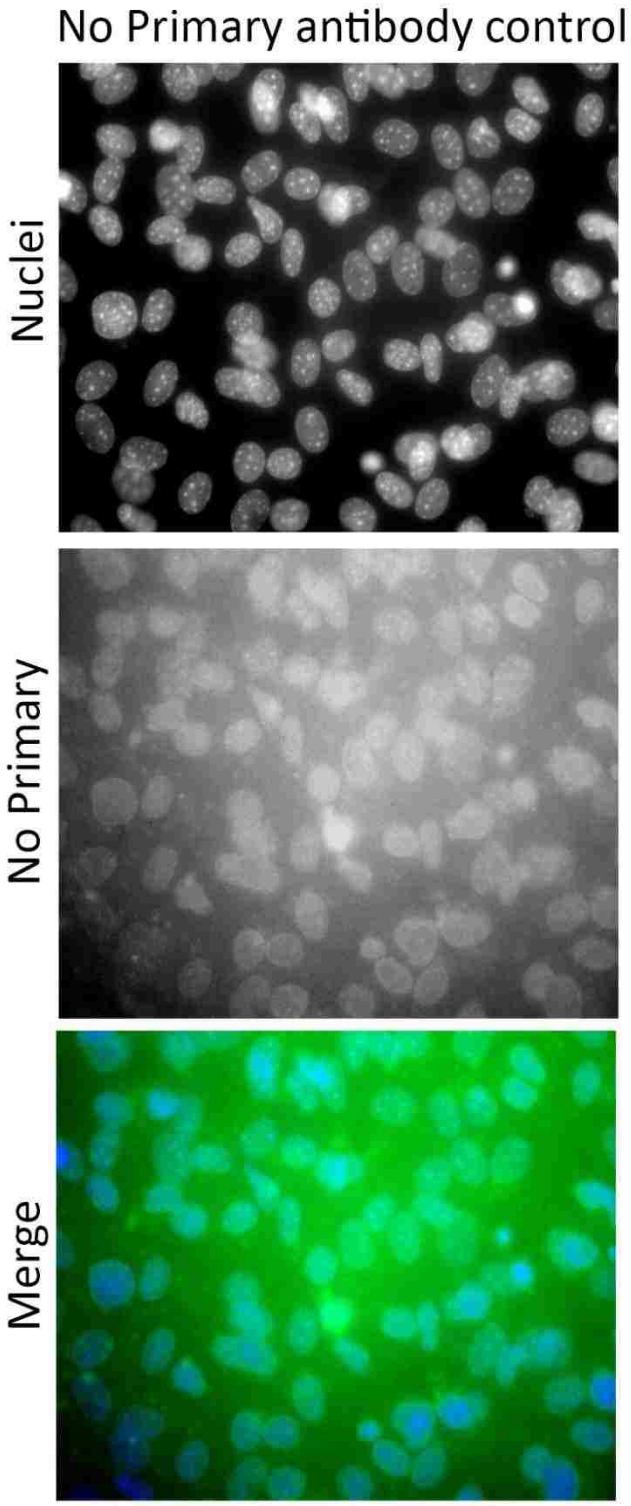

Figure 10: TAMP scaffolds auto-fluoresce or reflect light

Cells fixed on a TAMP scaffold were subjected to the same protocol as was performed for immunofluorescence staining except that primary antibody incubation was performed in blocking solution only (no antibody). The robust green in the image is likely from the auto-fluorescence or reflectance from the glassy material.

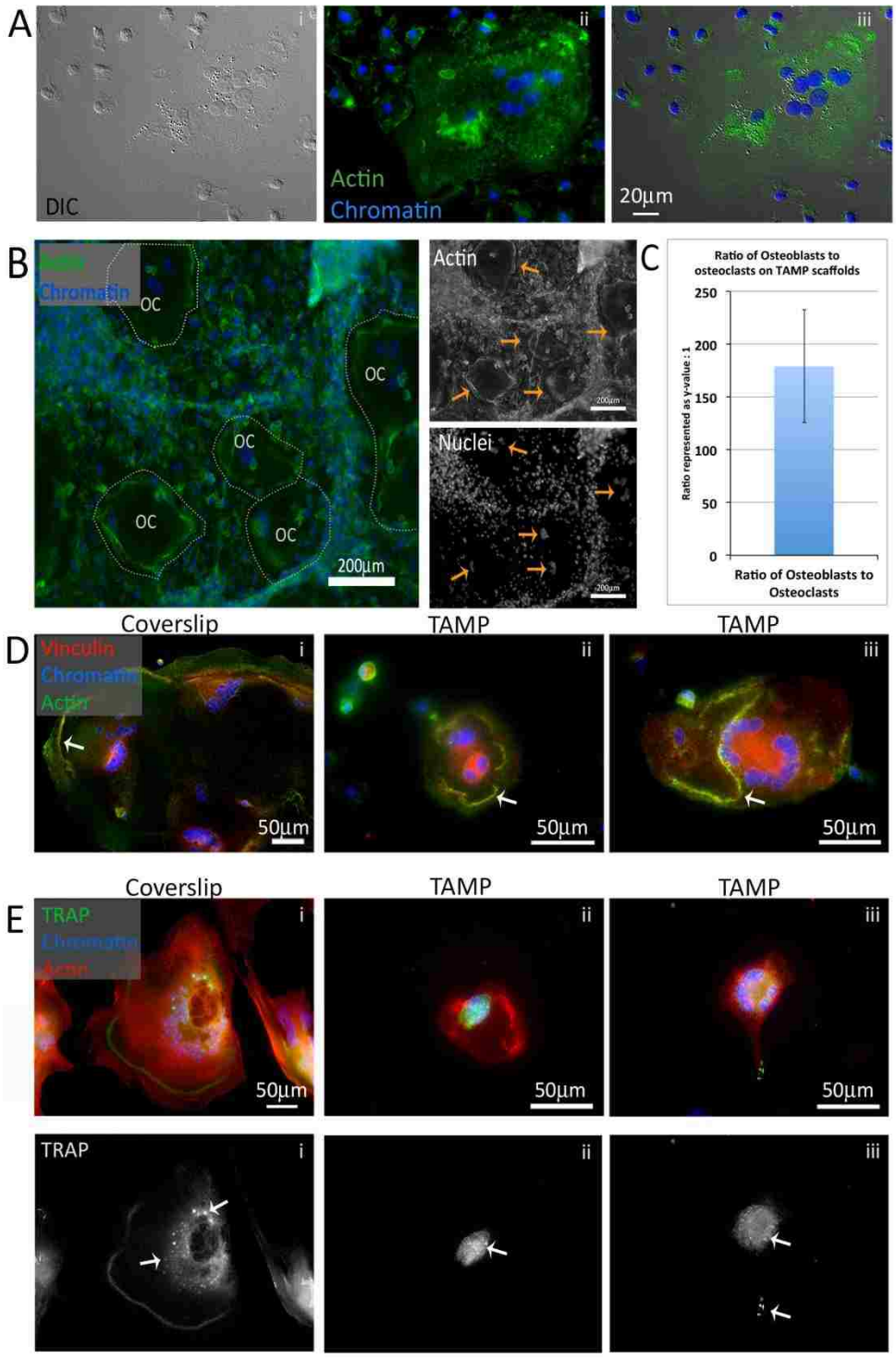

Figure 11: TAMP scaffolds support growth of osteoblast / osteoclast co-culture
Osteoclasts derived from bone marrow cultured with MC3T3-E1 cells on a coverslip are large cells with actin bands at the periphery of the cell and clusters of nuclei (A, phase (i);

fluorescence (ii): actin in green, chromatin (cell nuclei) in blue; merge (iii)). Co-cultured cells on TAMP scaffolds form a complex tissue-like structure (B, actin in green and nuclei in blue, osteoclasts are outlined with a dashed line and labeled with "OC"). The black and white single channel image of actin makes the actin bands easier to identify (marked with arrow), and the single channel nuclear image shows large empty spaces near clusters of nuclei (marked with arrow) suggesting that these large multinucleated cells are osteoclasts. Osteoblasts and osteoclasts were counted and found to be present in the co-culture in a ratio of 179 ±53:1 respectively (C). Co-culture cells were seeded onto coverslips (Ai, Bi) and scaffolds (Aii & Aiii, Bii & Biii), and incubated in Cellstripper to remove most other cells. This allowed for detection of sealing zones distinguished by the actin (green) and vinculin (red) bands (D), and tartrate resistant acid phosphatase (TRAP), an enzyme specific to osteoclasts (E, TRAP in green, actin in red, nuclei in blue). TRAP staining shown as single channel black and white images to more easily identify the punctate vesicular stain.

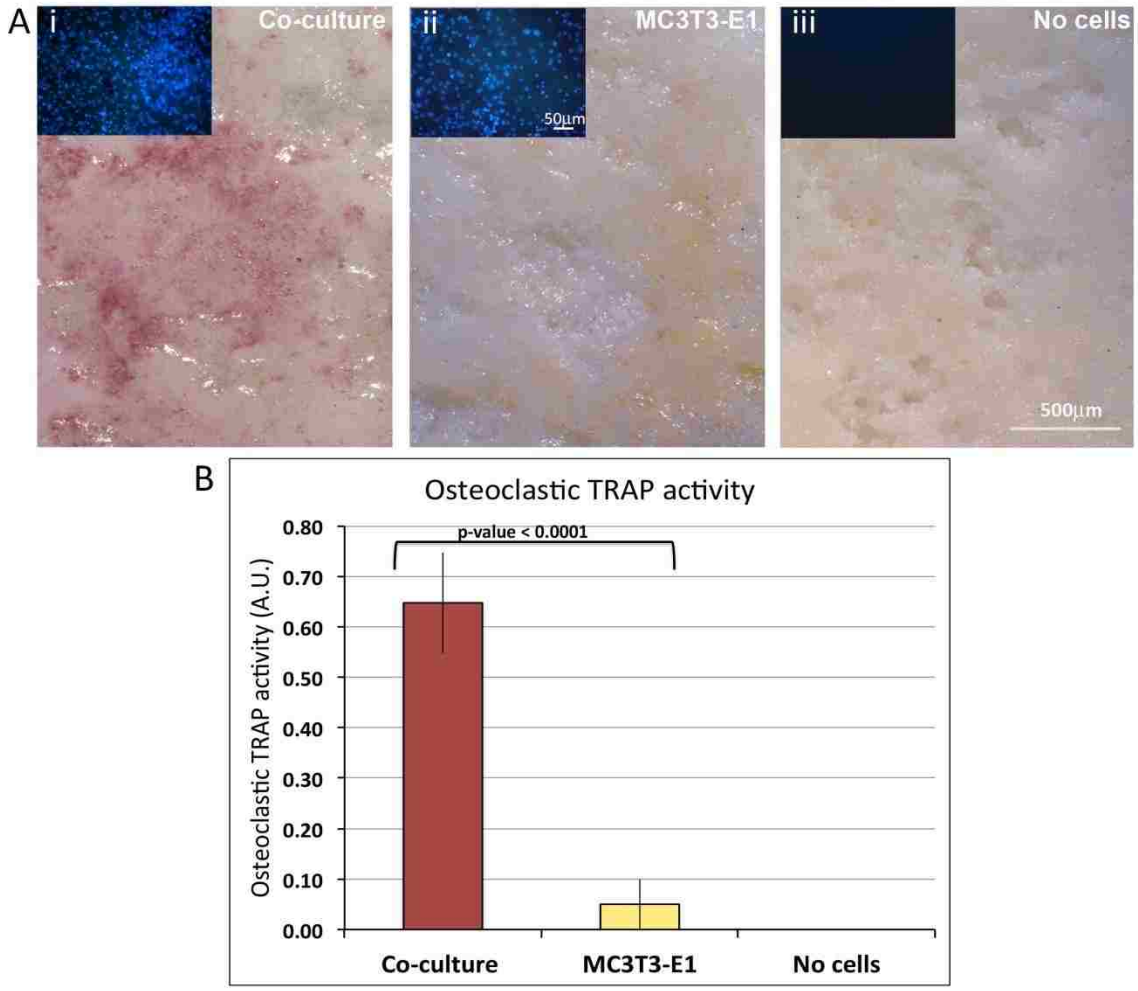

Figure 12: Osteoclasts are active on TAMP scaffolds

Osteoblast/osteoclast co-culture and MC3T3-E1 cells alone were grown on TAMP scaffolds for 10 days followed by staining for TRAP activity. The pink stain on the co-culture sample (Ai) indicates there are active osteoclasts present on the scaffolds versus the lack of pink stain observed on the scaffold with only MC3T3-E1 cells (Aii). The same scaffolds were stained by DAPI to show that cells were present on both samples (A insets, nuclei in blue). Blank scaffolds without cells were also stained and imaged to normalize the background staining (Aiii). ImageJ analysis of co-culture compared to MC3T3-E1 cells indicated that the co-culture was statistically more pink than the MC3T3-E1 cells confirming the presence of active osteoclasts on the TAMP scaffold (C).

Chapter 3 - How cells sense their non-biological extracellular environment: The role of surface nano-structure

3.1 - Abstract

Here we present evidence of the ability of MC3T3-E1 pre-osteoblasts to detect differences in nano-structure on two different substrates. The first substrate is a bioactive glass with a simple composition of 30 mol%CaO – 70 mol%SiO_2 and contains both nano- and macropores. The only variable between samples of this type of substrate is the nanopore size (3.7 nm vs. 17.7 nm), which is measured using BET (nitrogen adsorption analysis), while total surface area is kept constant. The second substrate, a bioactive glass with a more complex composition of 24.4 mol%Na2O–26.9 mol%CaO–2.6 mol%P2O5–46.1 mol%SiO2 called 45S5 Bioglass® [8], varies in the nano-structure due to phase separation, resulting in either a spinodal interconnected morphology or a droplet nucleation morphology as determined by SEM analysis ([68]). Cellular response to either substrate was measured to quantify the initial adhesion to the surfaces using immunofluorescence analyses. On the glass samples varying in nanopore size, we observed that cells preferred the smaller nanopores (Wang, Kowal et al., 2013; Tissue Engineering, PartA). Additionally, a clear preference was observed using the glass that differed in nano-structure in that more adherence was observed on the spinodal interconnected morphology than the droplet nucleation morphology.

In the case of both substrates, cells showed a significant preference to one of the nano-structures, indicating that remarkably, cells are able to sense morphological details of the substrates that are app. 1000 times smaller than the cells themselves. Research performed here aimed to uncover the underlying principles that allow cells to respond to such nano-scaled substrate details, allowing for the innovative design of tissue regenerative materials.

3.2 – Contribution

Nanoporosity significantly enhances the biological performance of engineered glass tissue scaffolds
(Wang, Kowal et. al. 2013)

My contribution to the Wang, Kowal el. al. 2013 paper was assisting with performing the experiments that resulted in Figure 13. From these data, we learned that cells were able to detect and respond to the difference in size of nanopores, suggesting that cells can in some way recognize topographical differences that are smaller than the cells themselves.

Role of phase separation on the biological performance of 45S5 Bioglass®
(Kowal[Ψ], Golovchak[Ψ] et. al. - in review)

[Ψ] both authors contributed equally

My contribution to the Kowal, Golovchak, et. al. manuscript (in review) includes data acquisition and analysis for figures 15, 16, 17, 18, and 19. From Figure 15, it was realized that more MC3T3-E1 pre-osteoblast cells had attached to the spinodal glass than to the droplet glass. In agreement with this result, cells were more spread out with more actin stress fibers and focal adhesions on the spinodal glass (Figure 16). We learned that both of the glass structures investigated behave in the same way when exposed to biological fluids with respect to calcium and phosphate dissolution and pH (Figure 17). In addition a layer of hydroxyapatite (HA) forms on the surface of both glasses after exposure to physiological solutions. The HA is similar in appearance by SEM analyses (Figure 18) at high magnification especially after exposure to PBS followed by medium. The HA has plate-like lamellae crystals forming; however, the packing or density of these crystals is slightly different between the spinodal and droplet glasses. Figure 19 in conjunction with data from Table 1 allowed us to determine that the BSA layer is likely to be thin since it is undetectable by SEM analyses on either glass type. Roman Golovchak performed and analyzed XPS and Raman experiments (Table 1, Figures 20

and 21) which demonstrated that protein adsorbed to the glass surface in different amounts and with different conformations. These results allowed us to conclude that the glass structure is influential in how proteins adsorb to the glass surface and in turn affects how cells respond to the glass, suggesting that it is critical to understand the mechanism behind cell-substrate interaction for the innovative design of bioscaffolds.

3.3 - Introduction

The importance of nanotopography on the ability of cells to attach to biomaterials is now well established [69, 70], and also has been demonstrated recently for bioactive glasses [9]. Shaojie Wang from Dr. Jain's lab developed ways to control the nanopore size of TAMP scaffolds while maintaining similar surface area between the samples. This was achieved by either sintering the glass to decrease the nanopore size or by incubating the glass in ammonium during the aging process to enlarge the nanopores. The pore size and surface area were both measured by BET, with samples resulting in an average nanopore size of 17.7nm and surface area of $81\pm2 m^2$/gram, and samples resulting in 3.7nm average nanopore size and $83\pm2 m^2$/gram surface area. Remarkably, these studies showed that cells are able to 'sense' the nanostructure of the substrate at a scale that is approximately 1000 times smaller than the cells themselves (as described below) and in the size-range of individual integrin cell-adhesion receptors (11-19 nm depending on the state of activity) [71-73].

It was later reported that even traditional 45S5 Bioglass® can be prepared with different morphologies related to phase separation, as determined by the melt quenching during glass fabrication procedure [68]. However, influence of the type of phase separation on the bioactivity of these materials has not been investigated. We investigated the influence of phase separated microstructure of these differently melt-quenched 45S5 Bioglass® varieties on their ability to adsorb proteins and adhere cells, in a first attempt toward establishing the role of different morphologies of Bioglass® at the micro- and nanometer scale on cell response. To understand the difference in the response of cells,

we have focused on the growth of hydroxyapatite (HA) layer and adsorption of proteins, since these processes influence the surface that is exposed to cells during attachment. In the past, the HA layer has been credited for the superior bioactive properties of 45S5 Bioglass® [74], however there is little published information about what role, if any, adsorbed proteins abundantly present in biological solutions may play toward cell attachment. Since adhered cells remain in contact with culture medium, potential changes in its chemistry have been monitored as well.

3.4– Results

3.4.1.a – Cellular response to TAMP with different pore sizes

MC3T3-E1 cells were seeded onto samples with nanopore sizes of 17.7nm and 3.7nm, yet the samples had similar surface areas. Cells were allowed to adhere and grow on the scaffolds for 12 and 48 hours before being fixed and analyzed for cell morphology and density. Cells on both samples were similar in morphology with a fibroblast-like appearance (Figure 13A); however, after 12 hours there was a difference in density with a preference of the cells to samples which had a smaller nanopore size (Figure 13A compare a to b, and quantitatively measured in B). In addition, after 48 hours, the preference for the smaller nanopores was no longer observed (Figure 13A compare c to d, and quantitatively measured in B). These data suggest that nanopore size may be critical for initial attachment of cells to their substrate. A more in-depth characterization of the mechanism behind these results is described below using Hench's traditional 45S5 Bioglass®.

3.4.1.b - Biolass® morphologies

By casting traditional 45S5 Bioglass® from different equilibration temperatures (≥1380 ˚C compared to ≤1370 ˚C), we produced Bioglass® samples with two types of phase separated morphologies: (i) spinodal type when the melt was quenched from temperature ≥1380 ˚C (Figure 16A), and (ii) droplet type when quenched from temperatures <1380 ˚C (Figure 1B) (21). The scale of droplet type phase separation in the

glass is on a submicron scale, whereas the scale of spinodal phase separation was found to be much smaller (Figure 14) [68].

In order to evaluate their chemical characteristics, the surfaces of the two Bioglass® varieties were analyzed by XPS in their pristine and polished states. Analyses described earlier [68] demonstrated that the overall chemical composition of both pristine glass varieties were nearly identical. In addition, their compositions were very similar to the calculated theoretical composition (Table 1). Both findings confirm their chemical identity as 45S5 Bioglass®. After polishing, a slight difference in the surface concentration of sodium and silicon was detected between the two sample types (Si: 13.9±1.7% in spinodal, and 18.6±1.9% in droplet; Na: 20.6±1.8% in spinodal, and 15.5±1.8% in droplet, Table 1). This difference may be due to Na^+ leaching out more efficiently from the droplet than the spinodal-type phase separated glass samples; or a more pronounced Na^+ ion migration during polishing towards the surface in spinodal samples [75]. However, these changes were observed in a thin surface layer after polishing only. The underneath bulk composition was found to be comparable for both droplet and spinodal-type phase separated glass samples, and close to the theoretical value of 45S5 Bioglass® [68].

3.4.2 - Attachment and morphology of cells seeded on Bioglass® varieties

MC3T3-E1 pre-osteoblast cells, frequently used in studies investigating the osteo-inductive properties of bioactive glasses [76, 24], were seeded onto the surface of spinodal and droplet type Bioglass® samples. Attached cells were fixed after 2 and 24 hours and processed for the detection of cell nuclei using fluorescent chromatin (DAPI, blue) staining (Figure 15A). Cell nuclei were counted to determine the number of cells that had attached to the surface of the glasses. After merely 2 hours, based on the number of attached cells a clear preference of the cells for the glass samples with spinodal morphology compared to the droplet morphology (n = 5) was observed. On average more than double the number of cells (spinodal: 203±4.4 cells vs droplet: 80.8±6.5 cells) attached to the surface of spinodal phase-separated glass samples compared to droplet

type phase-separated glass samples (Figure 15B). A similar result was observed after 24 hours (spinodal: 213±13.2 cells vs droplet : 84±7.5 cells, n = 4), with more than 2 times the number of cells attached to the spinodal glass than the droplet glass (Figure 15A, B). Together, these results indicate that MC3T3-E1 cells attached more efficiently to spinodal than to droplet type phase-separated Bioglass® samples.

To determine whether the preference of cells for spinodal glass was also supported by morphological features that typically are associated with cell attachment, after 2 hours of exposure we stained the actin cytoskeleton and focal adhesions in cells on both glass varieties. Cellular actin organization was detected by decorating actin with Alexa488-labelled phalloidin (green). The presence, number and robustness of assembled focal adhesions were assessed by fluorescence labeling using an antibody targeting vinculin (red), a protein localizing to focal cell adhesion complexes. We observed that cells growing on the spinodally phase separated Bioglass® samples assembled robust actin stress fibers that preferentially ended in pronounced focal adhesions as is typical of cells growing on stiff substrates. By comparison, cells growing on droplet type phase-separated glass samples assembled an array of much thinner, disoriented actin fibers and only a few, not well-developed vinculin-based focal adhesions (Figure 16A, images in column 1). This significant difference in morphological organization was further exemplified when monochromatic images representing the actin and vinculin channels were black/white inverted and thresholded to enhance the appearance of stress fibers and of focal adhesion complexes (Figure 16A, images in columns 2 and 3).

To quantify actin and vinculin signal strength, fluorescence intensity of both was measured inside defined squares that were placed in comparable peripheral cytoplasm regions of cells (green and red example squares shown in Figure 16A). Quantitative analyses (Figure 16B) showed that cells growing on spinodal glass, on average assembled 65% more stress fibers than cells growing on the droplet glass as indicated by increased peripheral actin fluorescence intensity (Figure 16B, a). In addition, we detected 38% more focal adhesion-localized vinculin in cells growing on spinodal samples, indicating that cells growing on spinodal type glass attached more readily to their substrate (Figure 16B, b). Lastly, we observed that the cells growing on spinodal type samples on average

occupied approximately 84% more surface/cell area compared to cells that attached to droplet type glass (Figure 16B, c), indicating that they spread out much faster. Together, these data demonstrate that the cells were able to recognize, differentiate and react to the underlying glass surface.

3.4.3 - Chemical behavior of Bioglass® varieties exposed to biological solutions

To better understand cell behavior in respect to Bioglass® substrate we next investigated Bioglass® performance upon exposure to biological solutions. As ions dissolving from Bioglass® may influence the formation of HA by increasing the local concentration of calcium and phosphate ions in solution [77, 78], or by changing the pH of the solution [15, 79, 80], and this may influence cellular activity [79, 80], we analyzed the concentration of calcium (Ca^{2+}) and phosphate (PO_4^{-3}) ions and the pH in the solutions before and after exposure to the differently phase separated Bioglass® samples. We chose to use PBS (phosphate buffered saline) and cell culture medium for these analyses, as both are physiological solutions that are used routinely when culturing cells as opposed to simulated body fluid (SBF) which is not appropriately formulated for the culture of mammalian cells [80].

As expected, since PBS does not contain Ca^{2+} ions, no calcium was detected in PBS solution before exposure to glass samples, and only a small amount of Ca^{2+} was detected in the PBS solution after incubation with either glass type (Figure 17A), suggesting some leaching and/or dissolution of the samples. However, no significant difference in Ca^{2+} concentration was observed between spinodal and droplet type glasses (0.90±0.27 and 1.30±0.07 mg/dL respectively, n=4). In contrast, the concentration of Ca^{2+} in cell culture medium decreased somewhat over time with exposure to both glass types (from 7.78±0.90 mg/dL for medium without glass exposure to 5.75±0.94 mg/dL for spinodal glass and 6.13±0.64 mg/dL for droplet glass after 24 hours), suggesting deposition of Ca^{2+} on the glass surfaces eventually leading to HA formation. However, again no significant difference for Ca^{2+} was found for the two Bioglass® varieties (2 hr

spinodal/droplet: 7.25±0.47/7.19±1.24; 24 hr spinodal/droplet: 5.75±0.94/6.13±0.69; Figure 17A).

A similar result was obtained for PO_4^{3-} (Figure 17B), with an overall decrease of PO_4^{3-} in solution over time, but no significant difference in the concentration of PO_4^{3-} between spinodal and droplet samples at any time point. The concentration of PO_4^{3-} in PBS solution decreased from 37.8±0.2 mg/dL (n=4) before glass exposure to 35.8±2.8 mg/dL for spinodal glass and 35.0±2.6 mg/dL for droplet glass. Additionally, the concentration of PO_4^{3-} in culture medium decreased from 9.7±2.3 mg/dL (before exposure) to 9.1±0.8 and 9.1±0.7 mg/dL after 2 hours and 6.3±0.6 and 6.2±0.8 mg/dL after 24 hours for spinodal and droplet glasses, respectively (Figure 17B), again correlating with the formation of HA on the glass sample surfaces.

A comparable result was also obtained when pH of Bioglass®-exposed biological solutions was determined. On average, the pH of PBS solution before exposure to glass was 7.72±0.05 and increased to 8.62±0.02 (spinodal) and 8.59±0.02 (droplet) after a 3-day incubation period. The pH of cell culture medium before exposure to glass was very similar to the pH of PBS (7.48±0.02, n=4) (Figure 17C), however in contrast to PBS remained almost unchanged during Bioglass® exposure. After 2-hour the pH measured 7.48±0.03 for spinodal and 7.44±0.08 for droplet glass exposed medium samples. After 24 hours, the pH dropped slightly to 7.45±0.03 for spinodal, and 7.39±0.02 for droplet glass exposed medium samples (Figure 17C). Together these data indicate that droplet and spinodal type Bioglass® varieties exhibit very similar dissolution characteristics in biological fluids.

3.4.4 - Formation of hydroxyapatite on Bioglass® varieties

Generally, good biological performance of bioactive glasses is attributed to the formation of a layer of hydroxyapatite (HA) on its surface, which is credited with providing the material with bioactivity [74]. As can be inferred from the comparison of the samples' surface composition obtained through XPS analysis and theoretical composition of HA (Table 1), a HA layer had indeed formed after a 3 day incubation

period in PBS solution. As indicated by our measurements summarized in Table 1, there is little observable difference in the concentration of calcium and phosphate on the two Bioglass® varieties, suggesting that the composition of the HA layers was essentially the same. Notwithstanding, to assess the physical structure of the respective HA layers, samples were imaged by SEM after exposure to PBS for 3 days at 37 °C. SEM analyses confirmed the formation of HA layers on both glass varieties (Figure 18). Both samples were found to be covered with dense, intertwined long lamella- or plate-like HA crystals. However, on the fine structure (18,000x magnification), the HA crystals on the spinodal type Bioglass® appeared larger in size and less densely packed compared to the crystals that formed on the droplet type Bioglass®. In addition, lower magnification analyses (6,000x magnification) indicated that on spinodal type Bioglass®, HA deposited as a more or less homogenous smooth layer of lamella-like crystals, whereas on droplet type Bioglass®, HA formed 'boulders' reminiscent of the underlying phase separation. In fact, the center-to-center distance between HA boulders correlated well with the phase-separation features of the droplet type Bioglass® samples (compare Figures 14 and 18).

Since Bioglass® samples were pre-incubated for 3 days in PBS followed by incubation in medium when cells were seeded on the glass samples, analyses of the structure of the HA coat that formed under these conditions was performed as well. The resulting SEM images convincingly show little variation in the structure of the HA crystals once the glass samples were submerged in cell culture medium after either 2 or 24 hours (Figure 18, middle and right panels). Moreover, pronounced HA 'boulders' that were detected on droplet-type Bioglass® samples after incubation in PBS solution partially disappeared, making the overall morphology of HA coats that formed on both Bioglass® varieties much more similar (Figure 18, middle and right panels).

3.4.5 - Adsorption of protein to Bioglass® variety surfaces – ESEM and XPS analyses

To investigate whether spinodal and droplet type Bioglass® varieties would absorb a coat of proteins to their surface when exposed to bodily fluids, we incubated the samples in a model protein solution, bovine serum albumin (BSA), that is abundantly present in blood serum as well as in the serum component of cell culture medium [81].

We first applied environmental scanning electron microscopic (ESEM) analyses of wet and dry Bioglass® samples that were incubated in BSA-solution or not. All samples appeared similarly un-contoured, both at lower (500x) and higher (5,000x) magnifications, suggesting that if a protein coat had formed, it must be thin and overall of homogenous appearance (Figure 19). Note these samples were not pre-incubated in PBS solution; hence no HA coat is present on the samples.

Next, we used XPS to better determine whether a coat of protein had adsorbed to the sample surfaces. A pronounced nitrogen (N) signal was detected by XPS analyses on all samples that were submersed in BSA-solution but not on the bulk glass, indicating that indeed a protein coat had formed on the surfaces of the BSA-incubated samples. Moreover, the percentage of nitrogen detected in the BSA-coated spinodal type Bioglass® samples was significantly higher compared to droplet type samples (20.5±1.5%, compared to 13.4±1.6%, Table 1), suggesting that more protein adsorbed to spinodal compared to droplet-type Bioglass® samples. Additionally, the amount of Ca and particularly the amount of Na detected by XPS on the glass samples immersed in BSA solution was significantly reduced (Ca on spinodal: 6.8±1.5 % before, 4.6±1.7 % after immersion; Ca on droplet: 6.9±1.5 % before, 4.3±1.8 % after immersion; Na on spinodal: 20.6±1.8 % before, 4.3±1.9 % after immersion; Na on droplet: 15.5±1.8 % before, 6.5±2.0 % after immersion, Table 1), further suggesting that a thin layer of protein had coated the Bioglass® surface.

Additionally, XPS analyses of the surfaces of spinodal and droplet Bioglass® samples after 2h pre-incubation in PBS (and hence with a layer of HA present on their surface) led to a significant difference in the detection of nitrogen (Table 1), indicating that BSA robustly adsorbed to both, HA and polished Bioglass® sample surfaces; and again, that more protein adsorbed to the HA layer on spinodal type Bioglass® compared to the amount adsorbed to HA-coated droplet-type Bioglass® surfaces (concentration of N ~22.0±0.5 vs 14.7±0.5 %, Table 1). Combined, our data indicate that indeed a thin protein film (still allowing detection of the underlying glass and HA chemistry) had formed on both Bioglass® surfaces (too thin for ESEM detection), with significantly more protein adsorbing to spinodal Bioglass® samples.

3.4.6 - Conformation of proteins adsorbed on Bioglass® samples – Raman spectroscopy

To investigate whether BSA adsorbed to spinodal and droplet phase separated Bioglass® varieties adopted different conformations we applied Raman spectroscopic analyses. Both infrared (IR) and Raman vibrational spectroscopies have been used successfully in the past to analyze the conformational state of proteins such as BSA adsorbed on different glass surfaces [82-86]. The amide groups of proteins possess nine characteristic vibrational modes or group frequencies [82]. Of these, the most useful for vibrational spectroscopic analysis of the secondary structure of proteins in aqueous media is the so-called Amide I band located between ~1600 and 1700 cm^{-1} [82-86]. This band represents primarily the C=O stretching vibrations of the amide groups coupled to the in-plane N-H bending and C-N stretching modes [82, 84, 85]. The exact frequency of this vibration is determined by the particular secondary structure adopted by the polypeptide chains. However, when conformations of proteins in solution are of interest, Raman spectroscopy is usually preferred over IR spectroscopy as the signal at 1645 cm^{-1} from water is very weak in Raman spectra (corresponding vibrations have very low Raman activity) and thus does not interfere with the reliable detection of the critical Amide I band. The Raman Amide I band representing the contours of BSA protein and shown in Figure 20 consists of a number of overlapping component bands, representing α-helices, β-sheets, β-turns and non-ordered structures comparable to previous analyses [82-86]. The exact assignments of the observed Raman peaks in the Amide I band (shown in Figure 21A-C) were made on the basis of known data [82, 84, 85], and are summarized in Figure 21D. Decomposition of the experimental Raman spectra of the Amide I band into Gaussians (Figure 21D) allows for evaluating the β-sheet/β-turn ratio, which is known to indicate biocompatibility of the material under consideration [82, 83, 86]. We determined a 2-3 times higher β-sheet/β-turn ratio and also an increased α-helix content for BSA-polypeptides adsorbed to spinodally phase separated Bioglass® in comparison to droplet type phase separated glass (Figure 21D). Interestingly, the α-helix content in BSA-polypeptides adsorbed on both Bioglass® varieties was lower compared to lyophilized BSA, further indicating that the conformation of BSA-polypeptides adsorbed on the

Bioglass® samples was modified (less ordered). This observation is in agreement with previous findings on proteins adsorbed to other biomaterials [87, 70].

3.5 - Discussion

Here we demonstrate using two types of bioactive glasses that sub-micron structure is influential to how cells sense their substrates. Initial experiments performed using TAMP scaffolds with different nanopore sizes yet similar surface areas suggested that the glass surface characteristics had an influence only during initial attachment of the cells, as after longer time points the difference was no longer observed. These data suggest that cells may recognize the glass surface initially and then secrete their own extracellular matrix making the glass surface nano-structure negligible. Still the mechanism by which the cells sensed the surface of the glass was not realized. Further analysis into this mechanism was performed using 45S5 Bioglass®.

Conventional 45S5 Bioglass® invented by Hench in the 1960s has mostly been considered to be a structurally homogeneous, single phase glass [88-90, 8]. However, this may not always be true [91-93], as the morphology of Bioglass can for example be modulated following a simple melt-quench procedure, resulting in spinodal versus droplet-type phase separation [68]. In the Bioglass® samples investigated here, the two types of phase-separation arise from the difference in the melt temperature just prior to casting and the quench rate during solidification [68]. We show that the type of phase separation can have a pronounced effect on cellular response. Thus, better understanding Bioglass®/cell interaction appears crucial for the future design of improved bioactive glass applications.

When seeding MC3T3-E1 pre-osteoblast cells on the two phase-separated Bioglass® varieties we found that, on average, more than double the number of cells attached to the surface of spinodal glass at 2 and 24 hours post seeding as compared to droplet-type phase-separated Bioglass® samples. Increased cell adhesion correlated with significantly increased cell spreading (individual cells on average covered 84% more area on spinodal glass samples), the formation of significantly more, and more robust stress

fibers (by 65%), and better-developed focal cell adhesions (by 38%). What then causes the difference in cellular behavior?

As adhered cells are surrounded by culture medium, it is feasible to postulate that spinodal and droplet Bioglass® varieties differently modify the culture medium (e.g. pH, and the ability to form a HA coat), which in turn would affect cell response. However, when we incubated spinodal and droplet-type phase-separated Bioglass® samples in biological solutions (PBS, cell culture medium), we only observed minimal changes in pH that remained well within the physiological range of biological systems [94, 95]; and both Bioglass® varieties exhibited very similar dissolution characteristics (concentration of Ca2+ and PO43- in solution over time).

SEM as well as XPS analyses showed that on both Bioglass® varieties a robust layer of HA formed within 3 days in PBS. The chemical composition and the fine structure of the HA crystals was similar on both Bioglass® varieties consisting of comparable dense, intertwined long lamella- or plate-like HA crystals (Figure 18), yet composed of crystals exhibiting a somewhat different size (Figure 18, panels 1). However, resulting surface roughness differences on this scale are unlikely to produce a discernable difference to the attachment and performance of MC3T3-E1 cells [96]. Interestingly, the morphology of the formed HA layer corresponded to the underlying Bioglass® morphology, with spinodal phase separated samples accumulating an overall homogeneous layer of HA crystals, while droplet-type phase-separated samples accumulated a layer of boulder-like HA clusters. As expected, the boulder center-to-center spacing correlated well with the phase-separated pattern of this Bioglass® variety (compare Figures 14 and 18). However, when samples were incubated in cell culture medium after exposure to PBS (as was done with Bioglass® samples examined for cell attachment), HA boulders partially disappeared and were much less pronounced, making both HA coats morphologically similar (Figure 18, middle and right panels), suggesting that differences in HA coat formation also only has a minor impact on cell response.

Intriguingly, XPS analyses further indicted that both Bioglass® varieties absorbed a layer of proteins, either adsorbed directly to the polished glass surface (if samples were not incubated in PBS solution or cell culture medium), or on top of the HA layer (see

Table 1). As XPS only probes the top ~10 nm of a sample surface, and in all cases the glass or HA chemistry was detectable underneath the protein coat (as indicted by the signal for Si, Ca, and Na, none of which is present in proteins, see Table 1), our results indicate that the protein coat likely is thin, consisting of only 1 – 2 layers of protein molecules, consistent with reports on protein films that adsorb to the surfaces other biomaterials [97-101, 70, 102]. In its mature, soluble form BSA is a globular protein, which consists of 583 amino acid residues, has a molecular weight of 66.5 kDa, and measures 14 x 4 x 4 nm in diameter [103, 104]. We chose bovine serum albumin (BSA) as a model protein, although it likely is not the protein species that directly interacts with integrin cell adhesion receptors (it has no arginine-lysine-aspartic acid-based amino acid integrin binding sequences, commonly known as RGD signals). However, BSA is abundantly present in blood and the serum component of cell culture medium (61% of all protein present [81], and thus has the potential to readily adsorb onto the surface of bioactive glasses when exposed to body fluids. Likely, BSA also mediates the adsorption of other, less abundant serum proteins (e.g. ECM proteins) [105], further supporting a critical role of BSA in mediating cellular response to biomaterials surfaces.

Interestingly, we found that significantly more protein adsorbed to spinodal Bioglass® samples compared to droplet-type samples (20.5±1.5%, compared to 13.4±1.6%, Table 1), suggesting that the adsorbed protein potentially formed a thicker, or more homogenously distributed film that may contribute to the better biological performance of the spinodal phase separated Bioglass® samples. Remarkably, Raman spectroscopy further indicated a 2-3 times higher β-sheet/β-turn ratio of BSA-polypeptides adsorbed to spinodally phase separated Bioglass® samples in comparison to BSA polypeptides adsorbed to droplet type phase separated samples. Higher β-sheet/β-turn ratios of adsorbed proteins have been correlated with an increased biocompatibility of protein-coated surfaces [82, 83, 86]. Furthermore, the **α**-helix content in BSA-polypeptides adsorbed to both Bioglass® varieties was lower compared to the α-helix content of solubilized BSA. As BSA in solution is a well-ordered protein, exhibiting approximately 60% **α**-helicity [106, 105, 104], the observed decrease in **α**-helicity indicates that BSA polypeptides are less folded when adsorbed to Bioglass®. These

observations correlate well with conformational alterations seen generally in proteins that adsorb to other surfaces [87, 70].

As it is now well accepted that proteins in solution (e.g. blood, lymph, or cell culture medium) are readily and robustly adsorbed on the surface of bioactive materials [97-99, 107, 100, 101, 70, 102], we expect that cells did not attach directly to the native Bioglass® surface or to the HA layer, but through a protein film that adsorbed onto the surface of the scaffolds (or the HA layer). Our work investigating nanopore size influence on cellular attachment is on the scale of ~10 nm [9] which correlates with the dimension of adsorbed proteins.

Whether the glass surface was activated by HA or not apparently did not significantly influence the amount of BSA that adsorbed to the surface of Bioglass®, as the amount of nitrogen detected by XPS analyses was comparable on both, HA-coated and as-polished, uncoated samples. Similarly, Garcia et al. found no difference in the amount of fibronectin (an extracellular matrix protein) that adsorbed to the surface of bioactive glass either unreacted or reacted for 1 day and 7 days in simulated body fluid (SBF) [108]. Furthermore, they found that cells attached more strongly to the glass that had been reacted to form HA and attributed it to the morphology of the adsorbed proteins. In this context, our results suggest that HA formation per se is not required for a glass to be considered bioactive, as proteins present in biological solutions will – upon exposure – likely absorb immediately to the glass surface. However, nanoscale structure of HA, when present, will likely modulate the level of bioactivity by influencing the amount and conformation of proteins that adsorb. Taken together, our results provide evidence that cell attachment to 45S5 Bioglass® is mediated by a protein layer whose conformational state on spinodally phase-separated glass samples evidently represents a more favorable attachment surface for MC3T3-E1 pre-osteoblast cells. This type of surface makes spinodal Bioglass® varieties biologically favorable over droplet-type phase separated varieties. Apparently, these characteristics are more conducive for cell attachment and proliferation on spinodal than droplet type phase separated Bioglass®.

3.6 - Conclusions

Several important conclusions can be drawn regarding how cells interact with bioactive glasses. The present results demonstrate that initial cell attachment to the bioactive glass surface is likely influenced by a thin film of protein that is adsorbed whether or not an HA layer is present. Thus, the cells do not interact with glass directly. Further, the results support the concept that cell-attachment to a bioactive glass is mediated by this protein layer whose magnitude and conformational state depend on the local chemistry and nanoscale structure of underlying bioactive glass/HA surface. Taken together, our results provide novel, exciting insight into the interactions of proteins and cells with bioactive scaffolds that should be considered for the future development and use of bioactive glass scaffolds. Additionally, the biological performance of 45S5 Bioglass® and of other bioactive glass and glass-ceramics can be improved further with a relatively simple, inexpensive fabrication procedure that provides optimized micro-nano structure of glass.

3.7 - Materials and Methods

3.7.1 - Glass fabrication

45S5 Bioglass® ($45SiO_2$ – $24.5Na_2O$ – $24.5CaO$ – $6P_2O_5$ by wt. %) was synthesized using melt quenching and casting in stainless steel molds. High purity (99.99 % or better; Alfa Aesar, MA, USA) carbonates ($CaCO_3$, Na_2CO_3), silicon dioxide (SiO_2) and calcium phosphate tribasic ($Ca_5OH(PO_4)_3$) powders (Alfa Aesar, MA, USA) were used as raw precursors, and melted in a platinum crucible. To induce spinodal phase decomposition, the melt was quenched from ≥1380 ^oC into preheated molds (termed "spinodal" glass). Quenching from ≤1370 ^oC produced 45S5 Bioglass® with pronounced droplet type phase separation (termed "droplet" glass) [68]. Post-cooling, cylindrical casts were cut into approximately 2 mm thin disks using a low-speed diamond-plate circular saw (IsoMet, Buehler, IL, USA), polished to optical quality using a series of silicon carbide abrasive papers with decreasing particle size (d) (paper #120 with d = 125 μm; #240 with d = 58 μm; #800 with d = 8 μm; #1200 with d = 3 μm) and finally with 1

μm size CeO2 powder on an automatic polishing machine (ATA, Sapphir500, Germany). Polished glass samples were cleaned in acetone prior to use.

.

3.7.2 - X-ray photoelectron spectroscopy of uncoated and protein-coated samples

Polished and acetone-cleaned glass samples were rinsed with deionized (DI) water, dried, and characterized initially with high-resolution X-ray photoelectron spectroscopy (XPS). Then the samples were submerged into an aqueous bovine serum albumin (BSA) protein solution (2.5 mg/ml) for 2 hours at room temperature. Additionally, a set of samples was sterilized by autoclaving and incubated in 1xPBS (phosphate buffered saline) at 37°C for 3 days prior to incubation in BSA/PBS (2.5 mg/ml) solution for 2 hours. All samples after immersion were washed with DI water to remove excess salts/protein and dried before XPS analyses. The high-resolution XPS measurements were performed with a Scienta ESCA-300 spectrometer using monochromatic Al Kα X-rays (1486.6 eV). XPS spectra were recorded in a normal emission mode, using a low energy (<10 eV) electron flood gun to neutralize surface charging from photoelectron emission. The XPS data consisted of survey scans over the entire binding energy (BE) range and selected scans over the core-level photoelectron peaks of interest. Data were collected from different locations of the same samples (at least 5/sample) as well as on different samples (n = 3/sample type) to confirm the reproducibility of results. This resulted in compositional data, calculated as a ratio between the areas of core level XPS peaks of constituent chemical elements and appropriate sensitivity factors, with maximum statistical uncertainty of 2%.

3.7.3 - Raman spectroscopy of protein-coated samples

To characterize the structure of proteins adsorbed on glass surface Raman spectroscopy measurements were performed in the 800-2000 cm^{-1} range with a Horiba Xplora confocal microscope (Horiba, NJ, USA), using a 532 nm laser for excitation. Spectra collected from five different locations of each sample were averaged to increase

confidence in the data. Peaks for BSA were assigned to known structural motifs (α-helix, β-sheet, and β-turn) according to published literature. To calculate β-sheet/β-turn ratio, the β-sheet band area was divided by the average area of the two assigned β-turn bands as per Gaussian fit.

3.7.4 - SEM and ESEM surface analyses of uncoated and protein-coated samples

Scanning electron microscopy (SEM) images of the microstructure of the prepared glasses were acquired from freshly fractured surface of the glass samples using a Hitachi 4300 (USA) SEM in high-vacuum mode at 12,000x and 18,000x magnification. To examine the Bioglass® samples with adsorbed protein coat under physiological (wet) conditions, polished specimens were imaged as reference before protein-incubation with a FEI XL-30 environmental scanning electron microscope (ESEM) at 250x, 500x, 1000x, and 5000x magnification using the gaseous secondary electron detector (GSE) at approximately 30% humidity. Then, samples were submerged in bovine serum albumin (BSA) (2.5 mg/ml)/DI water protein solution for 2 hours at room temperature and re-imaged immediately (wet) under the same conditions. After drying of the samples, a third set of images was acquired (dry).

Additionally, to examine formation of hydroxyapatite (HA) and/or other alterations of the glass surface that may occur upon exposure to medium containing phosphate ions, images were collected using a Zeiss 1550 electron microscope. As described above, samples were pre-incubated in PBS before exposure to BSA solution, then dried overnight in a desiccator before imaging at 1,000x, 6,000x, and 18,000x magnification.

3.7.5 - pH measurement, colorimetric calcium and phosphate concentration assays

Samples were autoclaved for sterilization followed by incubation in 1x PBS at 37 °C. After 3 days, the PBS was replaced with cell culture medium (described below) and incubated for 2 and 24 hrs. The medium was collected and pH measured immediately to prevent any potential changes due to environmental exposure. Calcium (Ca^{2+}) and phosphate ion (PO_4^{3-}) concentrations were measured in PBS solution and cell culture

medium using Quantichrom bio kits (BioAssays Systems, Hayward, CA; Cat. # DICA-500 and DIPI-500, respectively). The former assay was performed by generating a standard curve using the supplied reference solution. 5µl of medium sample was incubated with 200µl of working reagent. Reactions continued for 3 minutes at room temperature before absorbance was measured at 612nm using a Tecan Infinite M200 PRO spectrophotometer. Each solution was measured in triplicate. To determine Pi the Quantichrom Phosphate assay used a standard curve utilizing the supplied solution. 50µl of each sample were diluted 1:50 with DI water and incubated in a 96-well plate together with 100µl of working reagent at room temperature for 30 minutes. Absorbance was measured for each solution in triplicate at 620nm.

3.7.6 - Cells and cell assays

MC3T3-E1 subclone 4 mouse pre-osteoblast cells (CRL-2593) were purchased from American Type Culture Collection (ATCC, Manassas, VA). Cells were maintained at standard culture conditions at 37 °C in a 5% CO2 atmosphere and 100% humidity in complete medium as follows: Alpha-Modified Eagles Medium (α-MEM, Gibco/Invitrogen, Grand Island, NY, cat. # A10490-01) was supplemented with 10% fetal bovine serum (Atlanta Biologicals, Flowery Branch, GA, Cat. # S11150), 1% L-glutamine (HyClone, Logan, UT, Cat. # 25-005-C1) and 1% penicillin/streptomycin (Corning, Corning, NY, Cat. # 30-001-Cl) according to vendor's instructions.

Before cell seeding, polished and acetone-cleaned glass samples were sterilized by autoclaving and pre-incubated in 1xPBS for 3 days at 37 °C. MC3T3-E1 cells were seeded at a density of 35,000 cells/cm^2 onto respective glass disks placed into 3.5 cm diameter polystyrene tissue culture dishes (Corning, Corning, NY, Cat. # 353001). Cells were processed for analysis by fluorescence detection of nuclei by incubating in DAPI solution (Molecular Probes, Eugene, OR, Cat. # D1306), actin by incubating in Alexa488-phalloidin solution (Molecular Probes, Cat. # A-12379), and focal adhesions by immunofluorescence detection of the protein vinculin. In brief, cells were fixed using 3.7% formaldehyde followed by permeabilization with 0.2% Triton X-100. Then, cells

were blocked in 1% BSA/1xPBS at room temperature for 1 hour. The primary antibody, anti-vinculin (mouse monoclonal-Sigma, St. Louis, MO – Cat. #V9131; at 1:200), was diluted in blocking solution and incubated with cells overnight at 4 °C. A solution of 1xPBS containing DAPI (1 μg/ml:), Alexa488-phalloidin (1:100), and secondary antibody, Alexa568-conjugated goat-anti-mouse (1:200) (Molecular Probes/Invitrogen, Grand Island, NY, Cat. # A11031) was incubated with the cells at room temperature for 1 hour. Samples were placed with cells facing down in 1xPBS into glass-bottom culture dishes (LabTek) for microscopic examination. Cells were imaged using a Nikon Eclipse TE2000-E inverted fluorescence microscope equipped with 10x, 40x, 60x and 100x objectives and a forced-air cooled Photometrics CoolSnap HQ CCD camera (Roper Scientific, Martinsried, Germany). Images were captured using MetaVue (Molecular Devices, Sunnyvale, CA) software version 6.1r5.

For quantification of the number of cells attached to each sample, cell nuclei were counted for each of 6 images acquired with a 10x objective (approximate imaging field = 1 mm^2) for each sample (2 hour time point, n = 5; 24 hour time point, n = 4). Statistical analyses were performed by ANOVA followed by a Bonferroni correction to reduce the chance of obtaining a false positive, which reduced the p-value from $p = 0.05$ to $p = 0.0167$, increasing the stringency of the statistical analyses. Average cell size was determined on images of Alexa488-phalloidin stained cells (i.e. actin) by outlining the periphery of individual cells and measuring the cell area using ImageJ (droplet samples, n = 44; spinodal samples, n = 23 cells). Abundance of peripheral actin (stress fibers) was analyzed by drawing 7.5 μm x 7.5 μm squares (= 55 μm^2) near the periphery of Alexa488-phalloidin stained cells. Fluorescence intensity within the square areas was measured using ImageJ (droplet-type samples, n = 40; spinodal samples, n = 27). Similarly, abundance and robustness of focal adhesions was analyzed by drawing 10 μm x 10 μm squares (= 100 μm^2) near the periphery of vinculin stained cells and measuring fluorescence intensity within the squares (droplet-type samples, n = 15; spinodal samples, n = 12).

3.8 – Figures

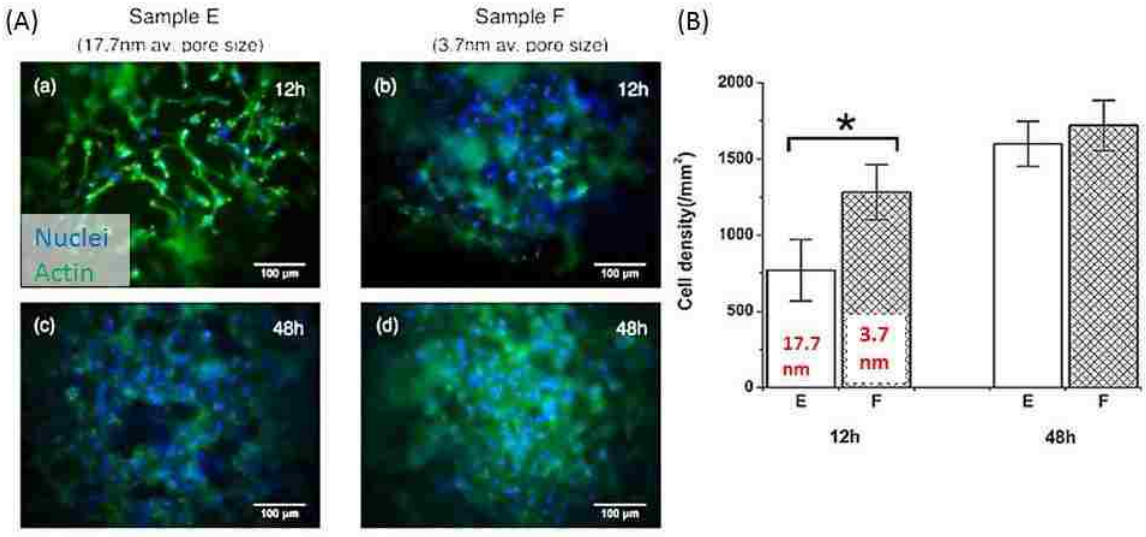

Figure 13: Cells sense differences in nanopore size

(A) Representative images of (a) samples E at 12h, (b) samples F at 12h, (c) samples E at 48h, and (d) samples F at 48h post cell seeding. MC3T3-E1 cells were stained for actin (green) to evaluate cell morphology and nuclei to quantify cell density. (B) Cell density on samples E and F 12 and 48 h after seeding showed a strong difference after 12h but not after 48h.

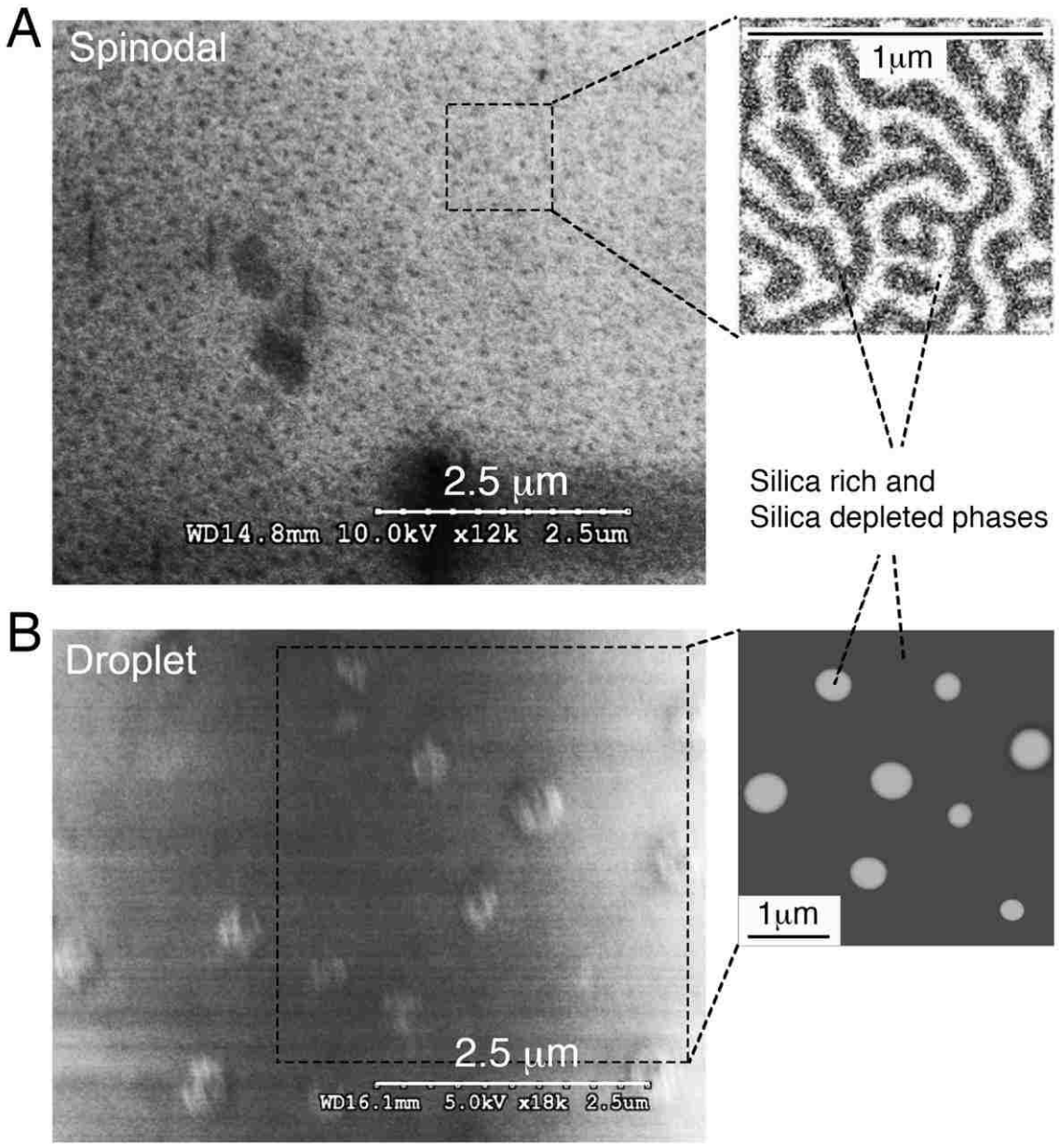

Figure 14: 45S5 Bioglass® varieties with different morphologies
45S5 Bioglass® samples with spinodal and droplet type phase-separation morphologies were prepared by quenching the melt from different equilibration temperatures following specific regimens. Representative SEM images of the two varieties are shown in A and B. Simplified schematics of the morphologies to the right illustrate that silicon enriched and depleted regions co-exist in the two 45S5 Bioglass® varieties.

Table 1
Composition of as-polished spinodal and droplet type phase-separated 45S5 Bioglass® samples before and after exposure to 0.25% (w/v) aqueous BSA-protein solution as determined by XPS surface analyses.

Sample	Composition in at%					
	O	Si	Ca	Na	P	N
Glass Composition, Theoretical	55.2	16.3	9.5	17.2	1.8	0
Spinodal, as polished	56.9±1.2	13.9±1.7	6.8±1.5	20.6±1.8	1.8±1.0	0
Spinodal, exposed to PBS solution	61.2±2.0	<1	20.9±2.0	<1	16.3±1.5	0
Spinodal, exposed to BSA solution	54.5±1.7	14.5±2.0	4.6±1.7	4.3±1.9	1.6±1.3	20.5±1.5
Spinodal, exposed to PBS then BSA solution	57.0±2.0	<1	10.8±2.0	<1	9.1±1.5	22.0±0.5
Droplet, as polished	57.0±1.2	18.6±1.9	6.9±1.5	15.5±1.8	1.9±1.1	0
Droplet, exposed to PBS solution	60.6±2.0	<1	22.2±2.0	<1	15.8±1.4	0
Droplet, exposed to BSA solution	56.3±1.8	18.4±2.0	4.3±1.8	6.5±2.0	1.7±1.5	13.4±1.6
Droplet, exposed to PBS then BSA solution	55.9±2.0	<1	15.8±2.0	<1	12.5±1.5	14.7±0.5
Hydroxyapatite (HA)	60.8		21.7		13.0	

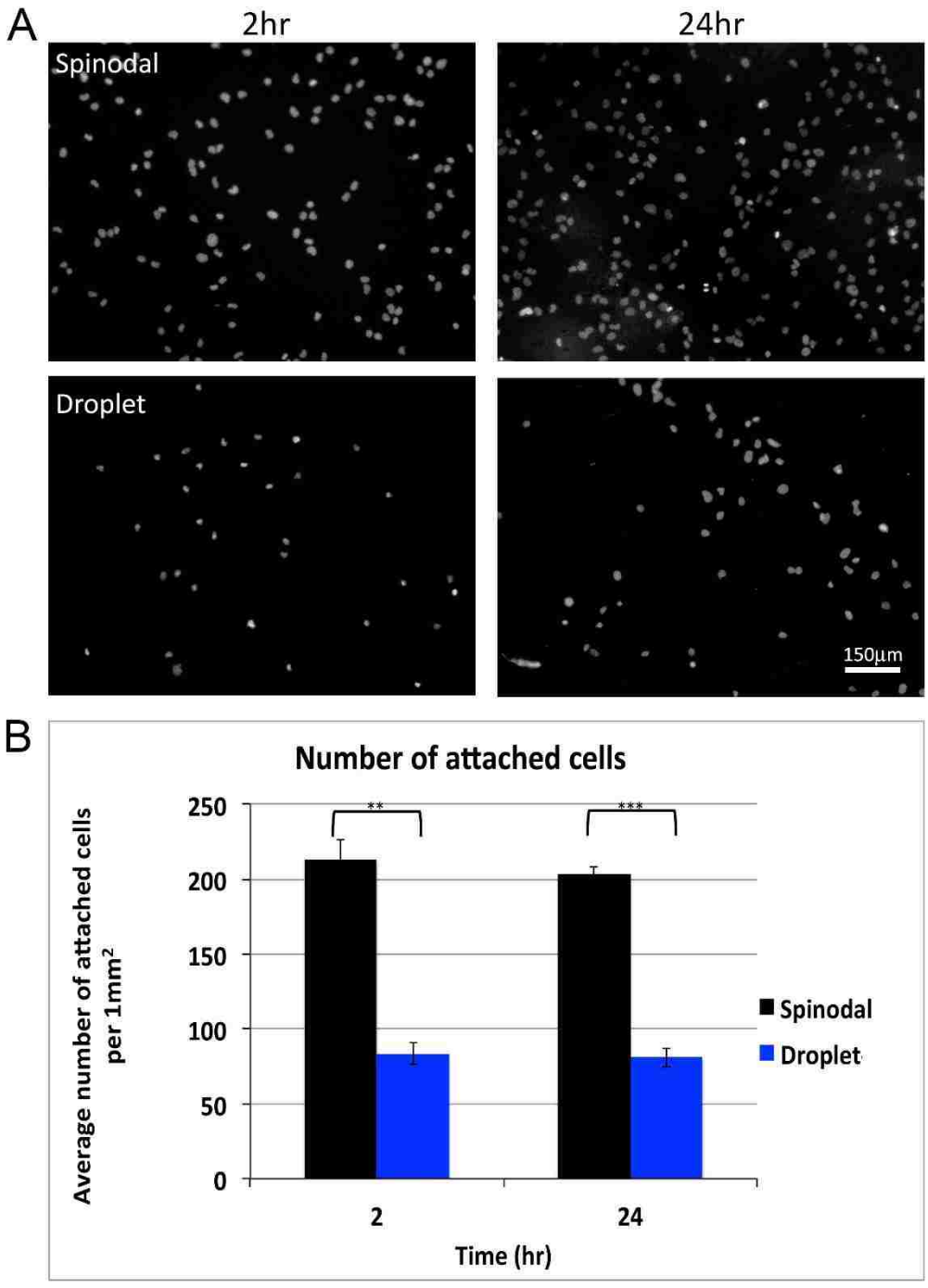

Figure 15: MC3T3-E1 pre-osteoblast cells attach more efficiently to spinodally phase separated Bioglass®

(A) Equal numbers of MC3T3-E1 pre-osteoblast cells were seeded onto polished, spinodal and droplet-type Bioglass® varieties. Cells were fixed 2 and 24 hours post seeding and cell nuclei stained with DAPI. Representative images are shown. (B) Quantitative analyses based on counting nuclei of 5 samples and of 5 areas for each glass type revealed that on average more than two times the number of cells attached to Bioglass® samples with spinodal compared to droplet type morphology.

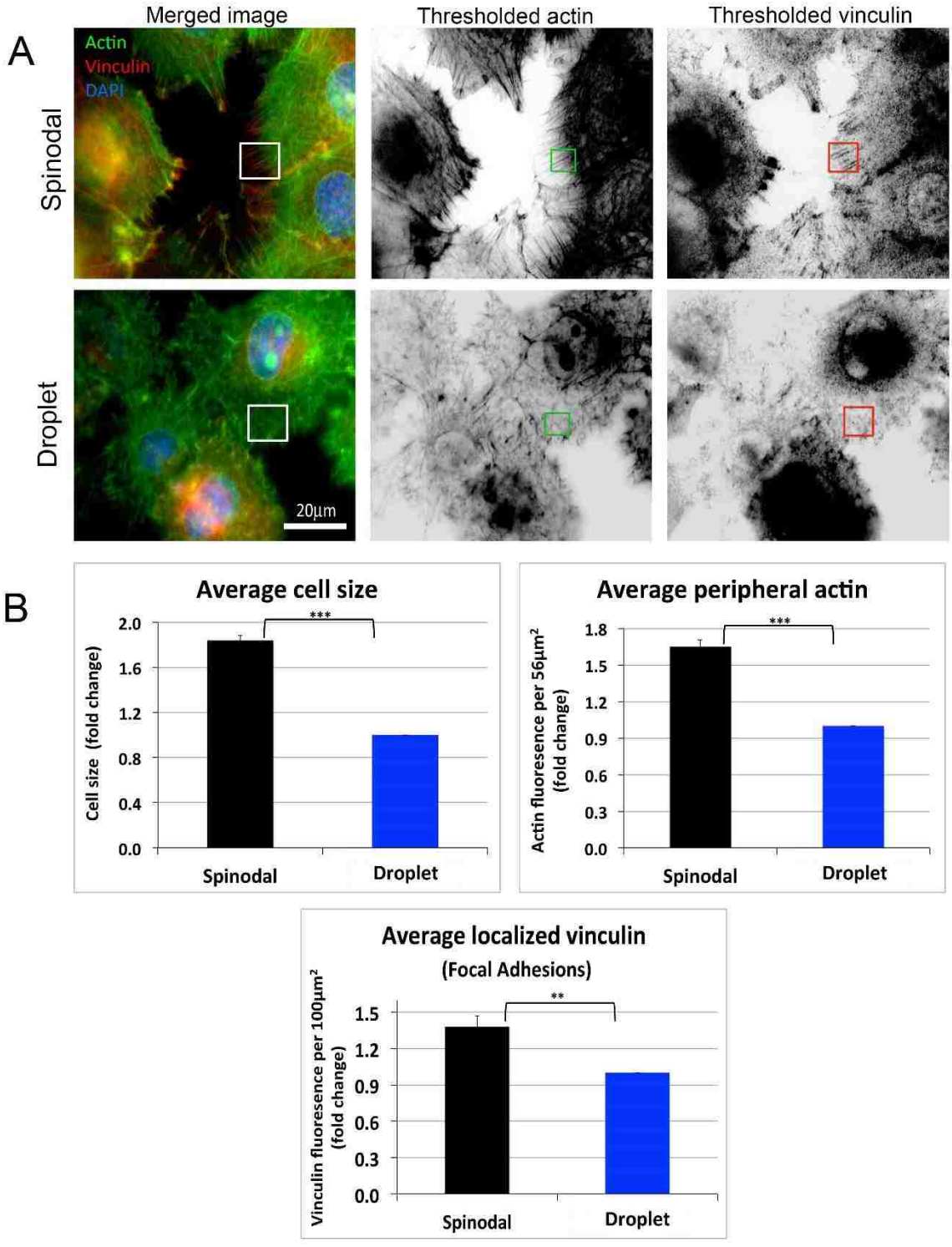

Figure 16: MC3T3-E1 pre-osteoblast cells attach more robustly to spinodally phase separated Bioglass®

(A) MC3T3-E1 pre-osteoblasts were seeded onto spinodal and droplet-type Bioglass® samples, fixed and stained 2 hours post seeding for actin (phalloidin, green), integrin-based focal adhesions (vinculin, red) and cell nuclei (DAPI, blue). Representative merged images are shown. Monochrome images of actin and vinculin fluorescence channels were black/white converted and thresholded for quantitative analyses. (B) Fluorescence intensities inside defined squares placed in cytoplasmic, plasma membrane-adjacent regions (example squares are shown in A) were quantified, averaged and graphed. Note that cells on spinodal-type samples assemble robust, well-organized stress fibers that often end in pronounced integrin-based focal adhesions. In contrast, cells growing on droplet-type samples assembled much less pronounced, less organized actin filaments and only a few, not well-developed focal adhesions.

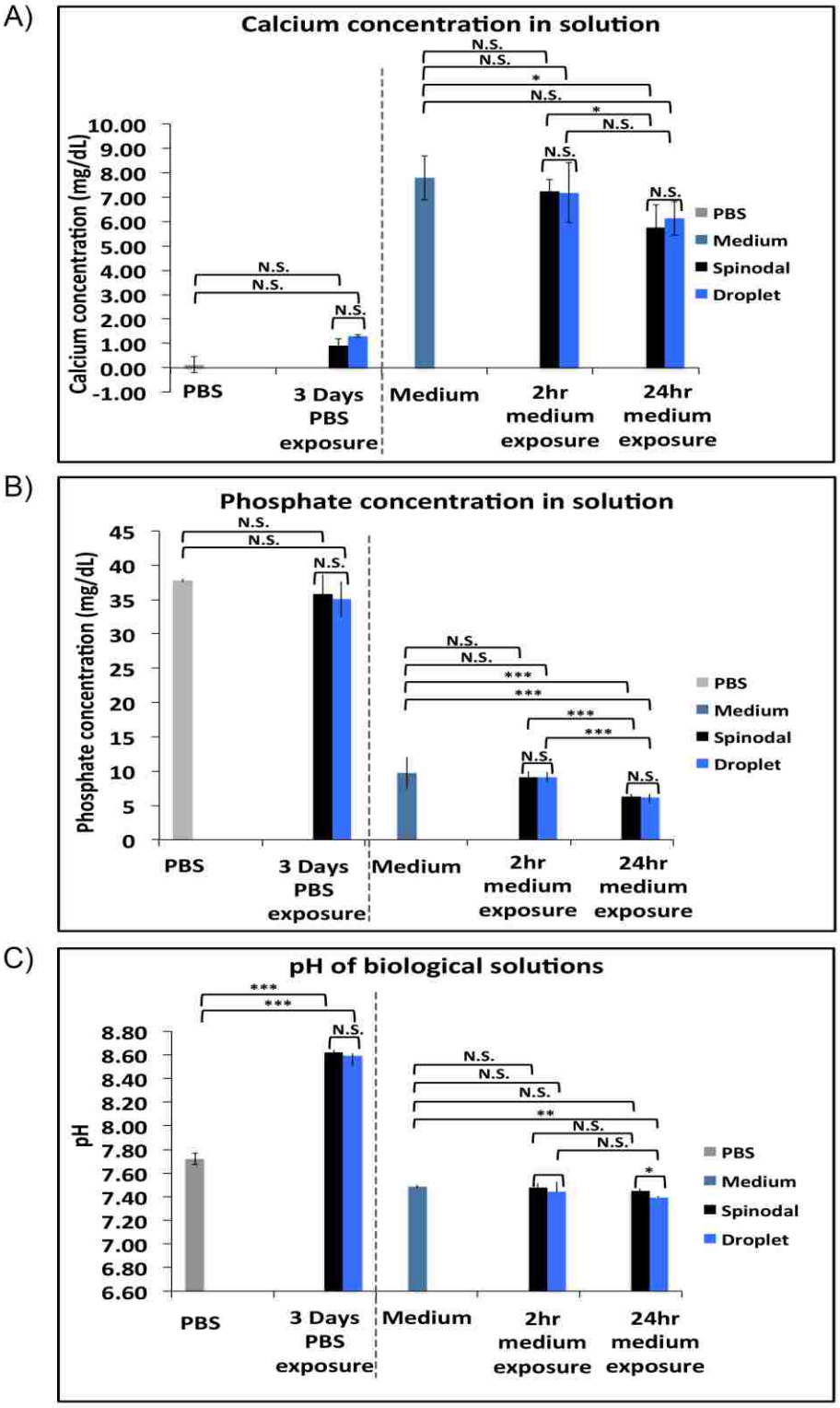

Figure 17: Effects of exposing spinodal and droplet phase separated Bioglass samples to biological solutions: calcium, phosphate, and pH

The concentration of Ca (A) and P_i (B) and the pH (C) was measured in phosphate buffered saline (PBS) and cell culture medium before and after exposure to either spinodal or droplet-type phase separated bioactive glass. Ca, P_i, and pH decreased slightly overtime, however no significant differences were detected between the two Bioglass® varieties.

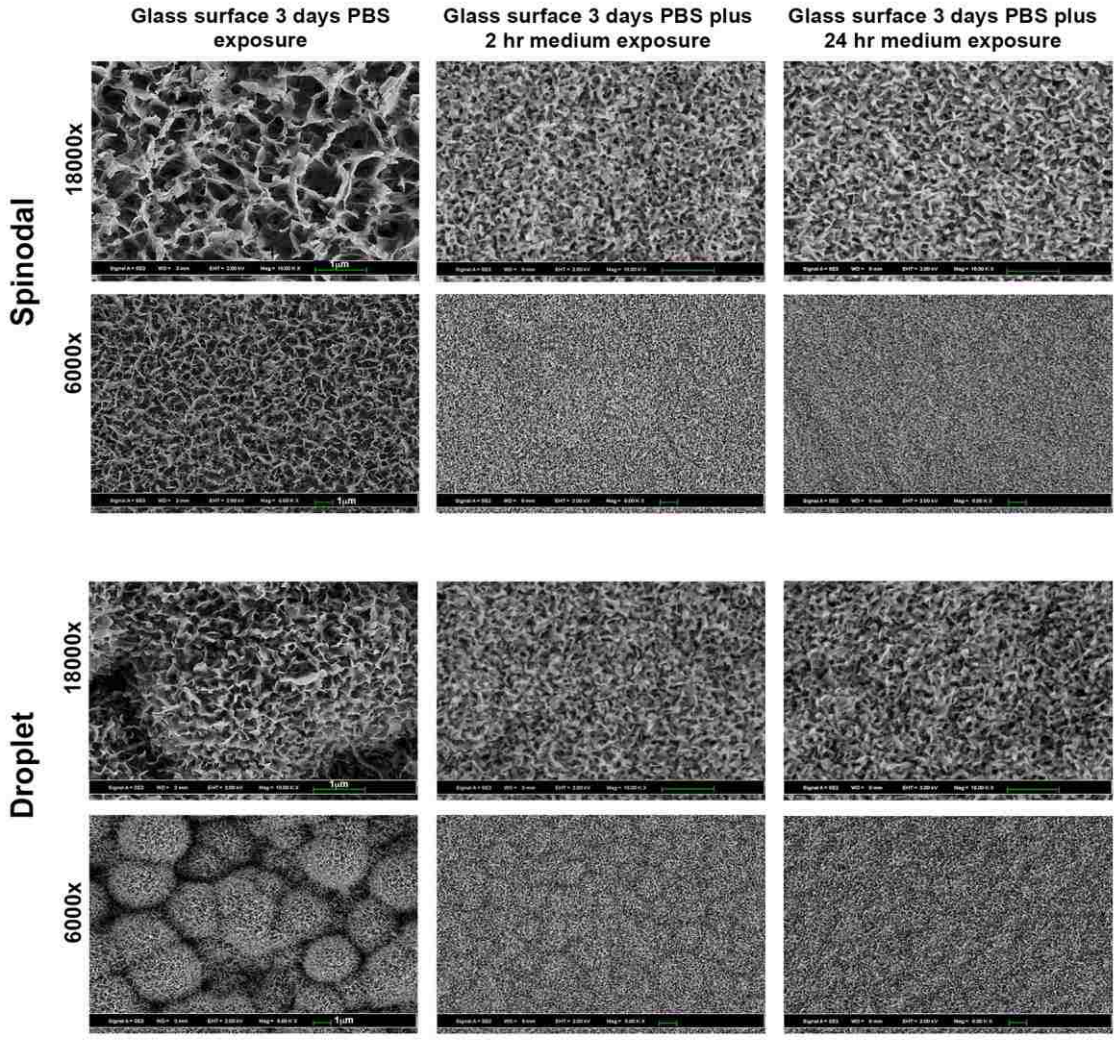

Figure 18: Surfaces of Bioglass® varieties after incubation in PBS and cell culture medium

Spinodal (top panel) and droplet type (bottom panel) phase-separated Bioglass® samples were investigated by scanning electron microscopy (SEM) after incubation in PBS for 3 days (left columns) and after an additional 2or 24 hour incubation in cell culture medium (middle and right columns respectively). A pronounced HA coat developed on both Bioglass® varieties that appeared more comparable when samples were incubated in PBS followed by cell culture medium as was done in cell culture experiments described in Figures 17 and 18.

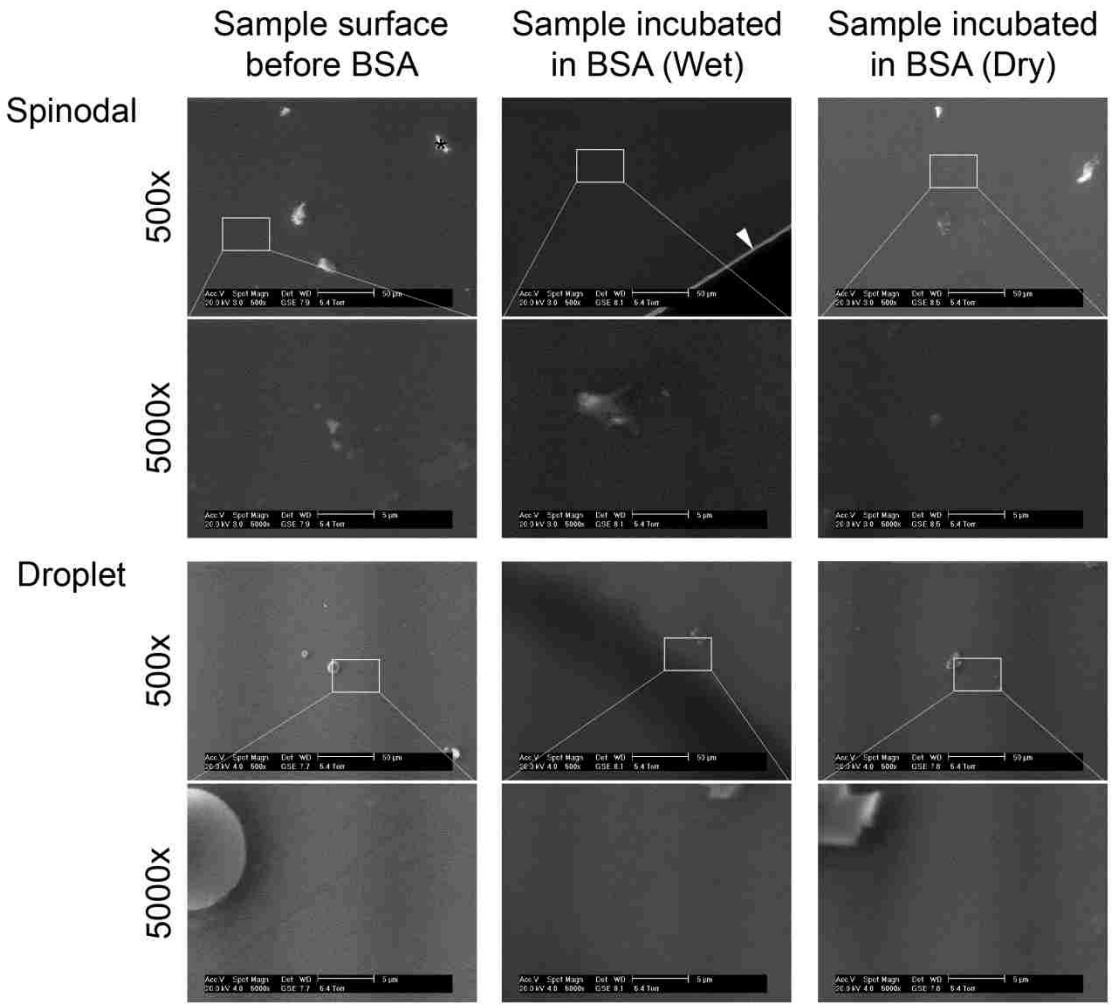

Figure 19: ESEM analyses of Bioglass samples before and after incubation in BSA-protein solution

Spinodal and droplet type phase-separated Bioglass® samples were investigated by environmental scanning electron microscopy (ESEM) before and after incubation in 0.25% aqueous BSA-protein solution imaged wet, and after drying. Samples appear un-contoured at both lower (500x) and higher (5000x) magnification under physiological conditions (wet) and after drying, indicating that the adsorbed protein layer is thin and below the applied SEM detection limit correlating with our XPS data (see below). Note contaminating dust particles (depicted with asterisk in image 1) and the edge of the glass sample (depicted with arrowhead in image 2) that served as reliable focusing guides.

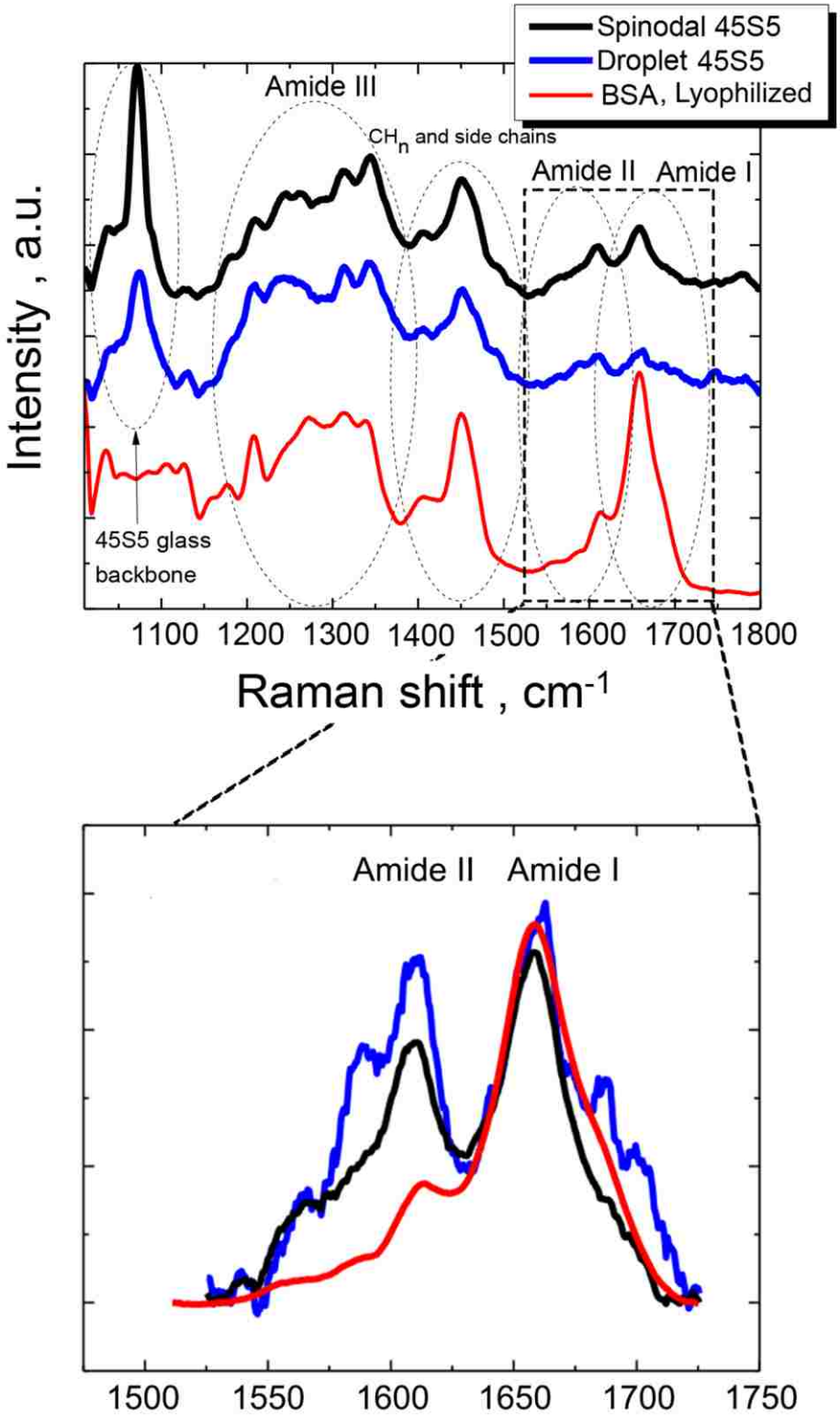
Spinodal 45S5
Droplet 45S5
BSA, Lyophilized
Amide III
CHn and side chains
Amide II
Amide I
45S5 glass
backbone
Intensity , a.u.
1100
1200
1300
1400
1500
1600
1700
1800
Raman shift , cm-1
Amide II
Amide I
1500
1550
1600
1650
1700
1750

Figure 20: Raman spectra of protein-coated Bioglass® varieties
Representative Raman spectra of lyophilized bovine serum albumin (BSA, red), and 45S5 Bioglass® varieties after incubation in aqueous BSA solution (spinodal, black; droplet, blue). Note the Amide I and II bands (enlarged and superimposed below) in all samples indicative of a protein layer that adsorbed on the glass sample surfaces.

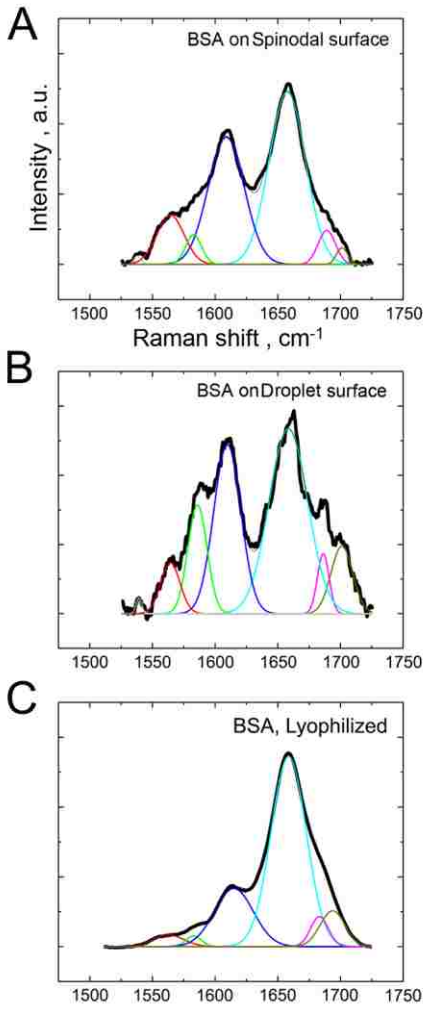

D

Position cm^{-1}	FWHM cm^{-1}	Relative area in %	Assignment
BSA adsorbed to Spinodal phase-separated 45S5 bioglass surface			
1564	25.9	10.0	Amide II
1583	15.2	4.0	Amide II
1609	34.0	34.0	β-sheet
1658	34.2	47.0	α-helix
1689	16.4	4.0	β-turn
1701	10.4	5.0	β-turn
BSA adsorbed to Droplet phase-separated 45S5 bioglass surface			
1564	18.2	6.0	Amide II
1586	18.0	12.0	Amide II
1610	25.5	27.0	β-sheet
1659	36.3	42.0	α-helix
1687	11.1	4.0	β-turn
1701	20.4	9.0	β-turn
BSA, Lyophilized			
1562	28.7	3.0	Amide II
1583	14.5	2.0	Amide II
1615	36.4	21.0	β-sheet
1659	33.0	61.0	α-helix
1683	16.7	5.0	β-turn
1694	23.2	8.0	β-turn

Figure 21: Gaussian fittings of Raman spectra indicate a different conformation of BSA adsorbed to spinodal and droplet Bioglass® varieties
Gaussian fittings (colored lines in graphs A to C) of Raman spectra of dried, BSA-protein coated spinodal (A), and droplet type phase separated 45S5 Bioglass® samples (B); and (C) of lyophilized BSA. (D) Quantitative analyses of Gaussian fittings of Raman spectra recorded for samples A to C and assignment of corresponding secondary protein

structures according to previously published studies. Note the increased β-sheet and α-helix content of BSA adsorbed to spinodal compared to droplet type phase-separated Bioglass® samples (depicted in red). FWHM = full width at half maximum of Gaussians.

Chapter 4 - Additional uses for the TAMP scaffolds - *Soft tissues*

4.1 – Abstract

The unique properties of our 30mol% CaO-70mol% SiO TAMP scaffolds may have potential for additional tissue engineering applications aside from bone tissue regeneration. For example, the porosity of the scaffold makes it similar to a porous membrane providing fluid / nutrient exchange to cells from all sides as opposed to tissue culture plastic. In addition, the cells might take cues from the scaffold topography that forms from the pores. These two features might provide researchers with a platform to grow cells in an environment that is more similar to the *in vivo* environment, allowing cells to maintain their normal structure / function (discussed in 4.2) or to even select for a specific cell type out of a mixture of cells (discussed in 4.3). The unique properties of the TAMP along with our ability to alter these properties allows for a broad range of potential applications.

4.2 – In vitro fertilization

During the process of *in vitro* fertilization, an egg is harvested from the mother-to-be and fertilized using sperm from the father-to-be. This fertilized egg is cultured in a dish for 3-5 days and then is implanted back into the mother-to-be [109]. The success rate of in vitro fertilization is in fact quite low, around only 30% [110], and is increased if a sample of the endometrial epithelial cells lining the uterus is collected and co-cultured with the egg, a technique called autologous endometrial co-culture (AEC) [111, 112]. These cells act as a nest and support development of the embryo. In the body, endometrial epithelial cells have a polarized morphology; however, when grown in culture, they lose their 3-dimensional structure and grow flat against the dish [113]. Since the TAMP scaffolds have a 3-dimensional structure and contain pores that allow the cells to be exposed to nutrients from all sides, the scaffolds might promote the

endometrial epithelial cells to retain their polarized morphology in culture. Evidence supporting this theory can be found in a study done by Cherney and Findlay, who observed that uterine epithelial cells (UEC) grown on Matrigel coated porous membranes maintained polarization [113]. However, Matrigel is a protein solution composed of the extracellular matrix produced by Engelbreth-Holm-Swarm (EHS) mouse sarcoma cells [114-117]; so even though it maintains polarization of the cells, this protocol is not likely to be approved by the FDA for use in fertility clinics.

4.2.1 – Results and discussion

Through collaboration with Dr. Stephen Somkuti at Abington Reproductive Medicine, we have characterized the growth of human uterine endometrial cells (hUECs) on our TAMP scaffolds. In brief, the surgeon takes a tissue biopsy of the lining of the uterus and stores the tissue in cell culture medium at 37°C until the sample can be transported to Lehigh that same day. Then the tissue is processed through digestion with collagenase to release the cells into solution. The cells are pelleted by centrifugation, collected, and plated for culture. The cells are grown in culture until they are nearing confluency before being frozen for storage. We followed this protocol of freezing before using the cells for experiments on the TAMP scaffolds because this is the protocol that Abington uses for AEC.

Initial experiments were performed to characterize the cells in their native state. Through this analysis, we could learn what morphological features to search for to indicate that the cells were growing polarized or more "naturally." To do this, a piece of tissue from a biopsy was fixed and prepared for analysis by SEM. The images showed that many of the cells were covered with cilia and microvilli (Figure 22 A, i and ii), suggesting that we should consider looking for cilia or microvilli to indicate polarization of the cells. Next we sought to determine which cells were present after tissue digestion. It was apparent that there were at least two cell types growing based on morphology. One cell type had a long stretched out shape that resembled a fibroblast. The other cell type had a smaller, rounder shape that resembled a glandular or epithelial cell (Figure

22B). The cells with the epithelial morphology tended to cluster together in groups. Although we expected to see two cell types from these digests, the results varied from patient to patient with some tissue digests resulting in a primarily epithelial morphology and others with a primarily fibroblast morphology. In order to identify these cell types, we utilized protein markers specific to the types of cells that were expected to be in the mixture (Chen et. al. 2013), stromal cells and endometrial epithelial cells. The stromal cells were expected to have the fibroblast-like morphology and to be positive for vimentin, whereas the epithelial cells were expected to be round and positive for cytokeratin. Uterine cells on coverslips were subjected to immunofluorescent staining of these protein markers, and analyses showed that while only some cells stained positive for cytokeratin (red), all cells stained positive for vimentin (green)(Figure 23, top panels). This result was unexpected, but still we see that there are two populations of cells present, those that are cytokeratin positive (likely epithelial cells) and those that are not (likely stromal cells). Once we determined that both cell types were likely present in the tissue digests, we looked to see whether both cell types would grow on the scaffold. Cells were seeded onto TAMP scaffolds and subjected to the same immuno-staining protocol for the coverslips. We overserved a similar result, with all cells staining positive for vimentin and some, but not all cells staining positive for cytokeratin, suggesting that both cell types grew on the scaffolds (Figure 23, bottom panels).

Finally, analysis was performed to determine whether cells were polarizing on the TAMP scaffolds. Initial experiments aimed at visualizing the morphology of the cells to determine whether the cells were stretching out across the glass surface or growing tall (polarized) on the scaffolds. To do this, we stained with Alexa488-phalloidin to visualize the actin cytoskeleton and DAPI to visualize the nuclei. Cells on a coverslip were more spread out by comparison to cells growing on a TAMP scaffold as evidenced by the bright cortically located actin bands near the periphery of the cells on TAMP. The difference in morphology of these cells and the transition from prominent stress fibers on coverslips to more diffuse and cortically localized actin bands on TAMP scaffolds suggests that cells on TAMP grow more 3-dimensionally and potentially tall (Figure 24). Since we had observed cilia on the surface of cells in the tissue sample by SEM, we next

looked for cilia on the surface of cells growing on TAMP. Both Arl13-b, a small GTPase that localizes to the ciliary shaft, and acetylated-tubulin were used as protein markers specific to the cilia. Uterine epithelial cells grown on coverslips had primary cilia on their surface (Figure 25), but did not have multiple motile cilia like the cells in the SEM images of the tissue. After a few unsuccessful attempts to visualize multiple cilia on cells growing on the TAMP scaffolds, besides one unconvincing pair of cells (Figure 25), we went back to the literature and realized that in reality, the number of ciliated cells is low. Even during the proliferative phase, the stage of the menstrual cycle that has the most ciliated cells, only around 20% of cells are ciliated [118, 119]. Future experiments would be better aimed at targeting microvilli or the localization of tight junctions in the membrane of the cells using confocal microscopy.

4.2.2 – Conclusions

The initial intention of this collaboration with Abington Reproductive Medicine was aimed at finding a way to increase the success of *in vitro* fertilization through providing the uterine endometrial cells with a more natural environment to grow, ultimately promoting development of the embryo during AEC. This project could however be taken in several different directions as outlined in more detail in section 5.2, including first using different methods of analysis to better show whether cells are polarized (look for microvilli, tight junctions, confocal and SEM analysis). In addition, parameters of the TAMP scaffolds (pore size, chemistry, etc) may be modified to enhance polarization of the cells. Finally, it may not even be necessary that cells polarize to indicate that they are growing in a more natural state, for example cellular secretion could be analyzed. The TAMP scaffolds could be used for other applications such as research requiring analysis to be performed on polarized cells in culture.

4.2.3 – Materials and methods

4.2.3.1 – Tissue digestion

Endometrial tissue was collected from a timed biopsy 5-9 days post luteinizing hormone surge and placed into a sterile container with RMPI medium (Sigma, St. Louis, MO, Cat.

R8758) that was supplemented with 10% fetal bovine serum (Atlanta Biologicals, Flowery Branch, GA, Cat. # S11150), 1% L-glutamine (HyClone, Logan, UT, Cat. # 25-005-C1) and 1% penicillin/streptomycin (Corning, Corning, NY, Cat. # 30-001-Cl). The tissue was kept at 37°C until it was collected from the surgicenter that same day by me and transported back to Lehigh. Once at Lehigh, the tissue was immediately processed by a series of digestions in warmed collagenase (Sigma, St. Louis, MO, Cat. # C6885). In brief, under the hood, tissue was removed from the sterile container and minced if samples were large enough to necessitate that. Next the tissue was transferred to a 15ml tube and incubated for 5 min at 37°C with agitation in 10ml of 0.2% collagenase, which had been prepared prior by solubilizing the collagenase in Hanks buffered saline solution and 0.5% penicillin/streptomycin. After agitation, tissue was allowed to settle for 5 minutes and the supernatant containing the cells was transferred to a new tube and centrifuged to pellet the cells, which were then re-suspended and plated for culture. Fresh collagenase was added to the tube with the tissue and the process was repeated a total of 4 times to make up 1-2 plates for culture. The remaining tissue pieces were plated in a separate dish. The following day, the plates were analyzed for cell growth and signs of contamination and half of the medium was exchanged for fresh medium to help remove red blood cells and other debris. Cells growth was observed for the next few days until they were nearing confluency, then they were cryopreserved in liquid nitrogen.

4.2.3.2 – Cell seeding

Cells were thawed quickly by incubation in a 37°C water bath before counting and seeding directly onto coverslips or PBS pre-incubated TAMP scaffolds (see section 1.5.1). 200,000 viable cells (determined by trypan blue) were seeded per well of a 24-well plate.

4.2.3.3 – SEM for tissue

A small portion of a tissue biopsy was fixed directly in 4% glutaraldehyde over night at 4°C before dehydration in a series of ethanol dilutions as described in section 2.6.4. The

tissue was coated with iridium and imaged using the Hitachi 4300 FEGSEM with secondary electron collection mode and 5.0kV accelerating voltage SEM.

4.2.3.4 - Immunofluorescence

Cells were processed for analysis by fluorescence detection of nuclei by incubating in DAPI solution (Molecular Probes, Eugene, OR, Cat. # D1306), actin by incubating in Alexa488-phalloidin solution (Molecular Probes, Cat. # A-12379), and vimentin, cytokeratin, and acetylated-tubulin by immunofluorescence detection. In brief, cells were fixed using 3.7% formaldehyde followed by permeabilization with 0.2% Triton X-100. Then, cells were blocked in 1% BSA/1xPBS at room temperature for 1 hour. The primary antibodies, anti-vimentin (rabbit monoclonal –D21H3, Cell Signaling, Beverly, MA, Cat. #5741; at 1:200) and anti-pan-cytokeratin (mouse monoclonal –C11, Santa Cruz Biotechnologies, Cat. #SC8018; at 1:200), or anti-acetylated-tubulin (rabbit polyclonal, Sigma, St. Louis, MO cat # 6-11B-1; at 1:250; at 1:200) and anti-γ-tubulin (rabbit polyclonal, Sigma, St. Louis, MO Cat. # T3559; at 1:500) were diluted in blocking solution and incubated with cells overnight at 4 °C. A solution of 1xPBS containing DAPI (1 µg/ml:) and secondary antibodies, Alexa568-conjugated goat-anti-rabbit or mouse (1:200) (Molecular Probes/Invitrogen, Grand Island, NY) or Alexa488-conjugated goat-anti-rabbit or mouse (1:200) (Molecular Probes/Invitrogen, Grand Island, NY) was incubated with the cells at room temperature for 1 hour. Samples were placed with cells facing down in 1xPBS into glass-bottom culture dishes (LabTek) for microscopic examination. Cells were imaged using a Nikon Eclipse TE2000-E inverted fluorescence microscope equipped with 10x, 40x, 60x and 100x objectives and a forced-air cooled Photometrics CoolSnap HQ CCD camera (Roper Scientific, Martinsried, Germany). Images were captured using MetaVue (Molecular Devices, Sunnyvale, CA) software version 6.1r5.

4.2.4 – Figures

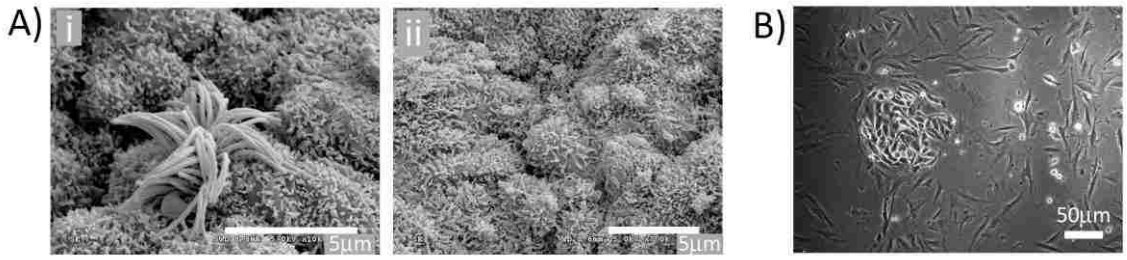

Figure 22: Morphological features of uterine endometrial cells
Cilia (i) and microvilli (ii) were imaged by SEM on the surface of cells in uterine endometrial tissue. Cells were isolated from these tissues by digestion in collagenase to releace the cells from the matrix. The resulting mixture of cells seemed to have two cell types, one with a fibroblast-like morphology and the other with an epithelial-like morphology.

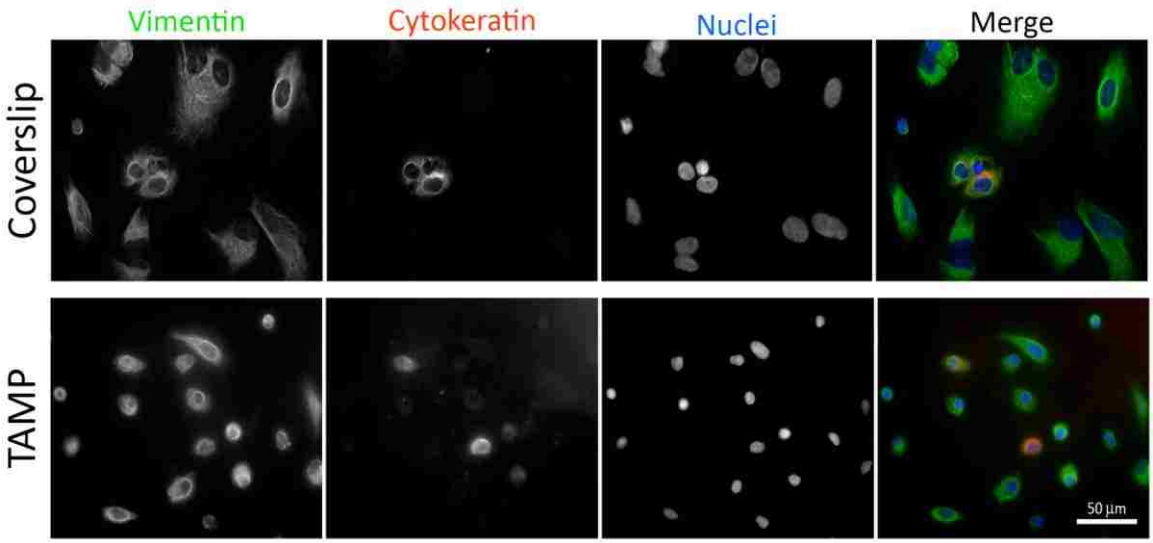

Figure 23: Both epithelial and stromal cells grow on TAMP scaffolds
Protein markers for stromal cells and epithelial cells were used to determine whether both cell types grew on the TAMP scaffolds. Stromal cells were expected to stain positive for vimentin while epithelial cells were expected to stain positive for cytokeratin. While all cells stained positive for vimentin, only a population of cells stained positive for

cytokeratin suggesting that both cell types were growing on the coverslips (top panels) and TAMP scaffolds (bottom panels).

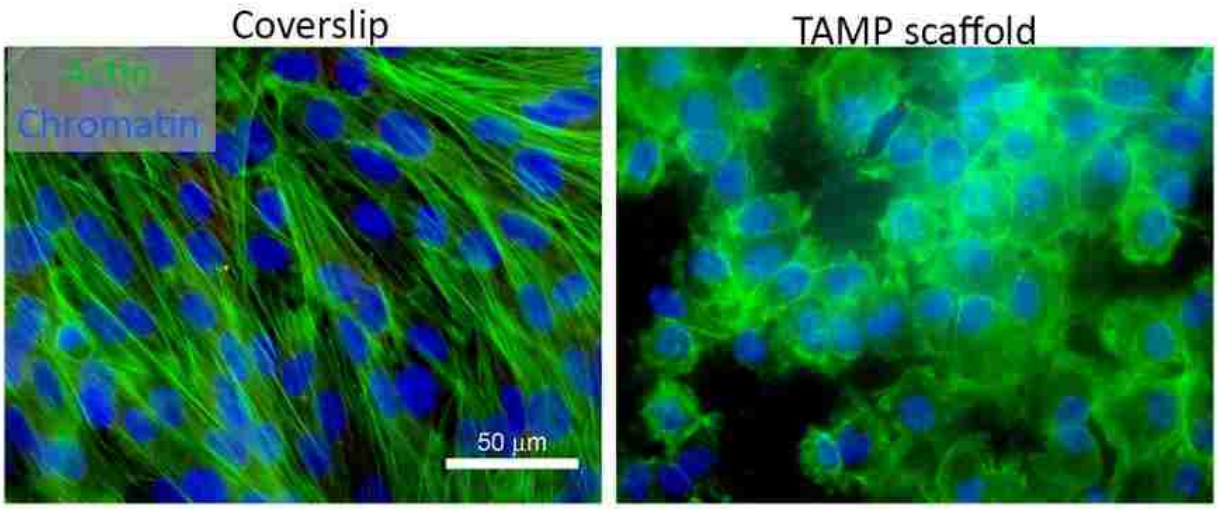

Figure 24: Uterine cells grow differently on coverslips compared to TAMP scaffolds
Uterine cells seeded onto coverslips and TAMP scaffolds have different morphologies based on actin cytoskeleton. Cells on coverslips are spread out with prominent actin stress fibers compared to cells on TAMP scaffolds which are smaller and more round with cortical actin bands at the perimeter of the cells which might suggest that cells on scaffolds are polarizing.

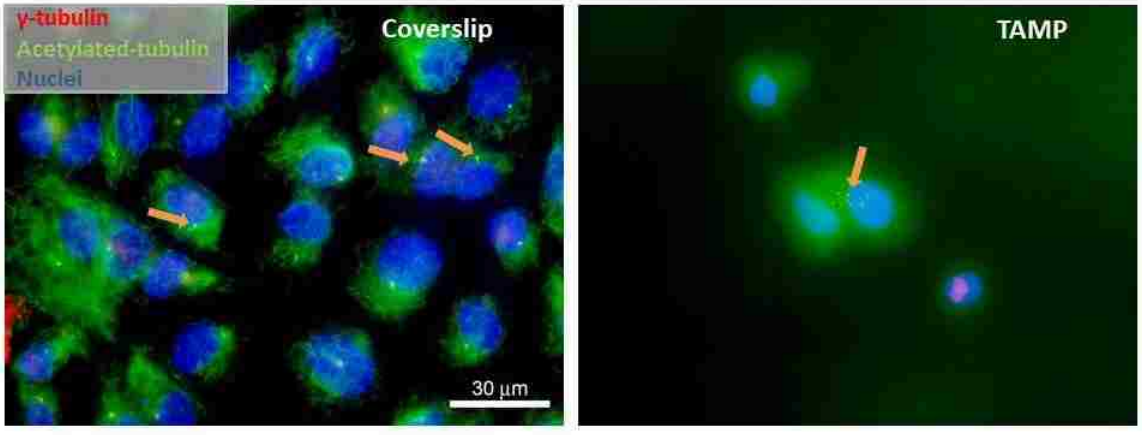

Figure 25: Cilia on uterine cells in culture
Uterine cells grown on coverlips have primary cilia as observed by acetylated- tubulin (green ciliary shaft) and γ-tubulin staining (red centrosomes), however we found a pair of cells on TAMP scaffolds that appears to have multiple red and green puncta unconvincingly suggesting that these cells might have cilia.

4.3 – Skin regeneration – burn wounds

Current methods of treating damage to the skin may result in severe complications. For example, in the case of severe burns, immediate excision of the damaged area and skin grafting is critical to reduce the likelihood of bacterial colonization that may lead to sepsis, organ failure, and ultimately death [120]. Because immediate excision of the wound is critical, culturing to expand the number of cells from autologous tissues is not an option. An alternative to growing tissue to cover the damaged area is a skin graft from another region of the body, generally the thigh or other discrete region. However, this creates another site on the patient for possible infection and pain, lengthened recovery time, or greater scarring [120]. Allogenic skin grafting, a graft from another individual, is another method of treating burn wounds, but immunosuppressive measures must be taken to ensure the graft is not rejected by the recipient, which may be detrimental since burn victims already have a very high risk of infection [121] . Contraction at the site of the healed wound presents another problem. Fibroblasts at the wound site will differentiate into myofibroblasts, which act in a fashion similar to muscle cells. Contraction due to these myofibroblasts is part of the normal process of healing, but in many cases, contraction may become so strong that it causes severe scarring or may even cause a loss of function by impairing range of motion [122].

The examples of potential complications involved with current treatments of skin damage described above clearly demonstrate that there is great need for better treatment of skin wounds. To this end, we investigated whether our TAMP material could be used to treat skin wounds. Initial experiments providing support of this hypothesis were done by our group (Shaojie Wang) in collaboration with Mona Marei at the Alexandria University in Egypt. TAMP scaffolds were implanted under the skin (soft tissue) of New Zealand rabbits and the result was the formation of soft tissue [9]. Additionally, in vitro experiments using normal dermal fibroblasts (ATCC CCL-110) demonstrated that fibroblasts attach to and proliferate on TAMP scaffolds (Figure 26) suggesting they may be suitable for the growth of skin cells.

4.3.1 – Results and discussion

A collaborative relationship with Dr. Sigrid Blome-Eberwein at the burn center of Lehigh Valley Hospital was established. Similar to the *in vitro* fertilization project with Abington Reproductive Medicine, we received human tissue samples that we digested to release the cells for culture. In this case, we received remnants of meshed skin grafts that we digested with trypsin [101]. Similar to the *in vitro* project, we expected the digests to result in a culture with two cell types, keratinocytes and dermal fibroblasts. From initial experiments, it appeared that both cells types might be growing on the TAMP scaffolds based on the morphology of cells stained for actin and focal adhesions (vinculin) (Figure 27), since there were both rounded and stretched cells. The two expected cell types could be distinguished based on morphology and proteins markers, with the fibroblast morphology as long, stretched out, and positive for collagen compared to round epithelial-like keratinocytes positive for cytokeratin. After subjecting cells grown on a coverslip to immunofluorescent staining for collagen and cytokeratin, we observed that the cellular morphology matched the expected staining pattern, such that fibroblast cells were positive for collagen (green) and keratinocytes were positive for cytokeratin (red) (Figure 28, top panels). We confirmed using this staining protocol that both cell types grew on the surface of our TAMP scaffolds (Figure 28, bottom panels); however, although the collagen stain was easily discernable for the fibroblasts on coverslips, the topography of the scaffolds combined with the fact that collagen is a secreted protein prevented accurate detection of collagen on the TAMP scaffolds. It does appear however, that both cell types are growing on the scaffold using this stain since there are nuclei not associated with red cytokeratin staining, this type of analysis should be repeated using vimentin to stain for the dermal fibroblasts.

4.3.2 – Conclusions

Keratinocytes and dermal fibroblasts isolated from human tissue samples could be successfully grown on TAMP scaffolds. These results suggest that further analyses to investigate the activity of the cells on the scaffolds should be performed. Additionally, one of the major issues with successful healing of a burn wound is that there is not a material available that supports the growth of fibroblasts as a bottom layer

with the keratinocytes as the top layer, the same cellular organization as the natural tissue. To address this problem, the TAMP could be prepared with different parameters that select for a specific cell type. Additionally, to use the TAMP scaffolds for clinical applications in wound healing, we would need to generate them in another form, either by weaving the glass into a fiber pad or by using the glass in powder form. These two potential modifications to the original TAMP scaffold preparation are discussed further in section 5.2.

4.3.3 – Materials and methods

4.3.3.1 – Tissue digestion

Skin tissue was collected by Dr. Sigrid Bome-Eberwein at Lehigh Valley Hospital and stored at 4°C before digestion with by a series of incubations in warmed trypsin (Corning, Corning, NY, Cat. # 25-053-CI). In brief, under the hood, tissue was removed from the sterile container and minced. Next the tissue was transferred to a 15ml tube and incubated for 5 min at 37°C with agitation in 5ml of trypsin. After agitation, tissue was allowed to settle for 5 minutes and the supernatant containing the cells was transferred to a new tube containing 5ml of D-MEM (Hyclone, Logan, UT, cat. # SH30021.01) that was supplemented with 10% fetal bovine serum (Atlanta Biologicals, Flowery Branch, GA, Cat. # S11150), 1% L-glutamine (HyClone, Logan, UT, Cat. # 25-005-C1) and 1% penicillin/streptomycin (Corning, Corning, NY, Cat. # 30-001-Cl), and centrifuged to pellet the cells, which were then re-suspended and plated for culture. Fresh trypsin was added to the tube with the tissue and the process was repeated a total of 4 times to make up 1-2 plates for culture. The remaining tissue pieces were plated in a separate dish. The following day, the plates were analyzed for cell growth and signs of contamination and half of the medium was exchanged for fresh medium to help remove red blood cells and other debris. Cells growth was observed for the next few days until they were nearing confluency, before seeding onto coverslips of PBS pre-incubated TAMP scaffolds.

4.3.3.2 - Immunofluorescence

Cells were processed for analysis by fluorescence detection of nuclei by incubating in DAPI solution (Molecular Probes, Eugene, OR, Cat. # D1306), actin by incubating in Alexa488-phalloidin solution (Molecular Probes, Cat. # A-12379), and collagen and cytokeratin by immunofluorescence detection using anti-collagen and anti-cytokeratin antibodies. In brief, cells were fixed using 3.7% formaldehyde followed by permeabilization with 0.2% Triton X-100 for DAPI and Phalloidin staining, or fixed and permeabilized in acetone for staining with primary antibodies. Then, cells were blocked in 1% BSA/1xPBS at room temperature for 1 hour. The primary antibodies, anti-pan-cytokeratin (mouse monoclonal –C11, Santa Cruz Biotechnologies, Cat. #SC8018; at 1:200) and anti-collagen I (mouse monoclonal, Abcam, Cambridge, UK cat # ab6308; at 1:200) were diluted in blocking solution and incubated with cells overnight at 4 °C. A solution of 1xPBS containing DAPI (1 µg/ml:) and secondary antibodies, Alexa568-conjugated goat-anti-rabbit or mouse (1:200) (Molecular Probes/Invitrogen, Grand Island, NY) or Alexa488-conjugated goat-anti-rabbit or mouse (1:200) (Molecular Probes/Invitrogen, Grand Island, NY) was incubated with the cells at room temperature for 1 hour. Samples were placed with cells facing down in 1xPBS into glass-bottom culture dishes (LabTek) for microscopic examination. Cells were imaged using a Nikon Eclipse TE2000-E inverted fluorescence microscope equipped with 10x, 40x, 60x and 100x objectives and a forced-air cooled Photometrics CoolSnap HQ CCD camera (Roper Scientific, Martinsried, Germany). Images were captured using MetaVue (Molecular Devices, Sunnyvale, CA) software version 6.1r5.

4.3.4 – Figures

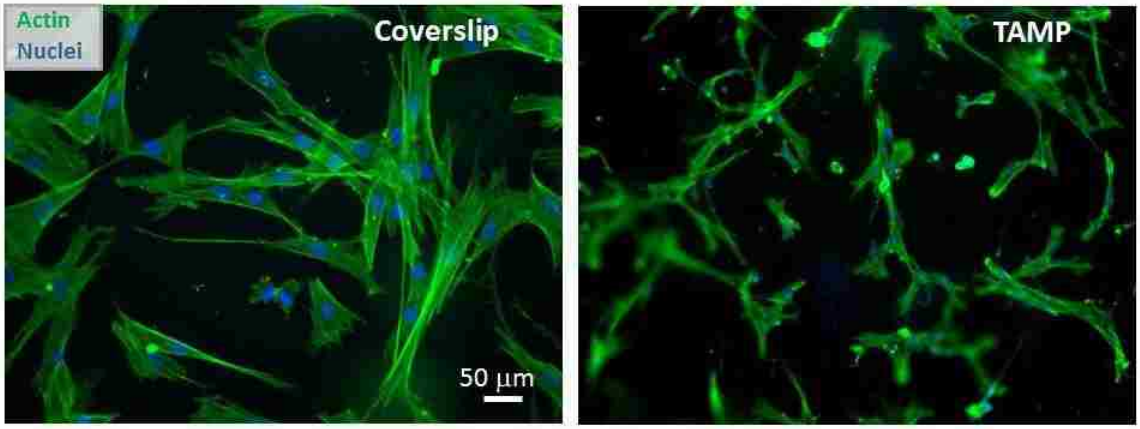

Figure 26: CCL-110 dermal fibroblasts grow on TAMP scaffolds
CCL-110 dermal fibroblasts seeded onto coverslips and TAMP scaffolds had similar morphologies as visualized by staining for DAPI (blue, nuclei) and A488-phalloidin (green, actin).

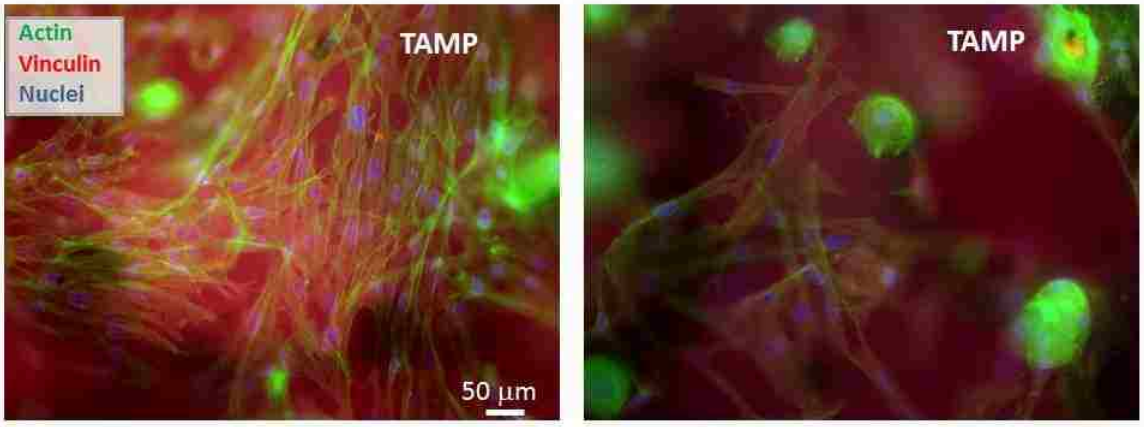

Figure 27: Cells from skin tissue digests have variable morphologies
Cells released from skin tissue by trypsin digestion were seeded onto TAMP scaffolds and stained for actin, vinculin, and nuclei. There are two cellular morphologies that can be observed growing on the scaffolds, a round epithelial-like cell and a stretched fibroblast-like cell.

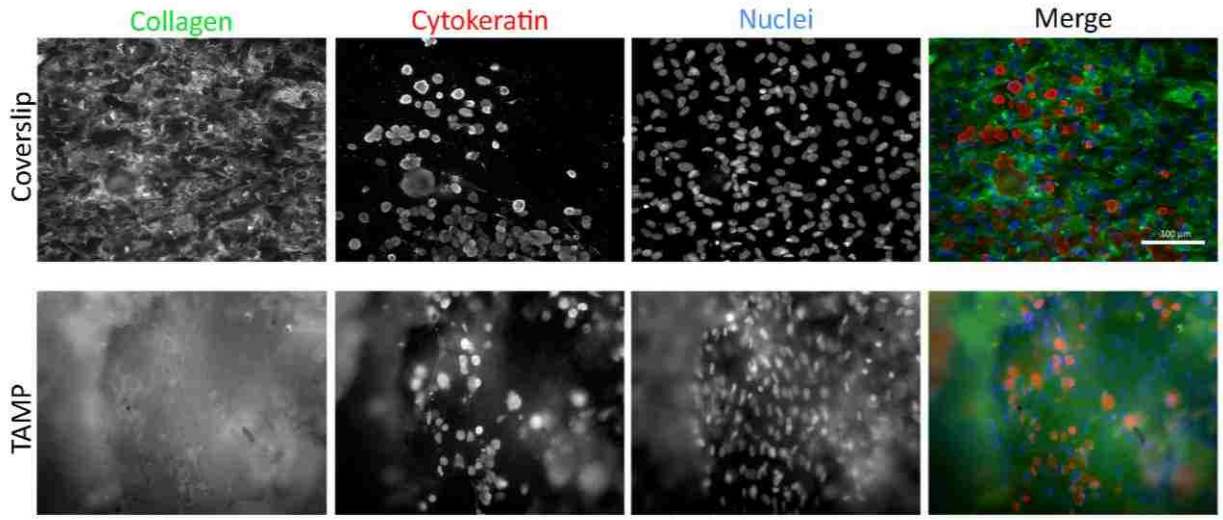

Figure 28: Both keratinocytes and dermal fibroblasts grow on TAMP scaffolds
Immuno-staining indicated that dermal fibroblasts stained positive for collagen (green) while keratinocytes stained positive for cytokeratin (red) indicating that both cells types were present in the tissue digest (top panels – coverslip) and grew on the TAMP scaffolds (bottom panels – TAMP).

Chapter 5 – Conclusions and future perspectives

5.1 - Conclusions

This dissertation aimed at analyzing cellular response to a novel material for tissue regeneration, TAMP scaffolds. Initial studies analyzed cellular adhesion and proliferation on the TAMP scaffolds and found that cells adhered by means of focal adhesions and proliferated and colonized both the surface and interior. Additional analyses were geared towards bone tissue regeneration because of the similarities of the structure of the TAMP scaffolds and that of bone, and because of the reported osteoinductive properties of the dissolution products of the scaffolds. We found using immunofluorescence, qRT-PCR, immunological and enzymatic assays that MC3T3-E1 pre-osteoblast cells differentiated into mature bone producing osteoblasts, and BMD pre-cursor cells matured into active osteoclasts, demonstrating potential for TAMP scaffolds utility in bone tissue regeneration.

Further analyses of the scaffolds were performed to determine the mechanism by which cells were sensing their substrate. Using two different types of bioactive glasses, we showed that substrate morphology was influential to the response of the cells. Further, we demonstrated that differences in glass morphology resulted in subtle yet potentially influential differences in the morphology of hydroxyapatite layer that forms on the surface of the glass after incubation in physiological solutions. Surface morphology from either glass itself or HA in-turn influences the conformation of proteins adsorbed to the surface. It is likely that these differences in protein conformation direct cellular response.

Finally, we explored the potential use of TAMP scaffolds for growing cells more naturally and for soft tissue regeneration since the porosity of the scaffolds makes them similar to a porous membrane providing fluid / nutrient exchange to cells from all sides, and providing specific topographical cues to the cells. In these studies, we used uterine endometrial cells isolated from tissue biopsies to analyze whether the features of the TAMP scaffolds would allow the cells to grow more naturally or polarized in culture.

We found that both epithelial cells and stromal cells from the tissue digests grow on the TAMP scaffolds; however, additional analyses are necessary to determine whether polarization is occurring (see below). In addition, keratinocytes and dermal fibroblasts isolated from human skin tissue samples were also shown to grow on the surface of the TAMP scaffolds. Further analyses are required to investigate how the TAMP scaffold may be used for burn wound healing.

5.2 – Future directions

There are several avenues that can be taken based on the data collected from the studies described here. Although the most comprehensive analysis was performed for bone tissue regeneration, making it the most promising application, the complexity of the next step in analysis might interfere with progress along this path. Moving to using animal models is the next logical step for the bone tissue analysis, and although we have already performed some *in vivo* tests through collaborators in Egypt with promising results [66], this type of analysis in the U.S. is not as simple. Significant funding, training, and approval would be required to initiate animal testing locally. Rather there is significant potential for progress on the skin project that can be done with somewhat readily available supplies to further investigate the use of TAMP scaffolds for skin regeneration.

As stated in section 4.3, there is a lack of effective material available to surgeons that promotes keratinocytes to grow as a top layer over proliferating dermal fibroblasts. This creates a real problem, as a portion of the wound fibroblasts become myofibroblasts, a necessary step in the wound healing process that may become hyperactivated resulting in severe scaring and contraction. Dr. Sigrid Blome-Eberwein is very enthusiastic about this project and frequently has skin tissue samples that are donated to Lehigh for research purposes. She is conveniently located just 20 minutes away at Lehigh Valley Health Network Regional Burn Center making progress on this project feasible. Since we know that both keratinocytes and dermal fibroblasts grow on the basic 70 mol% SiO2 -30 mol% CaO TAMP scaffolds, the next step would be to modify parameters to develop 2

unique scaffolds that would each select for one cell type. Parameters of the scaffolds that can be changed include chemistry or pore size using methods established by Ukrit Thamma. These analyses can be performed using the established immunofluorescent staining protocol for vimentin and cytokeratin described above (section 4.3.3.2). Once it has been confirmed that the different cell types preferentially grow on different scaffolds, the next analyses that could be performed would examine deposition, orientation, and organization of extracellular matrix proteins such as fibronectin and collagen for dermal fibroblasts and laminin for keratinocytes [123]. Analyses of the organization of these extracellular matrix proteins will be critical since this is known to influence scar formation. Parallel bundles of collagen are seen in the scar tissue of regenerated skin compared to the interwoven matrix observed in normal skin tissue [123, 124]. Additionally, analysis of the expression of certain types of cell-matrix adhesion complexes should be done, for example hemidesmosomes establish attachment of keratinocytes to the laminin basement membrane whereas several different integrins are involved in fibroblast attachment during wound healing [125, 123, 126]. Furthermore, analyses of the expression of α-smooth muscle actin could be performed to determine what portion of the fibroblast population become myofibroblasts [127-129].

Although the stiffness of the TAMP and pelleted TAMP scaffolds makes them not likely to be useful in wound healing due to their inflexibility, they should be used for the ease of imaging during initial studies. Once it has been determined that scaffolds with different parameters select for one cell type over the other, it will be necessary to find a means of producing the scaffolds in a flexible form. For example, it is possible to spin the glass pre-cursor into a fiber to make a fibrous pad [130, 131] that could be packed into the wound. Another potential method to make the TAMP more functional for this application would be to use the TAMP scaffolds in powder form. For example, cells isolated from tissue digests would be incubated with powder of one type to selectively bind the dermal fibroblasts, followed by incubation with powder to selectively bind the keratinocytes. Then the first powder with cells would be packed into the wound followed by the second powder. It might be necessary to separate the two powders using for example, a thin membrane that would dissolve away over time. Ukrit Thamma has

already established protocols for grinding and sieving the glass to a particular particle size. This avenue for TAMP scaffolds research in my opinion has the most potential, with a variety of changes that can be done to the parameters of the scaffolds and a fruitful supply of tissue samples from the Lehigh Valley Hospital collaboration.

The *in vitro* fertilization project can also be taken in a few different directions. This project has proven to be difficult as the samples are prone to contamination despite being cultured with penicillin / streptomycin and because sometimes samples do not grow in culture. In addition to these complications, the number of cells isolated from a tissue sample allows for seeding a maximum of one well from a 24-plate with a TAMP scaffold and two additional wells with 12 mm coverslips, making it difficult to analyze more than one aspect of the cells per tissue digest. With the hospital located more than an hour away and only performing surgeries on Wednesdays, it becomes somewhat difficult to get adequate samples for analyses. Nevertheless, there is valuable information that can be learned from these studies.

Additional analyses are required to determine whether or not cells are polarizing on the surface of the TAMP scaffolds. For example, imaging by SEM or using protein markers such as villin to demonstrate that microvilli are forming on the surface of the cells. Analysis for tight junction formation using ZO-1, claudin, or occludin antibodies and imaging by confocal microscopy to show that tight junctions are forming near the apical side of the cells [132] could be done also to show that cells are polarized. Secretion of certain factors could be monitored as well to determine whether or not cells are polarizing or growing more naturally. For example, PGF2a secretion by uterine epithelial cells is an indication of polarization [113], interleukin-1α is secreted by uterine endometrial epithelial cells to stimulate stromal cells to differentiate during decidualization / implantation [133], and granulocyte macrophage-colony stimulating factor secretion may be associated with improved IVF outcome [134]. Secretion analyses could be performed by using inserts designed for membrane studies. By cutting out the membrane from the insert using a razorblade and sanding the edges of TAMP scaffolds to make it fit into the plastic insert, followed by sealing the scaffold in place with aquarium silicon (Figure 29), one could create the separate compartments necessary for secretion

studies. If cells are found not to be polarizing on the TAMP scaffolds, parameters of the scaffolds can be modified to hopefully promote polarization. If polarization occurs, other cell types that also polarize should be analyzed to determine if the TAMP scaffolds have the same effect for cells from other tissues, and also to aid in exploring other potential applications, e.g. airway epithelial or intestinal cells.

To establish whether the TAMP scaffolds may be useful in designing a new AEC protocol to enhance the efficiency IVF, analyses should be performed using mouse embryos. These can be purchased from Embryotech and analyzed to determine whether they are developing more efficiently on the TAMP scaffolds than a regular tissue culture plastic dish. These analyses can be performed using already established protocols from the Abington Reproductive Medicine group.

5.3 – Figure

Figure 29: Cell culture inserts with TAMP scaffolds in place of membranes
Membranes were removed from the insert using a razorblade. TAMP scaffolds were polished to make them thin and smaller in diameter so they would fit in the inserts, then sealed in place using silicon aquarium sealant.

References

1. Yang S, Leong K-F, Du Z, Chua C-K. The design of scaffolds for use in tissue engineering. Part I. Traditional factors. Tissue engineering. 2001;7(6):679-89.
2. Ingham E, Fisher J. Biological reactions to wear debris in total joint replacement. Proceedings of the Institution of Mechanical Engineers, Part H: Journal of Engineering in Medicine. 2000;214(1):21-37.
3. Wong M, Eulenberger J, Schenk R, Hunziker E. Effect of surface topology on the osseointegration of implant materials in trabecular bone. Journal of Biomedical Materials Research Part A. 1995;29(12):1567-75.
4. Götz H, Müller M, Emmel A, Holzwarth U, Erben R, Stangl R. Effect of surface finish on the osseointegration of laser-treated titanium alloy implants. Biomaterials. 2004;25(18):4057-64.
5. Geetha M, Singh A, Asokamani R, Gogia A. Ti based biomaterials, the ultimate choice for orthopaedic implants–a review. Progress in materials science. 2009;54(3):397-425.
6. Pham C, Greenwood J, Cleland H, Woodruff P, Maddern G. Bioengineered skin substitutes for the management of burns: a systematic review. Burns. 2007;33(8):946-57.
7. Eisenbud D, Huang NF, Luke S, Silberklang M. Review skin substitutes and wound healing: current status and challenges. Wounds. 2004;16(1):2-17.
8. Hench L. The story of Bioglass. Journal of materials science Materials in medicine. 2006;17(11):967-78. doi:10.1007/s10856-006-0432-z.
9. Wang S, Kowal T, Marei M, Falk M, Jain J. Nanoporosity Significantly Enhances the Biological Performance of Engineered Glass Tissue Scaffolds. Tissue Engineering Part A. 2013;Not available-, ahead of print. doi:10.1089/ten.tea.2012.0585.
10. Vueva Y, Gama A, Tiexeira A, Almeida R, Wang S, Falk M et al. Monolithic Glass Scaffolds with Dual Porosity Prepared by Polymer-Induced Phase Separation and Sol-gel. Journal of the American Ceramic Society. 2010;93(7):1945-9.
11. Marques A, Almeida R, Thiema A, Wang S, Falk M, Jain H. Sol-gel derived glass scaffold with high pore interconnectivity and enhanced bioactivity. Journal of Materials Research. 2009;24(12):34953502.
12. Wang S, Falk MM, Rashad A, Saad MM, Marques AC, Almeida RM et al. Evaluation of 3D nano-macro porous bioactive glass scaffold for hard tissue engineering. Journal of materials science Materials in medicine. 2011;22(5):1195-203. doi:10.1007/s10856-011-4297-4.
13. Zhang D, Jain H, Hupa M, Hupa L. In-vitro Degradation and Bioactivity of Tailored Amorphous Multi Porous Scaffold Structure. Journal of the American Ceramic Society. 2012:1-8.
14. Brunauer S, Emmett PH, Teller E. Adsorption of gases in multimolecular layers. J Am Chem Soc. 1938;60(2):309-19.
15. Xynos ID, Edgar AJ, Buttery LD, Hench LL, Polak JM. Gene - expression profiling of human osteoblasts following treatment with the ionic products of Bioglass® 45S5 dissolution. Journal of Biomedical Materials Research Part A. 2001;55(2):151-7.

16. Jones JR, Tsigkou O, Coates EE, Stevens MM, Polak JM, Hench LL. Extracellular matrix formation and mineralization on a phosphate-free porous bioactive glass scaffold using primary human osteoblast (HOB) cells. Biomaterials. 2007;28(9):1653-63.
17. Christodoulou I, Buttery LD, Saravanapavan P, Tai G, Hench LL, Polak JM. Dose‐ and time‐ dependent effect of bioactive gel‐ glass ionic‐ dissolution products on human fetal osteoblast‐ specific gene expression. Journal of Biomedical Materials Research Part B: Applied Biomaterials. 2005;74(1):529-37.
18. Herman B, Pledger WJ. Platelet-derived growth factor-induced alterations in vinculin and actin distribution in BALB/c-3T3 cells. The Journal of cell biology. 1985;100(4):1031-40.
19. Yeung T, Georges PC, Flanagan LA, Marg B, Ortiz M, Funaki M et al. Effects of substrate stiffness on cell morphology, cytoskeletal structure, and adhesion. Cell Motil Cytoskeleton. 2005;60(1):24-34. doi:10.1002/cm.20041.
20. Solon J, Levental I, Sengupta K, Georges PC, Janmey PA. Fibroblast adaptation and stiffness matching to soft elastic substrates. Biophysical journal. 2007;93(12):4453-61.
21. Discher DE, Janmey P, Wang Y-l. Tissue cells feel and respond to the stiffness of their substrate. Science. 2005;310(5751):1139-43.
22. Robinson MS. Cloning of cDNAs encoding two related 100-kD coated vesicle proteins (a-adaptins). J Cell Biol. 1989;108(8):3.
23. Choi JY, Lee BH, Song KB, Park RW, Kim IS, Sohn KY et al. Expression patterns of bone‐ related proteins during osteoblastic differentiation in MC3T3‐ E1 cells. Journal of cellular biochemistry. 1996;61(4):609-18.
24. Quarles LD, Yohay DA, Lever LW, Caton R, Wenstrup RJ. Distinct proliferative and differentiated stages of murine MC3T3-E1 cells in culture: an in vitro model of osteoblast development. Journal of bone and mineral research : the official journal of the American Society for Bone and Mineral Research. 1992;7(6):683-92. doi:10.1002/jbmr.5650070613.
25. Sudo H, Kodama H-A, Amagai Y, Yamamoto S, Kasai S. In vitro differentiation and calcification in a new clonal osteogenic cell line derived from newborn mouse calvaria. J Cell Biol. 1983;96(1):191-8.
26. Felix R, Fleisch H. Increase in alkaline phosphatase activity in calvaria cells cultured with diphosphonates. Biochemical Journal. 1979;183(1):73-81.
27. Russell RG, Mühlbauer R, Bisaz S, Williams D, Fleisch H. The influence of pyrophosphate, condensed phosphates, phosphonates and other phosphate compounds on the dissolution of hydroxyapatitein vitro and on bone resorption induced by parathyroid hormone in tissue culture and in thyroparathyroidectomised rats. Calcified tissue international. 1970;6(1):183-96.
28. Owen TA, Aronow M, Shalhoub V, Barone LM, Wilming L, Tassinari MS et al. Progressive development of the rat osteoblast phenotype in vitro: reciprocal relationships in expression of genes associated with osteoblast proliferation and differentiation during formation of the bone extracellular matrix. Journal of cellular physiology. 1990;143(3):420-30.
29. Robling AG, Castillo AB, Turner CH. Biomechanical and molecular regulation of bone remodeling. Annu Rev Biomed Eng. 2006;8:455-98.

30. Soysa NS, Neil A, Aoki K, Ohya K. Osteoclast formation and differentiation: an overview. Journal of medical and dental sciences. 2012;59(3):65-74.
31. Teitelbaum SL. Bone resorption by osteoclasts. Science. 2000;289(5484):1504-8.
32. Väänänen HK, Zhao H, Mulari M, Halleen JM. The cell biology of osteoclast function. J Cell Sci. 2000;113(Pt 3):377-81.
33. Coetzee M, Haag M, Kruger MC. Effects of arachidonic acid, docosahexaenoic acid, prostaglandin E 2 and parathyroid hormone on osteoprotegerin and RANKL secretion by MC3T3-E1 osteoblast-like cells. The Journal of nutritional biochemistry. 2007;18(1):54-63.
34. Jimi E, Nakamura I, Amano H, Taguchi Y, Tsurukai T, Tamura M et al. Osteoclast function is activated by osteoblastic cells through a mechanism involving cell-to-cell contact. Endocrinology. 1996;137(8):2187-90.
35. Gruber H, Ivey J, Thompson E, Chesnut 3rd C, Baylink D. Osteoblast and osteoclast cell number and cell activity in postmenopausal osteoporosis. Mineral and electrolyte metabolism. 1985;12(4):246-54.
36. Hollberg K, Hultenby K, Hayman AR, Cox TM, Andersson G. Osteoclasts from mice deficient in tartrate-resistant acid phosphatase have altered ruffled borders and disturbed intracellular vesicular transport. Experimental cell research. 2002;279(2):227-38.
37. Minkin C. Bone acid phosphatase: tartrate-resistant acid phosphatase as a marker of osteoclast function. Calcified tissue international. 1982;34(1):285-90.
38. Suter A, Everts V, Boyde A, Jones SJ, Lüllmann-Rauch R, Hartmann D et al. Overlapping functions of lysosomal acid phosphatase (LAP) and tartrate-resistant acid phosphatase (Acp5) revealed by doubly deficient mice. Development. 2001;128(23):4899-910.
39. Roy A, Brower ME, Hayden JE. Sodium thymolphthalein monophosphate: a new acid phosphatase substrate with greater specificity for the prostatic enzyme in serum. Clinical Chemistry. 1971;17(11):1093-102.
40. LaCount MW, Handy G, Lebioda L. Structural origins of L (+)-tartrate inhibition of human prostatic acid phosphatase. Journal of Biological Chemistry. 1998;273(46):30406-9.
41. Fishman WH, Dart R, Bonner C, Leadbetter W, Lerner F, Homburger F. A new method for estimating serum acid phosphatase of prostatic origin applied to the clinical investigation of cancer of the prostate. Journal of Clinical Investigation. 1953;32(10):1034.
42. Jones JR. Reprint of: Review of bioactive glass: From Hench to hybrids. Acta biomaterialia. 2015;23:S53-S82.
43. Kodama H-a, Amagai Y, Sudo H, Kasai S, Yamamoto S. Establishment of a clonal osteogenic cell line from newborn mouse calvaria. 歯科基礎医学会雑誌. 1981;23(4):899-901.
44. Gough JE, Jones JR, Hench LL. Nodule formation and mineralisation of human primary osteoblasts cultured on a porous bioactive glass scaffold. Biomaterials. 2004;25(11):2039-46.

45. Wang Y, Sul HS. Pref-1 regulates mesenchymal cell commitment and differentiation through Sox9. Cell metabolism. 2009;9(3):287-302.
46. Varanasi V, Saiz E, Loomer P, Ancheta B, Uritani N, Ho S et al. Enhanced osteocalcin expression by osteoblast-like cells (MC3T3-E1) exposed to bioactive coating glass (SiO 2–CaO–P 2 O 5–MgO–K 2 O–Na 2 O system) ions. Acta biomaterialia. 2009;5(9):3536-47.
47. Hauschka PV, Lian JB, Gallop PM. Direct identification of the calcium-binding amino acid, gamma-carboxyglutamate, in mineralized tissue. Proceedings of the National Academy of Sciences. 1975;72(10):3925-9.
48. Franzen A, Heinegård D. Isolation and characterization of two sialoproteins present only in bone calcified matrix. Biochemical Journal. 1985;232(3):715-24.
49. Price PA, Otsuka A, Poser JW, Kristaponis J, Raman N. Characterization of a gamma-carboxyglutamic acid-containing protein from bone. Proceedings of the National Academy of Sciences. 1976;73(5):1447-51.
50. Filová E, Suchý T, Sucharda Z, Šupová M, Žaloudková M, Balík K et al. Support for the initial attachment, growth and differentiation of MG-63 cells: a comparison between nano-size hydroxyapatite and micro-size hydroxyapatite in composites. International journal of nanomedicine. 2014;9:3687.
51. Przybylowski C, Quinn T, Callahan A, Kaplan M, Golding A, Alesi C et al. MC3T3 preosteoblast differentiation on bone morphogenetic protein-2 peptide ormosils. Journal of Materials Chemistry. 2012;22(21):10672-83.
52. Ruckh TT, Carroll DA, Weaver JR, Popat KC. Mineralization content alters osteogenic responses of bone marrow stromal cells on hydroxyapatite/polycaprolactone composite nanofiber scaffolds. Journal of functional biomaterials. 2012;3(4):776-98.
53. Tsutsumi K, Saito N, Kawazoe Y, Ooi H-K, Shiba T. Morphogenetic study on the maturation of osteoblastic cell as induced by inorganic polyphosphate. Plos one. 2014;9(2):e86834.
54. Bronner F. Bone and calcium homeostasis. Neurotoxicology. 1991;13(4):775-82.
55. Blair HC. How the osteoclast degrades bone. Bioessays. 1998;20(10):837-46.
56. Linkhart TA, Linkhart SG, Kodama Y, Farley JR, Dimai HP, Wright KR et al. Osteoclast formation in bone marrow cultures from two inbred strains of mice with different bone densities. Journal of Bone and Mineral Research. 1999;14(1):39-46.
57. Väänänen HK, Laitala-Leinonen T. Osteoclast lineage and function. Archives of biochemistry and biophysics. 2008;473(2):132-8.
58. Boissy P, Saltel F, Bouniol C, Jurdic P, Machuca-Gayet I. Transcriptional activity of nuclei in multinucleated osteoclasts and its modulation by calcitonin. Endocrinology. 2002;143(5):1913-21.
59. Suda T, Takahashi N, Martin TJ. Modulation of osteoclast differentiation. Endocrine reviews. 1992;13(1):66-80.
60. Väänänen HK, Horton M. The osteoclast clear zone is a specialized cell-extracellular matrix adhesion structure. Journal of cell science. 1995;108(8):2729-32.
61. Salo J, Metsikko K, Palokangas H, Lehenkari P, Vaananen H. Bone-resorbing osteoclasts reveal a dynamic division of basal plasma membrane into two different domains. Journal of Cell Science. 1996;109(2):301-7.

62. Halleen JM, Räisänen S, Salo JJ, Reddy SV, Roodman GD, Hentunen TA et al. Intracellular fragmentation of bone resorption products by reactive oxygen species generated by osteoclastic tartrate-resistant acid phosphatase. Journal of Biological Chemistry. 1999;274(33):22907-10.
63. Detsch R, Mayr H, Ziegler G. Formation of osteoclast-like cells on HA and TCP ceramics. Acta biomaterialia. 2008;4(1):139-48.
64. Monchau F, Lefevre A, Descamps M, Belquin-Myrdycz A, Laffargue P, Hildebrand H. In vitro studies of human and rat osteoclast activity on hydroxyapatite, β-tricalcium phosphate, calcium carbonate. Biomolecular engineering. 2002;19(2):143-52.
65. Yamada S, Heymann D, Bouler JM, Daculsi G. Osteoclastic resorption of biphasic calcium phosphate ceramic in vitro. Journal of biomedical materials research. 1997;37(3):346-52.
66. El Shazley N, Hamdy A, El-Eneen H, El Backly R, Saad M, Essam W et al. Bioglass in Alveolar Bone Regeneration in Orthodontic Patients Randomized Controlled Clinical Trial. JDR Clinical & Translational Research. 2016;1(3):244-55.
67. Dobson K, Reading L, Haberey M, Marine X, Scutt A. Centrifugal isolation of bone marrow from bone: an improved method for the recovery and quantitation of bone marrow osteoprogenitor cells from rat tibiae and femurae. Calcified tissue international. 1999;65(5):411-3.
68. Golovchak R, Thapar P, Ingram A, Savytskii D, Jain H. Influence of phase separation on the devitrification of 45S5 bioglass. Acta Biomater. 2014;10(11):4878-86. doi:10.1016/j.actbio.2014.07.024.
69. Roach P, Farrar D, Perry CC. Interpretation of protein adsorption: surface-induced conformational changes. Journal of the American Chemical Society. 2005;127(22):8168-73. doi:10.1021/ja042898o.
70. Lord MS, Foss M, Besenbacher F. Influence of nanoscale surface topography on protein adsorption and cellular response. Nano Today. 2010;5:66-78.
71. Ye F, Hu G, Taylor D, Ratnikov B, Bobkov AA, McLean MA et al. Recreation of the terminal events in physiological integrin activation. J Cell Biol. 2010;188(1):157-73. doi:10.1083/jcb.200908045.
72. Nermut MV, Green NM, Eason P, Yamada SS, Yamada KM. Electron microscopy and structural model of human fibronectin receptor. The EMBO journal. 1988;7(13):4093-9.
73. Elbe JA. Integrin-ligand interaction. Springer Science & Business Media; 2013.
74. Hench LL. Bioceramics: from concept to clinic. Journal of the American Ceramic Society. 1991;74(7):1487-510.
75. Almeida RM, Hickey R, Jain H, Pantano CG. Low-Energy Ion Scattering spectroscopy of silicate glass surfaces. Journal of Non-Crystalline Solids. 2014;385:124-8.
76. Wang D, Christensen K, Chawla K, Xiao G, Krebsbach PH, Franceschi RT. Isolation and characterization of MC3T3-E1 preosteoblast subclones with distinct in vitro and in vivo differentiation/mineralization potential. Journal of bone and mineral research : the official journal of the American Society for Bone and Mineral Research. 1999;14(6):893-903. doi:10.1359/jbmr.1999.14.6.893.

77. Sepulveda P, Jones JR, Hench LL. In vitro dissolution of melt‐derived 45S5 and sol‐gel derived 58S bioactive glasses. Journal of biomedical materials research. 2002;61(2):301-11.
78. Filgueiras MR, LaTorre G, Hench LL. Solution effects on the surface reactions of three bioactive glass compositions. J Biomed Mater Res. 1993;27(12):1485-93. doi:10.1002/jbm.820271204.
79. Tsigkou O, Jones JR, Polak JM, Stevens MM. Differentiation of fetal osteoblasts and formation of mineralized bone nodules by 45S5 Bioglass conditioned medium in the absence of osteogenic supplements. Biomaterials. 2009;30(21):3542-50. doi:10.1016/j.biomaterials.2009.03.019.
80. Bohner M, Lemaitre J. Can bioactivity be tested in vitro with SBF solution? Biomaterials. 2009;30(12):2175-9. doi:10.1016/j.biomaterials.2009.01.008.
81. Price PJ, Gregory EA. Relationship between in vitro growth promotion and biophysical and biochemical properties of the serum supplement. In vitro. 1982;18(6):576-84.
82. Vanea E, Magyari K, Simon V. Protein attachment on aluminosilicates surface studied by XPS and FTIR spectroscopy. Journal of Optoelectronics and Advanced Materials. 2010;12(5):1206-12.
83. Tunc S, Maitz MF, Steiner G, Vazquez L, Pham MT, Salzer R. In situ conformational analysis of fibrinogen adsorbed on Si surfaces. Colloids and surfaces B, Biointerfaces. 2005;42(3-4):219-25. doi:10.1016/j.colsurfb.2005.03.004.
84. Surewicz WK, Mantsch HH. New insight into protein secondary structure from resolution-enhanced infrared spectra. Biochimica et biophysica acta. 1988;952(2):115-30.
85. Gruian C, Vanea E, Simon S, Simon V. FTIR and XPS studies of protein adsorption onto functionalized bioactive glass. Biochimica et biophysica acta. 2012;1824(7):873-81. doi:10.1016/j.bbapap.2012.04.008.
86. Byler DM, Susi H. Examination of the secondary structure of proteins by deconvolved FTIR spectra. Biopolymers. 1986;25(3):469-87.
87. Molino PJ, Higgins MJ, Innis PC, Kapsa RM, Wallace GG. Fibronectin and bovine serum albumin adsorption and conformational dynamics on inherently conducting polymers: a QCM-D study. Langmuir : the ACS journal of surfaces and colloids. 2012;28(22):8433-45. doi:10.1021/la300692y.
88. Thomas MV, Puleo DA, Al-Sabbagh M. Bioactive glass three decades on. Journal of long-term effects of medical implants. 2005;15(6):585-97.
89. Renny M, Turdean-Ionescu C, Stevensson B, Izquierdo-Barba I, García A, Arcos D et al. "Direct probing of the phosphate-ion distribution in bioactive silicate glasses by solid-state NMR: evidence for transitions between random/clustered scenarios. Chemistry of Materials. 2013;25(9):1877-85.
90. Renny M, Baltzar S, Mattias E. Na/Ca Intermixing around Silicate and Phosphate Groups in Bioactive Phosphosilicate Glasses Revealed by Heteronuclear Solid-State NMR and Molecular Dynamics Simulations. The Journal of Physical Chemistry B 2015;119(17):5701-15.

91. Pedone A, Charpentier T, Malavasi G, Menziani MC. New insights into the atomic structure of 45S5 bioglass by means of solid-state NMR spectroscopy and accurate first-principles simulations. Chemistry of Materials. 2010;22(19):5644-52.
92. O'Donnell MD, Watts SJ, Law RV, Hill RG. Effect of P 2 O 5 content in two series of soda lime phosphosilicate glasses on structure and properties–Part I: NMR. Journal of Non-Crystalline Solids. 2008;354(30):3554-60.
93. Lefebvre L, Chevalier J, Gremillard L, Zenati R, Thollet G, Bernache-Assolant D et al. Structural transformations of bioactive glass 45S5 with thermal treatments. Acta Materialia. 2007;55(10):3305-13.
94. Eagle H. The effect of environmental pH on the growth of normal and malignant cells. Journal of cellular physiology. 1973;82(1):1-8.
95. Ceccarini C, Eagle H. pH as a determinant of cellular growth and contact inhibition. Proceedings of the national academy of Sciences. 1971;68(1):229-33.
96. Jain RH, Wang S, Moawad HM, Falk MM, Jain H, editors. Glass bone implants: the effect of surface topology on attachment and proliferation of osteoblast cells on 45S bioactive glass. MRS Proceedings; 2009: Cambridge Univ Press.
97. Wright AK, Thompson MR. Hydrodynamic structure of bovine serum albumin determined by transient electric birefringence. Biophysical journal. 1975;15(2 Pt 1):137-41.
98. Wilson CJ, Clegg RE, Leavesley DI, Pearcy MJ. Mediation of biomaterial-cell interactions by adsorbed proteins: a review. Tissue engineering. 2005;11(1-2):1-18. doi:10.1089/ten.2005.11.1.
99. Wang K, Zhou C, Hong Y, Zhang X. A review of protein adsorption on bioceramics. Interface focus. 2012;2(3):259-77. doi:10.1098/rsfs.2012.0012.
100. Peters T, editor. The Plasma Proteins. Putman, F. W. ed.: Academic Press, New York; 1975.
101. Magyari K, Gruian C, Varga B, Ciceo-Lucacel R, Radu T, Steinhoff H-J et al. Addressing the optimal silver content in bioactive glass systems in terms of BSA adsorption. The Journal of Physical Chemistry B. 2014;2:5799-808.
102. El-Ghannam A, Ducheyne P, Shapiro IM. Effect of serum proteins on osteoblast adhesion to surface-modified bioactive glass and hydroxyapatite. Journal of orthopaedic research : official publication of the Orthopaedic Research Society. 1999;17(3):340-5. doi:10.1002/jor.1100170307.
103. Nilausen K. Role of fatty acids in growth-promoting effect of serum albumin on hamster cells in vitro. Journal of cellular physiology. 1978;96(1):1-14. doi:10.1002/jcp.1040960102.
104. Huang BX, Kim HY, Dass C. Probing three-dimensional structure of bovine serum albumin by chemical cross-linking and mass spectrometry. Journal of the American Society for Mass Spectrometry. 2004;15(8):1237-47. doi:10.1016/j.jasms.2004.05.004.
105. Vlasova I, Saletsky A. Raman spectroscopy in investigations of secondary structure of human serum albumin at binding of nanomarkers of fluorescein family. Laser physics. 2010;20(9):1844-8.

106. Wen Z, Hecht L, Barron L. alpha-Helix and associated loop signatures in vibrational Raman optical activity spectra of proteins. Journal of the American Chemical Society. 1994;116(2):443-5.
107. Roach P, Farrar D, Perry CC. Surface tailoring for controlled protein adsorption: effect of topography at the nanometer scale and chemistry. Journal of the American Chemical Society. 2006;128(12):3939-45. doi:10.1021/ja056278e.
108. Garcia AJ, Ducheyne P, Boettiger D. Effect of surface reaction stage on fibronectin-mediated adhesion of osteoblast-like cells to bioactive glass. J Biomed Mater Res. 1998;40(1):48-56.
109. Elder K, Dale B. In-vitro fertilization. Cambridge University Press; 2010.
110. Thurin A, Hausken J, Hillensjö T, Jablonowska B, Pinborg A, Strandell A et al. Elective single-embryo transfer versus double-embryo transfer in in vitro fertilization. New England Journal of Medicine. 2004;351(23):2392-402.
111. Rubio C, Simón C, Mercader A, Garcia-Velasco J, Remohí J, Pellicer A. Clinical experience employing co-culture of human embryos with autologous human endometrial epithelial cells. Human reproduction (Oxford, England). 2000;15:31-8.
112. Barmat LI, Liu H-C, Spandorfer SD, Kowalik A, Mele C, Xu K et al. Autologous endometrial co-culture in patients with repeated failures of implantation after in vitro fertilization–embryo transfer. Journal of assisted reproduction and genetics. 1999;16(3):121-7.
113. Cherny RA, Findlay JK. Separation and culture of ovine endometrial epithelial and stromal cells: evidence of morphological and functional polarity. Biology of reproduction. 1990;43(2):241-50.
114. Orkin R, Gehron P, Mcgoodwin EB, Martin G, Valentine T, Swarm R. A murine tumor producing a matrix of basement membrane. Journal of Experimental Medicine. 1977;145(1):204-20.
115. Kleinman HK, McGarvey ML, Liotta LA, Robey PG, Tryggvason K, Martin GR. Isolation and characterization of type IV procollagen, laminin, and heparan sulfate proteoglycan from the EHS sarcoma. Biochemistry. 1982;21(24):6188-93.
116. Kleinman HK, Martin GR, editors. Matrigel: basement membrane matrix with biological activity. Seminars in cancer biology; 2005: Elsevier.
117. Hughes CS, Postovit LM, Lajoie GA. Matrigel: a complex protein mixture required for optimal growth of cell culture. Proteomics. 2010;10(9):1886-90.
118. Masterton R, Armstrong E, More I. The cyclical variation in the percentage of ciliated cells in the normal human endometrium. Journal of reproduction and fertility. 1975;42(3):537-40.
119. Ferenczy A, Richart RM. Scanning and transmission electron microscopy of the human endometrial surface epithelium. The Journal of Clinical Endocrinology & Metabolism. 1973;36(5):999-1008.
120. Klein M, Heimbach D, Gibran N. Management of the Burn Wound. ACS Surgery. 2004;Principles and Practice.
121. Goldsby RA, Kindt TJ, Osborne BA, Kuby J. Immunology. 2003;5th edition(New York):W. H. Freeman and Company.

122. Grinnell F. Fibroblasts, Myofibroblasts, and Wound Contraction. The Journal of Cell Biology. 1994;124(4):401-4.
123. Martin P. Wound healing--aiming for perfect skin regeneration. Science. 1997;276(5309):75-81.
124. Enoch S, Leaper DJ. Basic science of wound healing. Surgery (Oxford). 2008;26(2):31-7.
125. Tsuruta D, Hashimoto T, Hamill KJ, Jones JC. Hemidesmosomes and focal contact proteins: functions and cross-talk in keratinocytes, bullous diseases and wound healing. Journal of dermatological science. 2011;62(1):1-7.
126. Mansbridge JN, Knapp M. Changes in keratinocyte maturation during wound healing. Journal of Investigative Dermatology. 1987;89(3):253-63.
127. Hinz B, Celetta G, Tomasek JJ, Gabbiani G, Chaponnier C. Alpha-smooth muscle actin expression upregulates fibroblast contractile activity. Molecular biology of the cell. 2001;12(9):2730-41.
128. Desmouliere A. Factors influencing myofibroblast differentiation during wound healing and fibrosis. Cell biology international. 1995;19(5):471-6.
129. Darby I, Skalli O, Gabbiani G. a-Smooth muscle actin is transiently expressed by myofibroblasts during experimental wound healing. Lab Invest. 1990;63(1):21-9.
130. Lu H, Zhang T, Wang X, Fang Q. Electrospun submicron bioactive glass fibers for bone tissue scaffold. Journal of Materials Science: Materials in Medicine. 2009;20(3):793-8.
131. Kim HW, Kim HE, Knowles JC. Production and Potential of Bioactive Glass Nanofibers as a Next- Generation Biomaterial. Advanced Functional Materials. 2006;16(12):1529-35.
132. Tsukita S, Furuse M, Itoh M. Multifunctional strands in tight junctions. Nature reviews Molecular cell biology. 2001;2(4):285-93.
133. Jacobs AL, Carson DD. Uterine epithelial cell secretion of interleukin-1 alpha induces prostaglandin E2 (PGE2) and PGF2 alpha secretion by uterine stromal cells in vitro. Endocrinology. 1993;132(1):300-8.
134. Spandorfer S, Barmat L, Liu HC, Mele C, Veeck L, Rosenwaks Z. Granulocyte Macrophage- Colony Stimulating Factor Production by Autologous Endometrial Co- Culture Is Associated with Outcome for In Vitro Fertilization Patients with a History of Multiple Implantation Failures. American Journal of Reproductive Immunology. 1998;40(5):377-81.

Vita

Tia J. Kowal

Work Address
111 Research Drive
Bethlehem, PA 18015
Email: tjk210@lehigh.edu

Education

LEHIGH UNIVERSITY 2010-current (ABD)
Doctor of Philosophy-Cell and Molecular Biology
Advisor: Matthias M. Falk, PhD
Dissertation Title: *Cell-bioactive glass scaffold interactions: Response to chemistry and topography*

MILLERSVILLE UNIVERSITY 2002 - 2007
Bachelors of Science degree in Biology
Minor in Chemistry

Relevant Coursework

Graduate courses: Advanced Cell Biology • Biochemistry I and II • Molecular Cell Biology I and II • Molecular Genetics • Teacher Development Workshop Series
BS degree: Cell Biology • Histology • Immunology • Neurobiology Microbiology • Stem Cells and Cloning • Genetics • A&P

Courses Taught

Guest Lecturer

-2016 Summer- (June 6th)- Bios 041-Summer Core Molecular Cell Biology I – *DNA replication and repair*

-2016 Spring- (February 9th)- Bios 421-Graduate level Molecular Cell Biology I – *Cellular response to extracellular matrix (ECM) properties – cancer and ECM stiffness*

Teaching Assistant

-2016 Summer I – Bios 041 – Core I: Cellular and Molecular Biology

-2016 Spring- Bios 346- Molecular Genetics lab

-2015 Fall- Bios 371- Elements of Biochemistry I

-2014 Spring- Bios 368- Cell Biology lab
– Designed and implemented additional experiments which resulted in a first author publication

-2013 Fall- Bios 116- Core II: Genetics lab
-2013 Spring- Bios 041- Core I: Cellular and Molecular Biology
-2012 Spring- Bios 041- Core I: Cellular and Molecular Biology

---

Fellowships And Awards

-Marjorie Nemes **Fellowship** – Lehigh University – Summer 2015
-ATCC **Photo contest** – Most popular photo award – 2015
-Graduate Student Spotlight – Lehigh University Department of Biological Sciences – Fall 2015
-College of Arts and Sciences Summer **Fellowship** – Lehigh University–June-July 2014
-Marjorie Nemes **Fellowship** –Lehigh University - Fall 2014

Nominations

- Nominated as Teaching assistant of the year: **Honorable Mention** – 2015 – Bios 116- Core II: Genetics lab
- Nominated as Teaching assistant of the year– 2013 – Bios 041 - Core I: Cellular and Molecular Biology

---

Peer Reviewed Publications

Kowal, **Tia J**., Hahn, Natalie C., Jain, Himanshu, Falk, Matthias M. Biological characterization of TAMP bioactive glass scaffolds for hard tissue regeneration (In Preparation).

Kowal, Tia J., Golovchak, Roman, Chokshi, Tanuj, Harms, Joe, Jain, Himanshu, Falk, Matthias, M. Role of Bioglass® nanotopography in protein and cell attachment (In Review).

Falk, Matthias M., **Kowal, Tia J**., Almaida, Rui M., Saad, Manal, Marei, Mona K., Thamma, Ukrit, Jain, Himanshu. Chapter 5: Sol-gel glass and Nano-Macro Porous bioscafolds. Bioactive glasses. **2016**. 105-135.

Falk, Matthias M., Fisher, Charles G., Kells-Andrews, Rachael M., **Kowal, Tia J.** Chapter 2: Imaging gap junctions in living cells: *Gap Junction Channels and Hemichannels*. Bai D. and Saez J., eds. Methods in Signal Transduction Series, CRC. 21-63. **2016**.

Kowal, Tia J., Falk, Matthias M. **2015**. Primary cilia on HeLa and other cancer cells. Cell Biology International Article first published online: 6 AUG 2015 DOI: 10.1002/cbin.10500

Wang, Shaojie, **Kowal, Tia J.**, Marei, Mona, Falk, Matthias M., Jain, Himanshu. **2013**. Nanoporosity significantly enhances the biological

performance of engineered glass scaffolds. Tissue Engineering Part A. July 2013, 19(13-14): 1632-1640. doi:10.1089/ten.tea.2012.0585.

Thévenin, Anastasia F., **Kowal, Tia J**., Fong, John T., Kells, Rachael M., Fisher, Charles G., and Falk, Matthias M. **2013**. Proteins and Mechanisms Regulating Gap Junction Assembly, Internalization and Degradation. Physiology. Vol. 28:93-116.

Falk, Matthias M., Fong, John T., Kells, Rachael M., O'Laughlin, Michael C., **Kowal, Tia J.**, Thevenin, Anastasia N. **2012**. Degradation of Edocytosed Gap Junctions by Autophagosomal and Endo-/lysosomal Pathways: A perspective. Journal of Membrane Biology. 2012 J Membrane Biol 245:465–476.

Jain, Raina H., Marzillier, Jutta Y., **Kowal, Tia J.,** Wang, Shaojie, Jain, Himanshu, and Falk, Matthias M. **2011**. Expression of mineralized tissue – associated proteins is highly upregulated in MC3T3-E1 osteoblasts grown on a borosilicate glass substrate. Advances in Bioceramics and Porous IV: Ceramic Engineering and Science Proceedings, R. Naragan & P. Colombo (Eds.), Vol. 32(1): 111-122.

Presented Talks

-2017- **Biological Sciences Graduate Student Seminar series**
February 14th: Lehigh University
The role of substrate nano-structure on cell behavior
Tia J. Kowal, Tanuj Chokshi, Ukrit Thamma, Himanshu Jain, Matthias M. Falk

-2016- **HHMI – BDSI – Bioconnect - RARE - *Invited Talk***
July 14th: Lehigh University
Anatomy of a Poster: Creating an effective scientific poster
Tia J. Kowal

-2015- **Materials Science and Technology - *Invited Talk***
October 6th: Columbus, OH
The role of substrate nano-structure on cell behavior
Tia J. Kowal, Tanuj Chokshi, Ukrit Thamma, Himanshu Jain, Matthias M. Falk

-2015- **HHMI – BDSI - *Invited Talk***
July 23rd: Lehigh University
Anatomy of a Poster: Creating an effective scientific poster
Tia J. Kowal

-2015- **Biological Sciences Graduate Student Seminar series**

April 7th: Lehigh University
Cell-bioactive glass scaffold interactions: Biological response to chemistry and topology
Tia J. Kowal

-2013- **Biological Sciences Graduate Student Seminar series**
March 19th: Lehigh University
Biological characterization of "Tailored Amorphous Multi-Porous" bioactive scaffolds for tissue
Tia J. Kowal

Coauthored Talks

-2015- **ACerS – GOMD** (Presented by Co-Advisor)
May 18th: Miami, FL
Symposium 2: Glasses in Healthcare – Fundamentals and Applications
Cell-Bioactive glass interactions: The role of substrate nano-structure
Tia J. Kowal, Tanuj Chokshi, Roman Golovchak, Matthias M. Falk, **Himanshu Jain**

-2013- **Materials Science and Technology** (Presented by Co-Advisor)
Oct 27th: Montreal, Canada
Next Generation Biomaterials Symposium
Control of Nano/Micro Structure of Bioactive Glass and Its Influence on Cell Response
Roman Golovchak, Tanuj Chokshi, Tia J. Kowal, Matthias M Falk, **Himanshu Jain**

-2012- **Innovations in Biomedical Materials** (Invited talk-Presented by Advisor)
Sept 10th: Raleigh, NC
Three Dimensional Scaffolds for Tissue Regeneration I
Performance of silicate TAMP bioscaffolds
Tia Kowal, Jutta Marzillier, **Matthias Falk**, Manal Saad, Mona Marei, Ukrit Thamma, Christine LaPorte, Himanshu Jain

-2012- **ACerS-Glass and Optical Materials** (Presented by Co-Advisor)
May 22th: St. Louis, MO
Session 4: Glasses for Biomedical Applications

In vitro and in vivo response of tailored amorphous multi porous (TAMP) bioscaffolds
Manal Saad, Mona Sabry, Mona Marei, Shaojie Wang, Tia Kowal, Jutta Marzillier, Matthias Falk, **Himanshu Jain**

Professional Affiliations

- American Society of Cell Biology – Member since 2010
- Materials Research Society – Member since 2011
- Biomedical Engineering Society – Member since 2012
- Sigma Xi – Member since 2014
- Women In Science & Engineering – Member since 2014

Professional Conferences

-2010-American Society of Cell Biology Meeting
Dec 10-15th: Philadelphia, PA
-2011-Materials Research Society Meeting
Nov 27-30th: Boston, MA
-2012-Delaware Membrane Protein Symposium: COBRE
May 14th: Newark, DE
-2012-Biophysical Society Pennsylvania Network Meeting
Sept 14th: Bethlehem, PA
-2012-Biomedical Engineering Society Meeting
Oct 24-27th: Atlanta, GA
-2013-Delaware Membrane Protein Symposium: COBRE
April 22nd: Newark, DE
-2013- Materials Research Society Meeting
Dec 1-6th: Boston, MA
-2014- BMES: Cell and Molecular BioEngineering Meeting
Jan 7-11th: La Jolla, CA
-2014- American Society for Cell Biology Meeting
Dec 6-10th: Philadelphia, PA
-2015- Materials Science and Technology
Oct 5-8th: Columbus, OH

Poster Presentations

-2010-Graduate School open house poster presentation
Oct 16th: Lehigh University
-2011-**Materials Research Society Meeting** Poster Presentation
Nov 29th: Boston, MA - Session KK
Role of Nanoporosity on the performance of Bioactive Nano-Macro Dual-Porous Glass Scaffolds
Shaojie Wang, **Tia Kowal**, Ahmad Rashad, Mona Marei, Matthias Falk, Himanshu Jain

-2012-Graduate School open house poster presentation
Jan 26th: Lehigh University
Biological Characterization of TAMP Scaffolds for Hard Tissue Regeneration
Tia Kowal, Shaojie Wang, Jutta Marzillier, Paulina Krzyszczyk, Himanshu Jain, Matthias Falk

-2012-**IMI Day and NSF Site Visit** Poster Presentation
Sept. 13th: Lehigh University
Biological Characterization of TAMP Scaffolds for Hard Tissue Regeneration
Tia Kowal, Shaojie Wang, Jutta Marzillier, Paulina Krzyszczyk, Himanshu Jain, Matthias Falk

-2012-**Biomedical Engineering Society Meeting** Poster Presentation
Oct 24-27th: Atlanta, GA- Novel Biomaterials/Scaffolds
Biological Characterization of TAMP Scaffolds for Hard Tissue Regeneration
Tia Kowal, Shaojie Wang, Jutta Marzillier, Paulina Krzyszczyk, Himanshu Jain, Matthias Falk

-2013-Graduate School open house poster presentation
Feb 4th: Lehigh University
Biological Characterization of TAMP Scaffolds for Hard Tissue Regeneration
Tia Kowal, Shaojie Wang, Jutta Marzillier, Paulina Krzyszczyk, Himanshu Jain, Matthias Falk

-2013-**College of Arts and Sciences poster presentation**
March 25th: Lehigh University
Biological Characterization of TAMP Scaffolds for Hard Tissue Regeneration
Tia Kowal, Shaojie Wang, Jutta Marzillier, Paulina Krzyszczyk, Himanshu Jain, Matthias Falk

-2013-**Thought and Action: 2013 Academics Symposium**
April 4th: Lehigh University
Biological Characterization of TAMP Scaffolds for Hard Tissue Regeneration
Tia Kowal, Shaojie Wang, Jutta Marzillier, Paulina Krzyszczyk, Himanshu Jain, Matthias Falk

-2013-**Materials Research Society Meeting** Poster Presentation
Dec 5th: Boston, MA – Session H
Biological Characterization of TAMP Scaffolds for Hard Tissue Regeneration
Tia Kowal, Shaojie Wang, Jutta Marzillier, Mona Marei, Himanshu Jain, Matthias Falk

-2014-Graduate School open house poster presentation
Jan 3th: Lehigh University

Cell-bioactive glass scaffold interactions: The role of substrate nano-structure
Tia Kowal, Tanuj Chokshi, Ukrit Thamma, Himanshu Jain, Matthias M. Falk

-2014- **BMES: Cell and Molecular BioEngineering Meeting Poster**
Jan 7-11th: La Jolla, CA
Cell-bioactive glass scaffold interactions: The role of substrate nano-structure
Tia Kowal, Tanuj Chokshi, Ukrit Thamma, Himanshu Jain, Matthias M. Falk

-2014- **Lehigh University Biological Sciences Undergraduate Research Symposium** Poster Presentation (presented by undergraduate)
April 10th: Lehigh University
Osteoblast-Osteoclast Co-culture investigations on TAMP Scaffolds for Hard Tissue Regeneration
Natalie Hahn, **Tia Kowal**, Himanshu Jain, Matthias M. Falk

-2014- **Lehigh University Biological Sciences Undergraduate Research Symposium** Poster Presentation (presented by undergraduate)
April 10th: Lehigh University
MC3T3-E1 Preosteoblasts respond differently to 45S5 Bioglass Samples Varying in Nanostructure
Tanuj Chokshi, **Tia Kowal**, Roman Golovchak, Himanshu Jain, Matthias Falk

-2014- **American Society for Cell Biology** Poster Presentation
December 9th: Philadelphia, PA
Cell-bioactive glass scaffold interactions: The role of substrate nano-structure
Tia J. Kowal, Tanuj Chokshi, Ukrit Thamma, Himanshu Jain, Matthias M. Falk

-2015-Graduate School open house poster presentation
Jan 29th: Lehigh University
Cell-bioactive glass scaffold interactions: The role of substrate nano-structure
Tia J. Kowal, Tanuj Chokshi, Ukrit Thamma, Himanshu Jain, Matthias M. Falk

-2015- **Lehigh University Biological Sciences Undergraduate Research Symposium** Poster Presentation (presented by undergraduate)
April 21th: Lehigh University
An In vitro bone model for tissue regeneration
Natalie Hahn, **Tia Kowal**, Himanshu Jain, Matthias M. Falk

-2015- **Lehigh University College of Arts and Sciences Undergraduate Research Symposium** Poster Presentation (presented by undergraduate)
April 29th: Lehigh University
An In vitro bone model for tissue regeneration
Natalie Hahn, **Tia Kowal**, Himanshu Jain, Matthias M. Falk

-2016-Graduate School open house poster presentation
Feb 4th: Lehigh University
Cell-bioactive glass scaffold interactions: The role of substrate nano-structure
Tia J. Kowal, Tanuj Chokshi, Ukrit Thamma, Himanshu Jain, Matthias M. Falk

-2017- **Lehigh University College of Arts and Sciences Undergraduate Research Symposium** Poster Presentation (presented by undergraduate)
April 20th: Lehigh University
Identification of Skin and Endometrial Marker Proteins to Distinguish Between Cell Types Growing on TAMP Scaffolds
Jannah Wing, **Tia Kowal**, Himanshu Jain, Sigrid Blome-Eberwein, Steve Somkuti, Matthias M. Falk

-2017- **Lehigh Valley Molecular and Cell Biology Symposium Undergraduate Research Symposium** Poster Presentation (presented by undergraduate)
April 27th: DeSales University
Identification of Skin and Endometrial Marker Proteins to Distinguish Between Cell Types Growing on TAMP Scaffolds
Jannah Wing, **Tia Kowal**, Himanshu Jain, Sigrid Blome-Eberwein, Steve Somkuti, Matthias M. Falk

---

Persons Mentored

Undergraduates

-2011 to 2012- Paulina Krzyszczyk – Bioengineering Student
-2011 Spring- Diego Liriano – Biology Student
-2012 to 2014- Natalie Hahn – IDEAS student
-2013 to 2014- Tanuj Chokshi – Biology student
-2016 to 2017- Jannah Wing – IDEAS student

Visiting Scientists

-Fall 2011 - Jui Chakraborty - India
-Spring 2011- Ahmad Rashad - Egypt
-Spring 2011 - Di Zhang - Finland

Community Outreach

-2017 PA DNA day ambassador and organizer – Liberty High School – DNA repair module – April 25, 2017

-2017 Broughal Middle School Bio Fair volunteer –Protein synthesis and trafficking station – March 21, 2017

-2016 Judge for Third Annual Allentown School District Science Fair –June 2, 2016

-2016 GRAD Experience–The Cell: How cells communicate to one another–May 23rd Alumni Weekend

-2016 Broughal Middle School Bio Fair volunteer –Protein synthesis and trafficking station – March 23, 2016

-2016 PA DNA day ambassador and organizer – Liberty High School - Personalized medicine module – April 26, 2016

-2015 Judge for Second Annual Allentown School District Science Fair –May 28, 2015

-2015 Broughal Middle School Bio Fair volunteer –Protein synthesis and trafficking station – March 20, 2015

-2014 Broughal Middle School Bio Fair volunteer –Protein synthesis and trafficking station – March 15, 2014

-2014 AAUW bookfair – science book pricing and sale

-2014 Allentown School District Science Fair Judge